The Sveconorwegian orogeny

(Article begins on next page)

13 January 2025

2    # The Sveconorwegian orogeny

3

4

5    Bernard Bingen [1] , Giulio Viola [2] , Charlotte Möller [3] , Jacqueline Vander Auwera [4] , Antonin

6    Laurent [5], Keewook Yi [6]

7

8

9    1 Corresponding author, Geological Survey of Norway, 7491 Trondheim, Norway;

10   bernard.bingen@ngu.no; ORCID; 0000-0002-4901-2016

11   2 Department of Biological, Geological and Environmental Sciences, BiGeA, University of

12   Bologna, 40126 Bologna, Italy; giulio.viola3@unibo.it

13   3 Department of Geology, Lund University, Sölvegatan 12, SE-223 62 Lund, Sweden;

14   charlotte.moller@geol.lu.se

15   4 Department of Geology, University of Liège, 4000 Liège, Belgium; jvdauwera@uliege.be

16   5 Université de Lyon, UJM-Saint-Etienne, CNRS, UCA, IRD, LMV UMR 6524, F-42023

17   Saint-Etienne, France; antonin.laurent@univ-st-etienne.fr

18   6 Korea Basic Science Institute, 363-883 Chungbuk, South Korea; kyi@kbsi.re.kr

19

20

21   **GRAPHICAL ABSTRACT**

Sveconorwegian orogeny
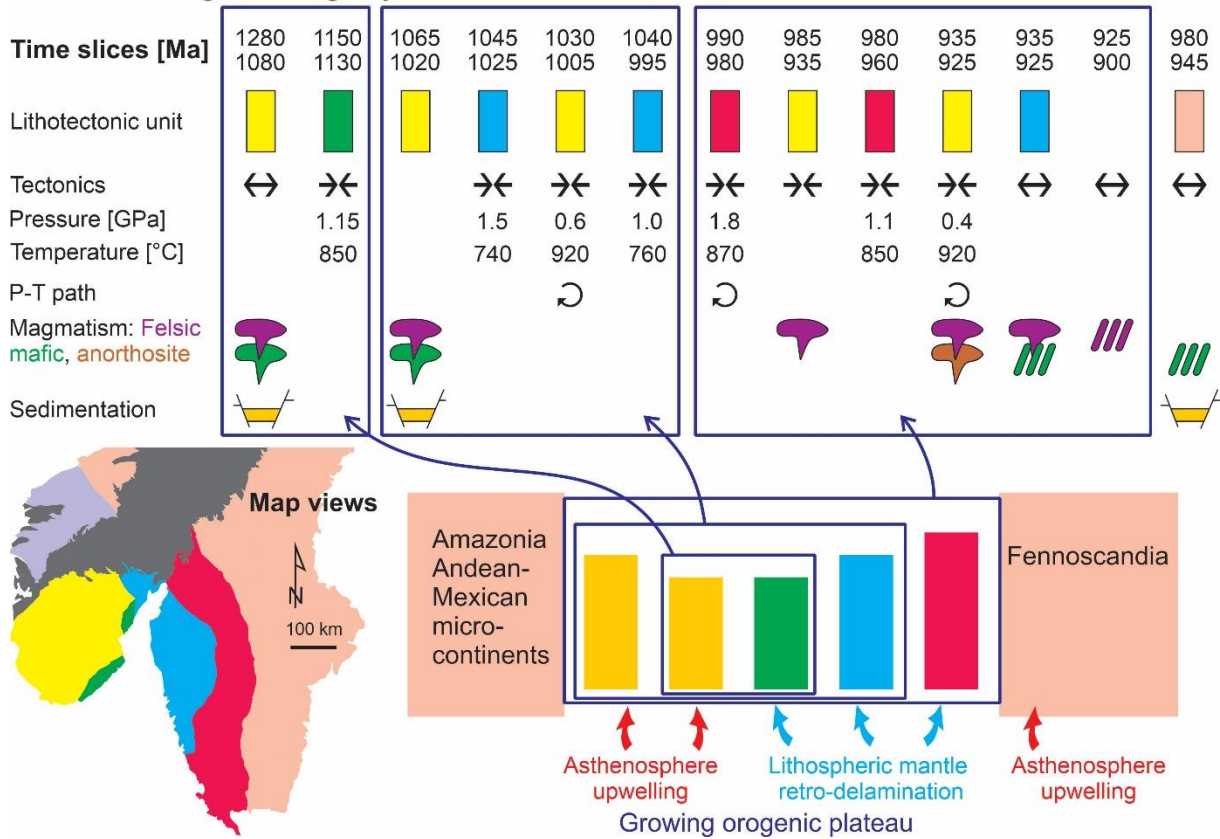
23 **ABSTRACT**

24 This article reviews the geology of the Sveconorwegian orogen in south Scandinavia and

25 existing tectonic models for the Mesoproterozoic to Neoproterozoic Sveconorwegian

26 orogeny. It proposes an updated geodynamic scenario of large, hot, long-duration continental

27 collision starting at c. 1065 Ma between proto-Baltica and another plate, presumably

28 Amazonia, in a Rodinia-forming context. An orogenic plateau formed at 1280 Ma as a back-

29 arc Cordillera-style plateau, and then grew further stepwise after 1065 Ma, as a collisional

30 Tibetan-style plateau. Voluminous mantle- and crustal-derived Sveconorwegian magmatism

31 took place in the hinterland in the west of the orogen, mainly: (i) bimodal magmatism at

32 1280–1145 Ma, overlapping with extensional intramontane basin sedimentation, (ii) the calc-

33 alkaline Sirdal magmatic belt at 1065–1020 Ma, (iii) the hydrous ferroan hornblende-biotite

34 granite (HBG) suite at 985–925 Ma and (iv) the anhydrous ferroan massif-type anorthosite-

35 mangerite-charnockite (AMC) suite at 935–915 Ma. High-alumina orthopyroxene megacrysts

36 in anorthosite imply mafic underplating at 1040 Ma and remelting of the underplates at 930

37 Ma. Overlapping with magmatism, protracted low-pressure, granulite-facies metamorphism

38 reached twice ultra-high temperature conditions, of 0.6 GPa-920 °C at 1030–1005 Ma and 0.4

39 GPa-920 °C at 930 Ma. These features imply shallow asthenosphere under the crust. Towards

40 the foreland in the east, metamorphism shows increasing high-pressure signature eastwards

41 with time, with peak P-T values of 1.15 GPa-850 °C at 1150–1120 Ma in the Bamble-

42 Kongsberg lithotectonic units, 1.5 GPa-740 °C at c. 1050 Ma in the Idefjorden lithotectonic

43 unit, and 1.8 GPa-870 °C at c. 990 Ma in the Eastern Segment under eclogite-facies

44 conditions. These are attributed to retreating delamination of the dense sub-continental

45 lithospheric mantle and growth of the orogenic plateau towards the foreland. After c. 930 Ma,

46 convergence came to a halt, the orogenic plateau collapsed, and 16 km of overburden was

47 removed by extension and erosion.

48

49 **Keywords:** Sveconorwegian, Mesoproterozoic, Rodinia, continental collision, orogenic

50 plateau - lithospheric mantle delamination

51

52 **Highlights:**

53 - Review of the geology of the Sveconorwegian orogen in south Scandinavia.

54 - Review of geodynamic models for the Mesoproterozoic to Neoproterozoic Sveconorwegian

55 orogeny.

56 - Model of large, hot, long-duration continental collision for the Sveconorwegian orogeny.

57 - Orogenic plateau construction is associated with retreating delamination of the continental

58 lithospheric mantle.

59 - Protracted shallow asthenosphere lead to crustal melting and ultra-high temperature

60 granulite-facies metamorphism.

61    - Massif-type anorthosite-mangerite-charnockite plutonism resulted from remelting of mafic

62    underplates at 1.1 GPa under high heat flow conditions.

63    - The Sveconorwegian orogeny contributed to assembly of Rodinia supercontinent

## 1    Introduction

65    Late-Mesoproterozoic orogenic belts are interpreted as products of the closure of oceanic

66    realms and the collision between continents to form supercontinent Rodinia at the end of the

67    Mesoproterozoic (Hoffman, 1991; Li et al., 2008). The Rodinia paradigm is robust, and

68    supported by a peak in the abundance of late Mesoproterozoic detrital zircons (Hawkesworth

69    et al., 2009). This notwithstanding, paleogeographic models for Rodinia configuration and

70    plate tectonic models for Rodinia assembly remain in essence ill-defined (Torsvik, 2003).

71    Proto-Baltica (Proterozoic Baltica = East European Craton, here after called Baltica) is a core

72    piece of Rodinia in almost all models (Fig. 1) (Li et al., 2008; Merdith et al., 2017), and the

73    Sveconorwegian orogen at the western margin of Baltica provides key geological evidence for

74    the assembly of Rodinia (Bingen et al., 2008a; Bingen et al., 2008c; Bogdanova et al., 2008;

75    Cawood and Pisarevsky, 2017; Cawood et al., 2010; Falkum and Petersen, 1980; Gee et al.,

76    2015; Gower et al., 2008; Hartz and Torsvik, 2002; He et al., 2018; Ibanez-Mejia et al., 2011;

77    Lorenz et al., 2012; Pisarevsky et al., 2014; Roberts, 2013; Roberts and Slagstad, 2015;

78    Slagstad et al., 2019; Slagstad et al., 2020; Slagstad et al., 2018; Slagstad et al., 2017;

79    Stephens and Wahlgren, 2020b; Torsvik et al., 1996; Weber et al., 2010).

80        The Sveconorwegian orogen is well exposed and accessible in its type area in southwest

81    Scandinavia (south Norway and southwest Sweden). It represents therefore an excellent

82    natural laboratory to study Precambrian geodynamics (Bingen and Viola, 2018; Laurent et al.,

83    2018a; Möller and Andersson, 2018; Slagstad et al., 2018; Stephens and Wahlgren, 2020b;

84    Vander Auwera et al., 2011; Viola and Henderson, 2010).

85     The body of geological data on the Sveconorwegian orogen has been steadily growing over

86    the last 20 years, leading to contrasting conceptual models. This article reviews the existing

87    structural, metamorphic, magmatic, geochronological and isotopic record across the entire

88    Sveconorwegian orogen, and discusses the orogenic models that have been proposed in the

89    literature. In fact, there is a lively debate in the literature on whether the Sveconorwegian

90    orogeny was a collisional or a non-collisional (Andean) orogeny (Bingen et al., 2008a; Möller

91    and Andersson, 2018; Slagstad et al., 2020; Slagstad et al., 2017; Slagstad et al., 2013;

92    Stephens and Wahlgren, 2020b). We address this debate and conclude proposing an updated

93    model of large, hot, and long-duration continent-continent collision for the Sveconorwegian

94    orogeny at the margin of Baltica / Fennoscandia. This model involves the stepwise

95    propagation of an orogenic plateau towards the foreland and hinterland of the orogen,

96    associated with retreating delamination of the continental lithospheric mantle. It takes into

97    account a number of key features of the orogeny, including the zoning of metamorphism, the

98    distribution of magmatism and the genesis of massif-type anorthosites.
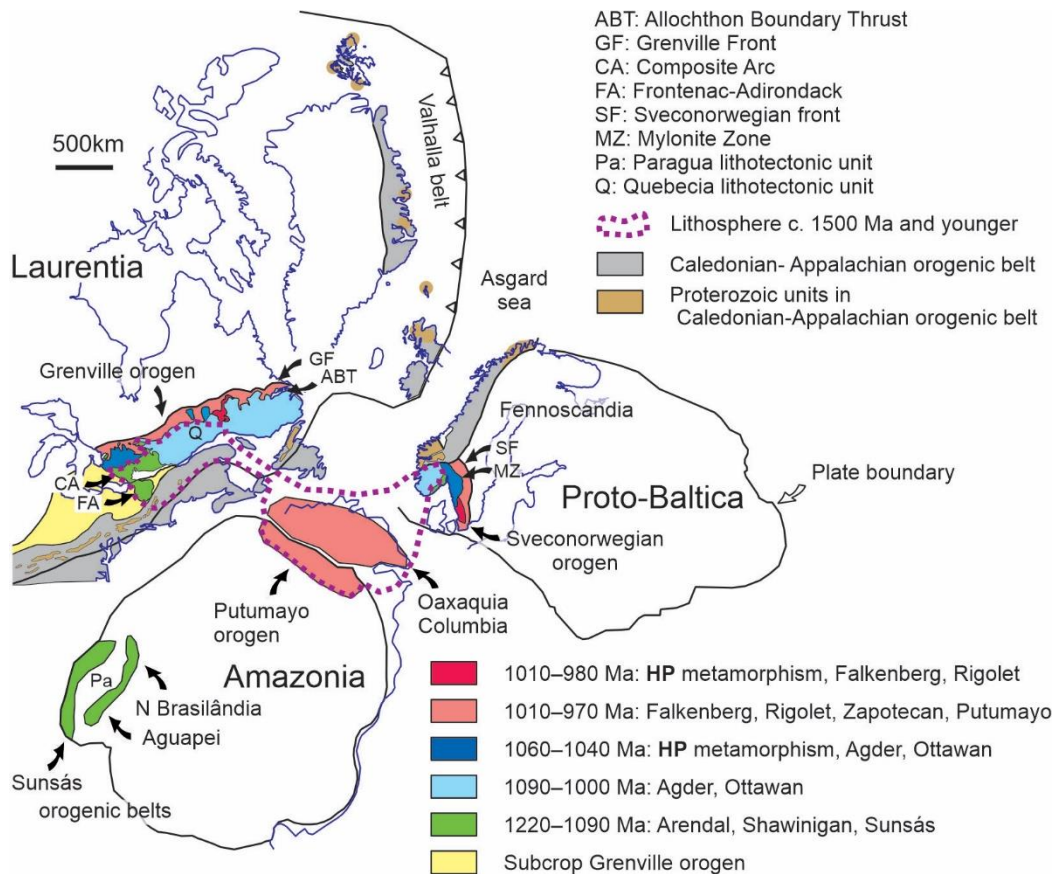
99    -------------------

**Figure 1.** Archetypal paleogeographic reconstruction of proto-Baltica (Baltica), Laurentia and

Amazonia in their Rodinia framework at the Mesoproterozoic-Neoproterozoic boundary

(Cawood and Pisarevsky, 2017; Hoffman, 1991; Li et al., 2008). The first order architecture

of the Meso- to Neoproterozoic orogenic belts is shown, with emphasis on the geochronology

of metamorphism (Hynes and Rivers, 2010; Ibanez-Mejia et al., 2011; Rivers, 2008; Tohver

et al., 2005). The high-pressure (HP) metamorphic belts are shown separately. The names of

the main tectonometamorphic phases in the different orogens are listed in the legend, with

Arendal, Agder, Falkenberg for the Sveconorwegian orogen, Shawinigan, Ottawan, Rigolet

for the Grenville orogen, Putumayo for the Putumayo orogenic belt, Zapotecan for the

Oaxaquia lithotectonic unit, and Sunsás for the Sunsás, Aguapei and N Brasilândia belts.

--------------------

**Table 1.** Chart of geological events in the Sveconorwegian orogen.

--------------------
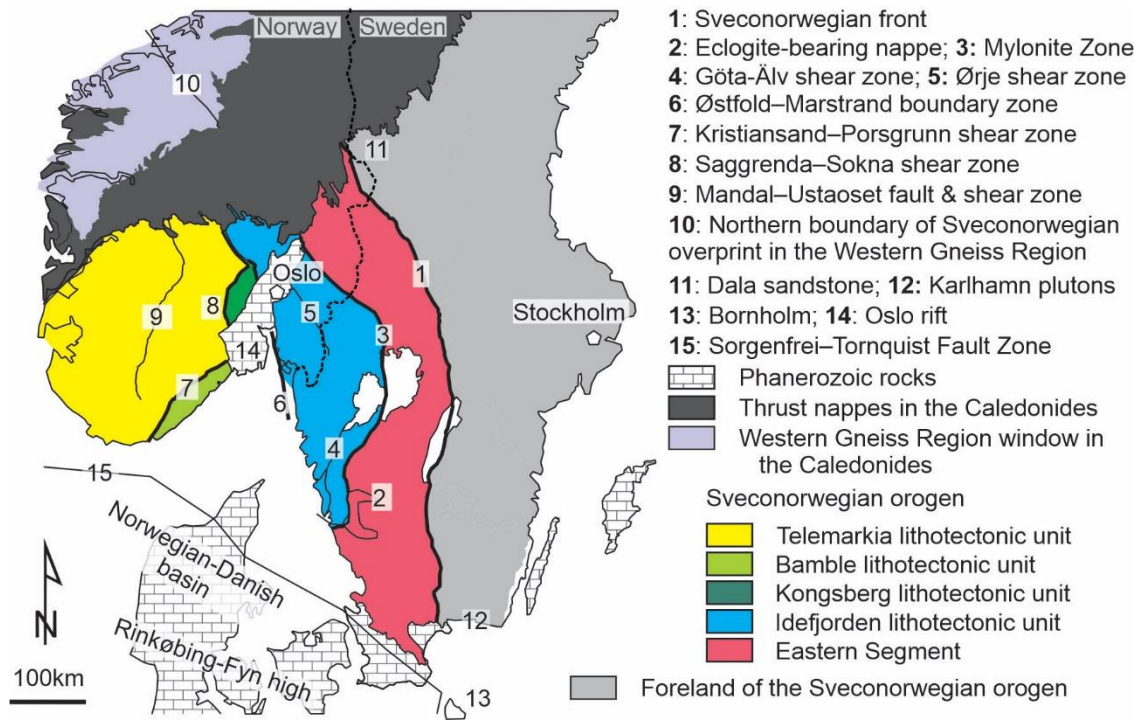
**Figure 2.** Sketch map of the Sveconorwegian orogen, with nomenclature of lithotectonic units and main shear and fault zones.

--------------------

## 2    Context

### *2.1    The Sveconorwegian orogen and Sveconorwegian orogeny*

The Sveconorwegian orogen is located along the southwestern margin of Fennoscandia, which is the northern part of proto-Baltica (Fig. 1; Fig. 2; Table 1) (Bogdanova et al., 2008; Koistinen et al., 2001; Stephens et al., 2020). The Sveconorwegian orogen consists of Paleoproterozoic to Mesoproterozoic continental lithosphere reworked during the Sveconorwegian orogeny at the transition between the Mesoproterozoic and the Neoproterozoic (Stenian to Tonian). This lithosphere was generated during the Svecokarelian (1910–1750 Ma), post-Svecokarelian (1710–1660 Ma), Gothian (1660–1520 Ma), Telemarkian (1520–1480 Ma) and Hallandian (1465–1380 Ma) accretionary orogenies.

128      The exposed Sveconorwegian orogen is presently c. 550 km wide and has a general N–S

129      structural grain (Fig. 2) (Berthelsen, 1980; Demaiffe and Michot, 1985; Falkum, 1985;

130      Falkum and Petersen, 1980). In the east, it is separated from the Paleoproterozoic foreland by

131      the nearly 700 km long Sveconorwegian front (Möller and Andersson, 2018; Möller et al.,

132      2015; Stephens and Wahlgren, 2020a; Wahlgren et al., 1994).

133      In the north, the Sveconorwegian orogen was reworked during the Caledonian orogeny

134      (Fig. 2). Precambrian rocks with a Meso- to Neoproterozoic overprint are observed in the

135      Western Gneiss Region, the largest basement window in the Caledonides (Røhr et al., 2013;

136      Tucker et al., 1990) and are also found in Caledonian thrust nappes of the Lower and Middle

137      Allochthons of the Caledonides (Augland et al., 2014; Corfu, 2019; Lundmark and Corfu,

138      2008; Roffeis and Corfu, 2014; Wiest et al., 2018). In the south, the Sveconorwegian

139      basement is overlain by Phanerozoic sedimentary rocks and affected by Carboniferous-

140      Permian and younger faulting and rifting along the WNW–ESE trending Sorgenfrei-Tornquist

141      Fault Zone and NNE–SSW trending Oslo rift (Fig. 2) (Bergerat et al., 2007; Erlström, 2020;

142      Larsen et al., 2008; Torgersen et al., 2015). As inferred from geophysical data and a few deep

143      wells in Denmark, a Sveconorwegian basement probably underlies the Norwegian-Danish

144      Basin (Ringkøbing-Fyn high), reaching the southern boundary of the Baltica plate (Trans-

145      European Suture Zone and Elbe line) (Lassen and Thybo, 2012; Olesen et al., 2004; Olivarius

146      et al., 2015; Thybo, 2001).

147      The Sveconorwegian orogen can be conceptually subdivided into five, orogen-parallel

148      lithotectonic units (INSPIRE_Directive, 2007), called, from east to west, the Eastern

149      Segment, and the Idefjorden, Kongsberg, Bamble, and Telemarkia lithotectonic units (also

150      referred to as units in short in the following text) (Fig. 2) (Bingen et al., 2008c). These

151      lithotectonic units are separated by major Sveconorwegian shear zones and are characterized

152      by distinct geological histories.

153      The first high-grade metamorphism attributed to the Sveconorwegian orogeny dates back

154    to between 1150 and 1120 Ma and is recorded in the Bamble and Kongsberg lithotectonic

155    units. It is referred to as the Arendal phase in Bingen et al. (2008a; 2008c). As elaborated

156    further below, this early-Sveconorwegian event can be interpreted as the outcome of a

157    geodynamic evolution starting after the Hallandian orogeny, i.e. after c. 1340 Ma, and

158    hereafter referred to as the pre-Sveconorwegian. The main Sveconorwegian orogeny started at

159    c. 1065 Ma, and can be summarized by three orogenic phases (Bingen et al., 2008a; Bingen et

160    al., 2008c): the Agder phase (1065–1000 Ma), the Falkenberg phase (1000–970 Ma) and the

161    Dalane phase (970–900 Ma). As more geological data become available, however, these three

162    phases are becoming increasingly difficult to discriminate in time and they are not used

163    systematically in the following text. Intrusion of pegmatite fields and lamprophyre dykes

164    sealed the orogeny at c. 915–900 Ma (Müller et al., 2015; Müller et al., 2017; Wahlgren et al.,

165    2015).

166    *2.2   Rodinia assembly*

167    Several paleogeographic and tectonic models have been proposed for the configuration and

168    assembly of supercontinent Rodinia at the end of the Mesoproterozoic (Hoffman, 1991; Li et

169    al., 2008; Merdith et al., 2017; Torsvik, 2003). Classical models (Fig. 1), integrating

170    paleomagnetic data and geological information from the Proterozoic to the Phanerozoic,

171    suggest that Rodinia formed by the reassembly of continents previously assembled into

172    supercontinent Nuna (Columbia) during the Paleo- and Mesoproterozoic (Evans and Mitchell,

173    2011; Johansson, 2009; Pisarevsky et al., 2014; Rogers and Santosh, 2002; Zhang et al.,

174    2012). These models locate Laurentia in the centre of Rodinia, with Baltica to the east and

175    Amazonia south of Laurentia, respectively (Fig. 1) (Cawood and Pisarevsky, 2017; Dalziel,

176    1997; Gong et al., 2018; Hoffman, 1991; Li et al., 2008; Merdith et al., 2017; Torsvik et al.,

177    1996). Alternative Baltica–Laurentia reconstructions are proposed by Torsvik (2003), Lorenz

178    et al. (2012) and Slagstad et al. (2019).

179        It is beyond the scope of this paper to review Rodinia assembly models. In the following

180    text and in several figures, updated geological, geochronological and isotopic data from the

181    Sveconorwegian orogen are compared with data from the Grenville orogen of Laurentia, the

182    Putumayo and Sunsás orogens of Amazonia and Mesoproterozoic lithotectonic units in the

183    Andes (Garzón, Las Minas inliers) and Mexico (Oaxaquia). The goal is to show that it is

184    realistic to consider the Sveconorwegian orogen as part of a large orogenic zone between

185    Laurentia, Amazonia and Baltica (Fig. 1). The comparative analysis offers a broader

186    perspective for the Sveconorwegian orogeny in a Rodinia context.

187    --------------------
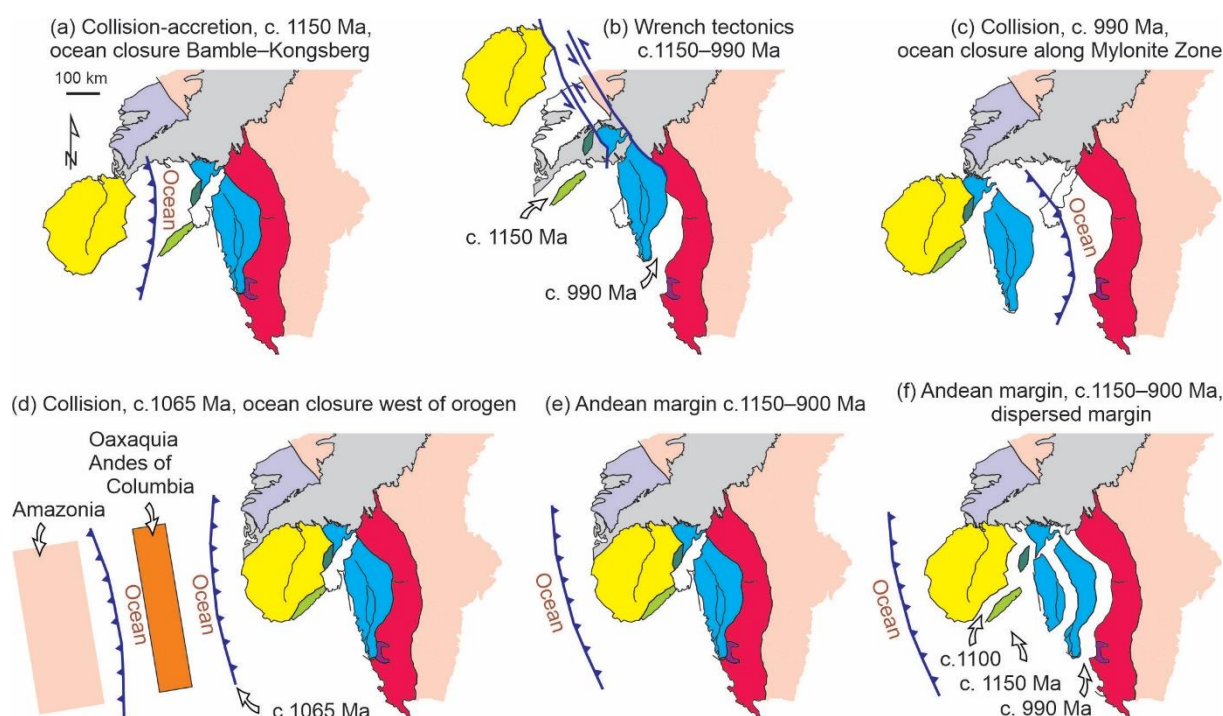


189    **Figure 3.** Conceptual tectonic models, in map view, for the Sveconorwegian orogeny,

190    reviewed in this paper. Same colour coding as in Fig. 2. (a) Early-Sveconorwegian accretion

191    of the Telemarkia lithotectonic unit, with suturing along the Bamble-Kongsberg lithotectonic

192    units (Bingen et al., 2005). (b) Wrench tectonics involving large-strike-slip displacements

193    between the five lithotectonic units of the orogen, all endemic to Fennoscandia (Lamminen

194    and Köykkä, 2010; Stephens and Wahlgren, 2020b). (c) Collision at c. 990 Ma between

195    Baltica (Fennoscandia) and a continent comprising the four western lithotectonic units of the

196    orogen (Möller and Andersson, 2018; Petersson et al., 2015b). (d) Collision at c. 1065 Ma

197    between Baltica (Fennoscandia) and another continental plate (Amazonia) with closure of

198    oceanic basins to the west of the exposed orogen (Bogdanova et al., 2008; Cawood and

199    Pisarevsky, 2017; Ibanez-Mejia et al., 2011). (e, f) non-collisional (Andean) models, with

200    orogeny controlled by a subduction system outboard of Fennoscandia during the entire

201    duration of orogeny from c. 1150 to 900 Ma. (e) The margin was either well assembled before

202    the orogeny (Falkum and Petersen, 1980; Slagstad et al., 2013) or (f) dispersed and re-

203    assembled during the orogeny (Slagstad et al., 2020).

204    --------------------

205    *2.3   A diversity of orogenic models*

206    Many large-scale tectonic models have been proposed to explain the Sveconorwegian

207    orogenic evolution. In Fig. 3, six possible conceptual end-member models are sketched in

208    map view. They range from collisional (Himalaya-Tibet type) to non-collisional (Andean

209    type), and some involve accretion of exotic lithotectonic units to Fennoscandia. In Fig. 3 a,

210    the early-Sveconorwegian closure of an ocean between the Telemarkia and Idefjorden

211    lithotectonic units resulted in the formation of the Bamble-Kongsberg lithotectonic units at c.

212    1150–1120 Ma, and accretion of an exotic Telemarkia lithotectonic unit (Bingen et al., 2005).

213    In Fig. 3 b, the five lithotectonic units are all endemic to Fennoscandia. Only large-scale

214    movements between them are considered, steered by large scale wrench tectonics, which is

215    controlled by strike-slip shearing along the main Sveconorwegian shear zones (Bingen et al.,

216    2005; Lamminen and Köykkä, 2010; Stephens and Wahlgren, 2020b). In Fig. 3 c, closure of

217    an oceanic basin at c. 990 Ma between the Eastern Segment and the Idefjorden lithotectonic

218    unit along the Mylonite Zone, resulted in collision between Baltica (Fennoscandia) and a

219    continent composed of the four western lithotectonic units of the orogen ('Sveconorwegia')

220    (Möller and Andersson, 2018; Petersson et al., 2015b). In Fig. 3 d, an (Himalaya-Tibet type)

221    collision at and after c. 1065 Ma between Baltica (Fennoscandia) and one (or several)

222    continental plate(s) (possibly Amazonia, Laurentia, and intervening terranes exposed in

223    Mexico and the Andes of Colombia) involved closure of oceanic basins to the west of the

224    exposed orogen (Bingen et al., 2008c; Bogdanova et al., 2008; Cawood and Pisarevsky, 2017;

225    Ibanez-Mejia et al., 2011; Stephens and Wahlgren, 2020b; Weber et al., 2010). In Fig. 3 e and

226    f, non-collisional (Andean type) models feature an eastward subduction of an oceanic plate

227    below the western margin of Baltica (Fennoscandia) during the entire Sveconorwegian

228    orogeny, from 1150 to 900 Ma, in the absence of a final collision. The lithotectonic units in

229    the orogen either were assembled already before the Sveconorwegian orogeny (Fig. 3 e)

230    (Falkum and Petersen, 1980; Slagstad et al., 2013) or, alternatively, they were dispersed

231    during the pre-Sveconorwegian time interval (1280–1150 Ma) and then re-assembled during

232    the Sveconorwegian orogeny after 1150 Ma (Fig. 3 f) (Slagstad et al., 2020). These six

233    models are not mutually exclusive because terrane assembly (Fig. 3 a, c) can be anticipated

234    before a collision (Fig. 3 d) or during a protracted subduction history (Fig. 3 e, f), and because

235    deformation partitioning (Fig. 3 b) can take place before, during and after a collision or during

236    protracted subduction. Arguments supporting or dismissing aspects of each of these orogenic

237    models are discussed in more detail below.

238    *2.4    Secular evolution of the Earth, mantle delamination and orogenic plateau*

239    Estimates of heat flow and heat production through Earth history suggest that the

240    asthenosphere was c. 100°C hotter in the Mesoproterozoic than at present (Gerya, 2014;

241    Herzberg et al., 2010; Johnson et al., 2013; Korenaga, 2008; Sizova et al., 2014). A hotter

242    asthenosphere implies a weaker rheology of lithospheric plates. The tectonic consequences of

243  a hotter asthenosphere on the dynamics of orogeny are multiple and include, but are not

244  limited to, ductile thick-skinned deformation, lower topography, more proximal

245  sedimentation, shallower slab breakoff, widespread partial melting in the lower to middle

246  crust, widespread syn-orogenic magmatism, ultrahigh temperature granulite-facies

247  metamorphism (above 900°C), decoupling between crust and lithospheric mantle, and

248  remelting of basaltic underplates to produce anorthosite plutons (Brown, 2006, 2013; Gerya,

249  2014; Rey and Houseman, 2006; Sizova et al., 2014; Vander Auwera et al., 2011;

250  Vanderhaeghe, 2012). These consequences can be evaluated qualitatively in the Proterozoic

251  geological record (Cagnard et al., 2011; Chardon et al., 2009). However, they are difficult to

252  assess and quantify individually (Sizova et al., 2014).

253      There is wide consensus that after the Archean, plate tectonics has imposed dominant

254  horizontal movements to orogenies. However, an evaluation of the composition and

255  temperature of the lithosphere through Earth history suggests that, after the Archean, the sub-

256  continental lithospheric mantle was, on average, denser than the asthenosphere (Griffin et al.,

257  2009; Poudjom Djomani et al., 2001). The sub-continental lithospheric mantle was therefore

258  gravitationally unstable in the Proterozoic, like in the Phanerozoic, and prone to delamination

259  and foundering (subduction) (Bird, 1979; Chen et al., 2017; Krystopowicz and Currie, 2013).

260  Delamination of the lithospheric mantle is compensated by upwelling of asthenosphere. The

261  parameters and geometry of delamination in convergent orogens were explored numerically

262  by Li et al. (2016). Delamination is promoted by the density contrast between the lithospheric

263  mantle and the asthenosphere, rheological weakness of the lower crust and the lithospheric

264  mantle, convergence rate, and eclogitization of the lower crust.

265      The Sveconorwegian orogeny is characterized by widespread crustal partial melting, low-

266  pressure–ultrahigh-temperature metamorphism and massif-type anorthosite plutonism, typical

267  of hot orogens. Orogenic models for the Sveconorwegian orogeny should integrate the

268     evolution of the mantle (and not only the crust). They require consideration of vertical

269     movements of the lithospheric mantle and the asthenosphere in addition to horizontal

270     movements of the lithospheric plates.

271       Orogenic plateaus are a hallmark of large and hot convergent orogens (Beaumont et al.,

272     2006; Godin et al., 2006; Jamieson and Beaumont, 2013; Li et al., 2016; Rey et al., 2001;

273     Royden et al., 2008; Vanderhaeghe, 2012). An orogenic plateau consists of elevated and

274     thickened crust spreading by gravitational forces, above a lithospheric mantle thinned by

275     delamination. Temperature in the crust is regulated by self-heating and basal heating from the

276     mantle. The crust of a plateau is characterized by a little viscous low- to middle-crust,

277     weakened by partial melting, called infrastructure, overlain by a brittle upper crust, called

278     superstructure or orogenic lid (Jamieson and Beaumont, 2013; Rey et al., 2001;

279     Vanderhaeghe, 2012). In the infrastructure, metamorphism typically carries a high-

280     temperature signature, overprinting pre-plateau metamorphic signatures (for example early

281     high-pressure metamorphism) (Godin et al., 2006). Due to the difference in viscosity, the

282     infrastructure and superstructure are structurally decoupled. The infrastructure can flow under

283     the superstructure (channel flow), leading to a situation where the superstructure is in

284     extension, while the infrastructure is in compression. An orogenic plateau can be anticipated

285     to grow with time if convergence is maintained (Li et al., 2016; Royden et al., 2008).

286       The Sveconorwegian orogen consists of a patchwork of high-grade gneiss complexes and

287     low-grade rocks (Fig. 4). In this paper, these are interpreted as the remnants of the

288     infrastructure and superstructure of an orogenic plateau, respectively.

289     --------------------

290
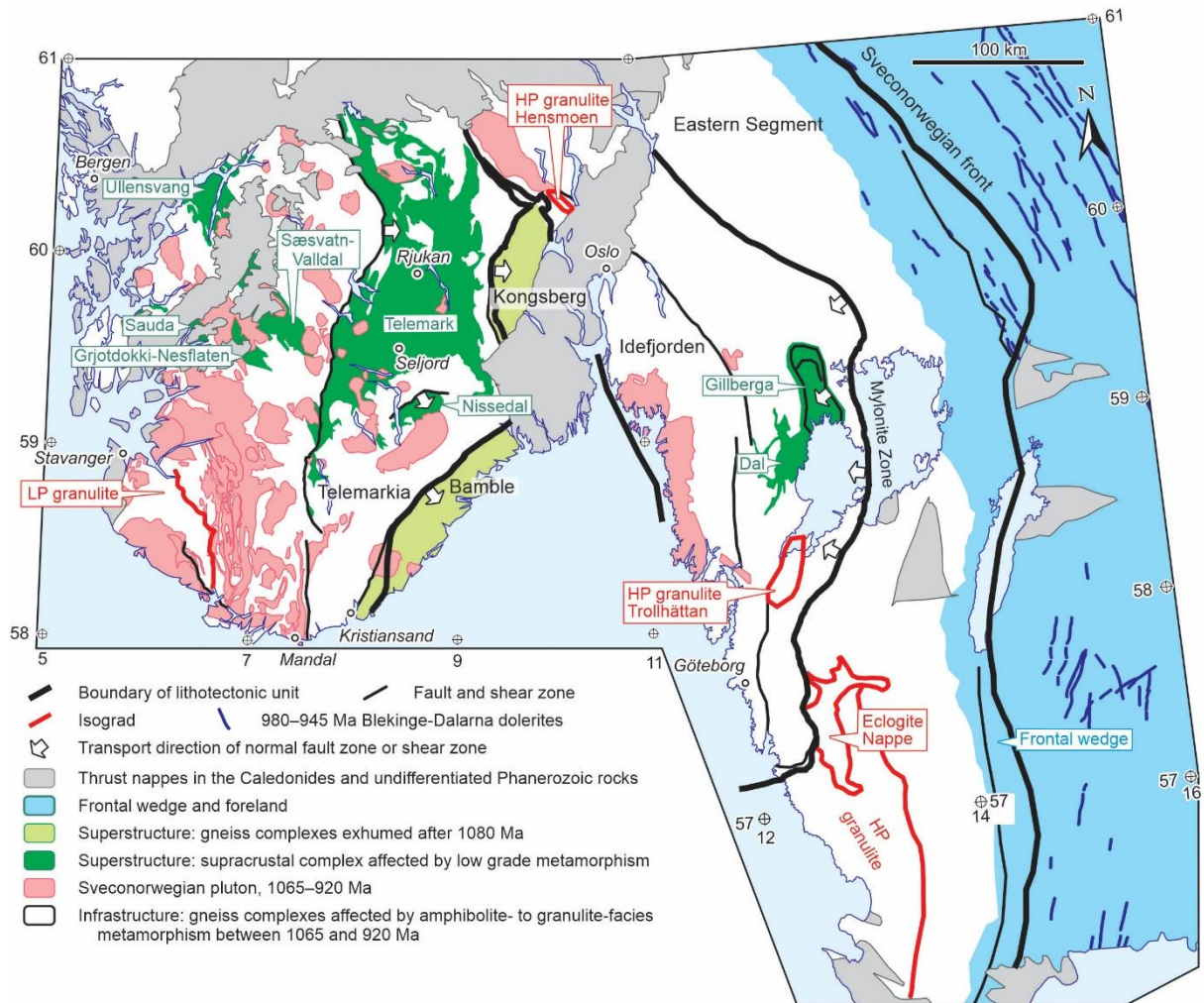
291　**Figure 4.** Sketch map of the Sveconorwegian orogen, showing the extent of the infrastructure

292　and superstructure (orogenic lid) of the orogen during the main Sveconorwegian orogeny

293　(1065–920 Ma) and Sveconorwegian plutons (1065–920 Ma).

294　--------------------

**Figure 5.** Sketch map of the Sveconorwegian orogen, with emphasis on Sveconorwegian events younger than c. 1100 Ma. Localities of samples in Auli and Eidsvoll analysed in this study are shown. Age intervals in the legend rounded in 5 Ma intervals.

--------------------
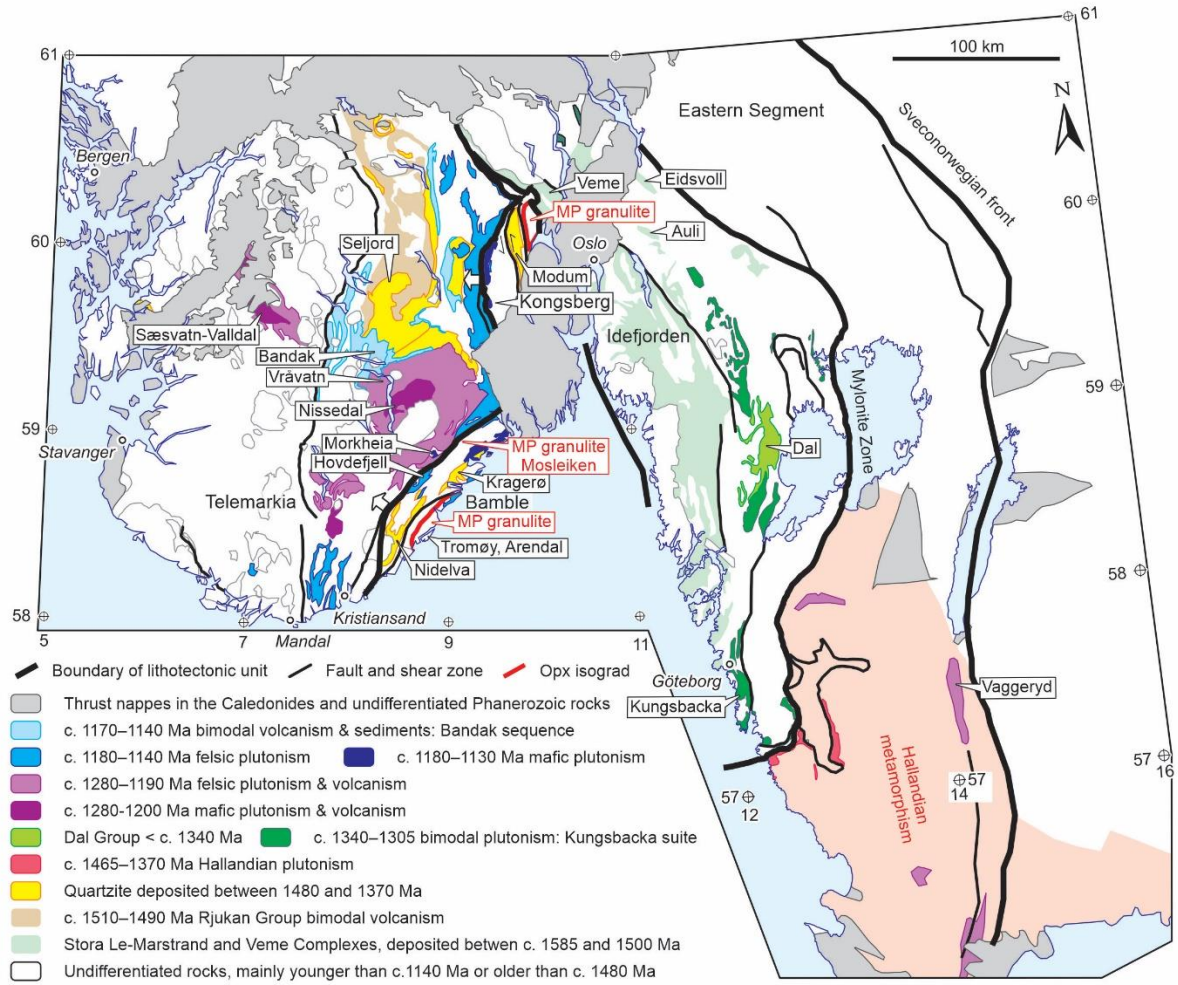
**Figure 6.** Sketch map of the Sveconorwegian orogen, with emphasis on pre- and early-
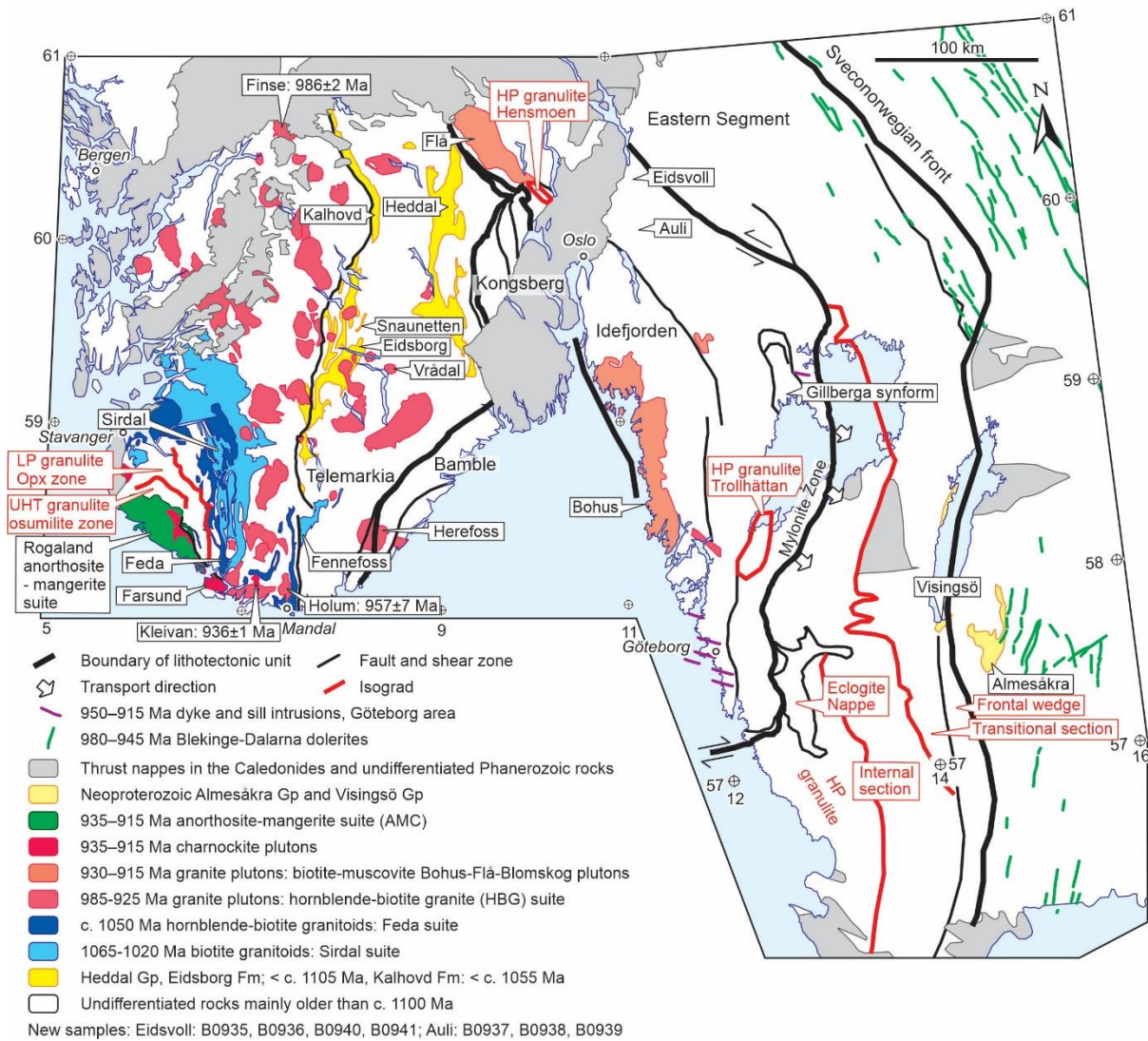
Sveconorwegian events and rocks.

--------------------
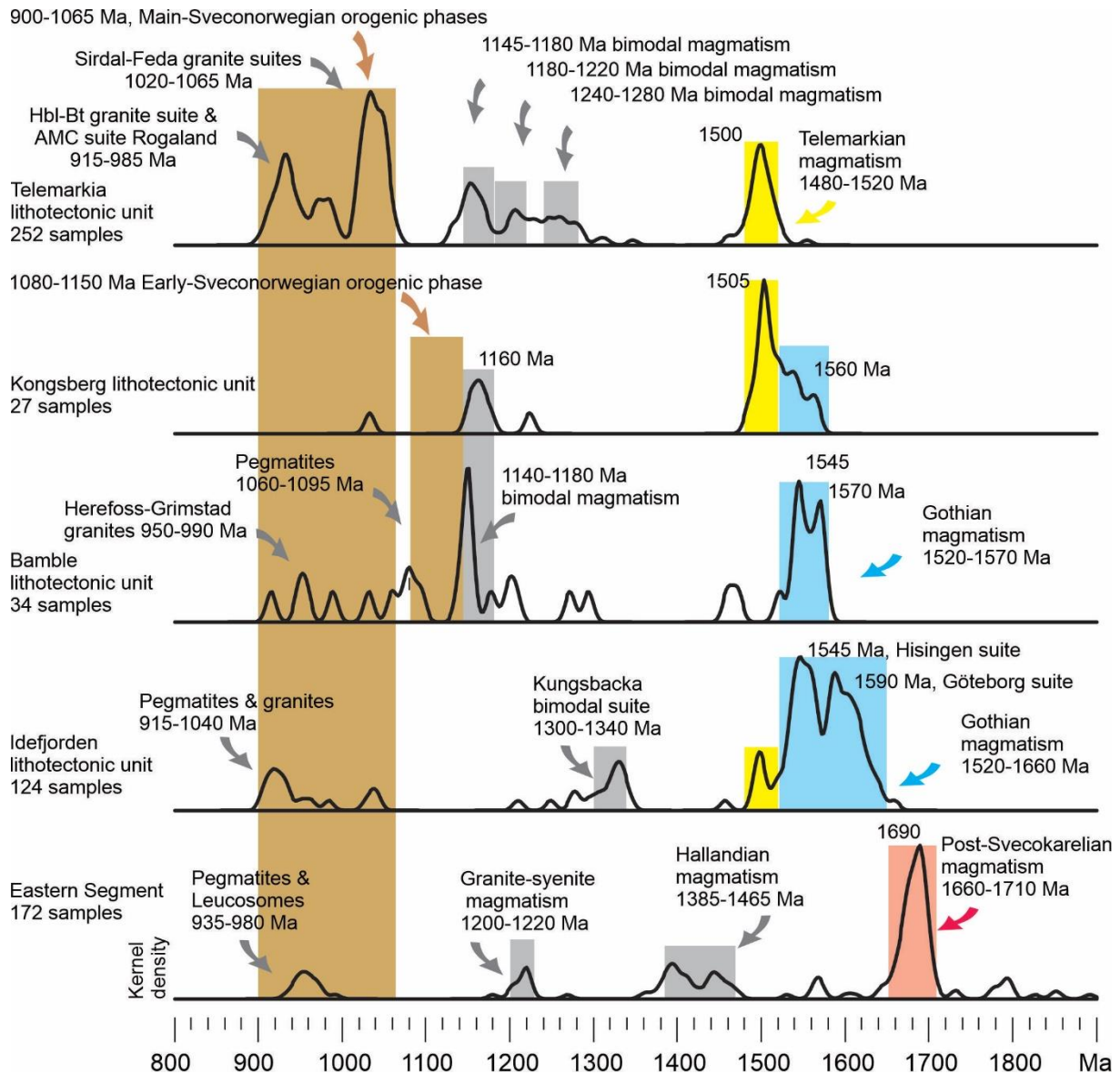
**Figure 7.** Kernel density estimators summarizing the geochronology of magmatic rocks in the

five lithotectonic units of the Sveconorwegian orogen, on a compilation of published data.

The plots are generated with "DensityPlotter" (Vermeesch, 2012) (each published age is

entered as one value, with a bandwidth of 6 Ma; the height of the five curves is identical and

normalized to the one of the largest peak). The compilation is provided in the supplementary

material, with referencing.

--------------------

312

**Figure 8.** Hafnium isotopic composition of magmatic rocks in the Sveconorwegian orogen

and Fennoscandia foreland, expressed as $\varepsilon_{Hf}$ (initial value) as a function of intrusion age.

Interpretations of the distribution of data are discussed in the text. The five lithotectonic units

are shown with distinct colours and summarized by an evolution vector. The Oaxaquia

lithotectonic unit (Mexico) and the inliers in the Andes of Colombia are shown for

comparison. Each symbol represents the average value for one sample, of the isotopic
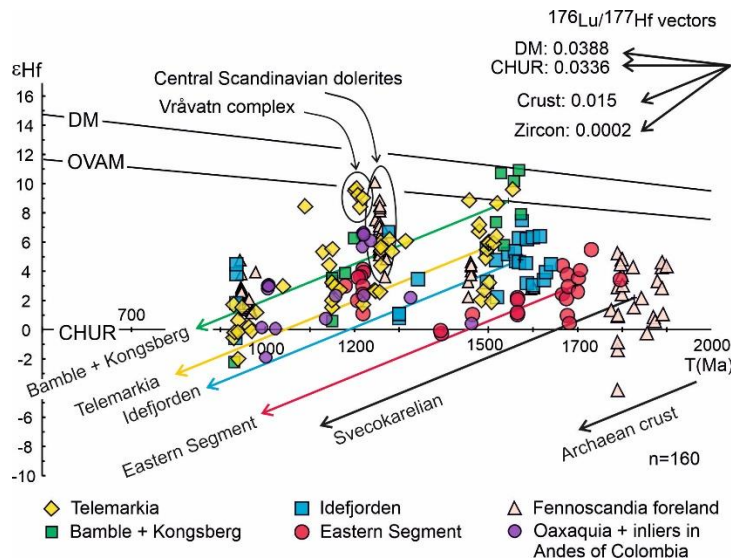
composition of several analyses of zircon or baddeleyite or of one whole-rock analysis (only a

few samples), at the recommended time of intrusion (zircon or baddeleyite U–Pb age). Total

of 220 samples. Sources of data: Sveconorwegian orogen and foreland: Andersen et al. (2009;

2002b; 2007), Lamminen et al. (2011) , Pedersen et al. (2009), Petersson et al. (2015a;

2015b), Roberts et al. (2013); Söderlund et al. (2005); Oaxaquia and inliers in the Andes of

Colombia: Ibanez-Mejia et al. (2015), Weber et al. (2010); DM: depleted mantle (Griffin et

al., 2000); OVAM: oceanic volcanic arc mantle (Dhuime et al., 2011); CHUR: chondritic

reservoir (Bouvier et al., 2008). The top right inset shows the $^{176}Lu/^{177}Hf$ ratio and evolution

vectors of isotopic reservoirs and typical zircon.

--------------------

## 3 Geology of the Sveconorwegian orogen

330    The geology of the Sveconorwegian orogen is reviewed below from east to west, using the

331    nomenclature summarized in Table 1 and the maps of Fig. 2, Fig. 4, Fig. 5 and Fig. 6. A

332    compilation of the geochronology of magmatic rocks is provided in Fig. 7, and a compilation

333    of Lu–Hf isotopic data in Fig. 8.

### 334    *3.1    Fennoscandian foreland*

335    The Fennoscandian foreland of the Sveconorwegian orogen (Fig. 2) comprises mainly

336    metamorphosed Paleoproterozoic magmatic rocks (plutonic and volcanic rocks) and

337    siliciclastic sedimentary rocks, dating back to between c. 1960 Ma and 1740 Ma (Bergman et

338    al., 2008; Korja et al., 2006; Lahtinen et al., 2009; Stephens, 2020). These rocks were

339    assembled during the accretionary Svecokarelian orogeny. They were unconformably overlain

340    and crosscut by post-Svecokarelian volcanic and plutonic complexes formed between c. 1710

341    and 1680 Ma (Appelquist et al., 2011; Brander et al., 2012; Högdahl et al., 2004; Ripa and

342    Stephens, 2020a). These rocks are attributed in the literature to the Phase 2 of the

343    Transcandinavian Igneous Belt and are little deformed to undeformed. They are interpreted to

344    have formed in a supra-subduction geodynamic setting after the Svecokarelian orogeny.

345    Younger Mesoproterozoic magmatic rocks intruded this basement, including granite plutons

346    (1530–1220 Ma ; Andersson et al., 2002b; Brander and Söderlund, 2009; Cecys and Benn,

347    2007; Johansson et al., 2016), dolerites (c. 1460 Ma; Söderlund et al., 2005), and the so-called

348    Central Scandinavian dolerites ($1271 \pm 1$ to $1246 \pm 2$ Ma; Brander et al., 2011; Ripa and

349    Stephens, 2020c; Söderlund et al., 2006).

350    The c. 1 km thick unconformable Jotnian sandstone was deposited in a gentle continental

351    sag basin between c. 1580 Ma and 1270 Ma and it is not deformed (Lundmark and

352    Lamminen, 2016; Ripa and Stephens, 2020b). The southernmost part of the Fennoscandian

353    foreland was reworked during the Hallandian orogenic event between 1465 and 1385 Ma

354    (Fig. 6) (Bogdanova et al., 2008; Brander and Söderlund, 2009; Ulmius et al., 2015; Wahlgren

355    and Stephens, 2020).

356       Sveconorwegian-related brittle deformation reached far into the Fennoscandian foreland

357    (Andréasson and Rodhe, 1994; Elminen et al., 2018; Mattila and Viola, 2014; Saintot et al.,

358    2011; Viola et al., 2009; Viola et al., 2013). The Blekinge-Dalarna dolerites form a weakly

359    arcuate N-S trending dyke swarm parallel to the Sveconorwegian front (Fig. 4; Fig. 5). They

360    intruded between $978 \pm 2$ and $946 \pm 1$ Ma, in the easternmost part of the Sveconorwegian

361    orogen and its foreland (Gong et al., 2018; Ripa and Stephens, 2020d; Söderlund et al., 2005).

362    The c. 1200 m thick, sandstone dominated, Almesåkra Group represents possible remnants of

363    a Sveconorwegian fold-and-thrust belt, to the east of the Sveconorwegian front (Fig. 5) (Ripa

364    and Stephens, 2020d; Rodhe, 1987). Locally preserved peperitic contacts between the

365    Blekinge-Dalarna dolerites and these sediments suggest that the sandstone was

366    unconsolidated during intrusion of the dolerites and therefore that the two rock types are

367    broadly coeval.

368       The Neoproterozoic, c. 1400 m thick, microfossil-bearing, Visingsö Group is exposed

369    along the Sveconorwegian front in Sweden (Fig. 5). Its deposition is bracketed between $886 \pm$

370    9 Ma (detrital zircon U–Pb data) and c. 740 Ma (biostratigraphy). It can be considered as the

371    infill of a post-Sveconorwegian, fault-controlled basin (Loron and Moczydłowska, 2018;

372    Moczydłowska et al., 2018; Pulsipher and Dehler, 2019; Wickström and Stephens, 2020).
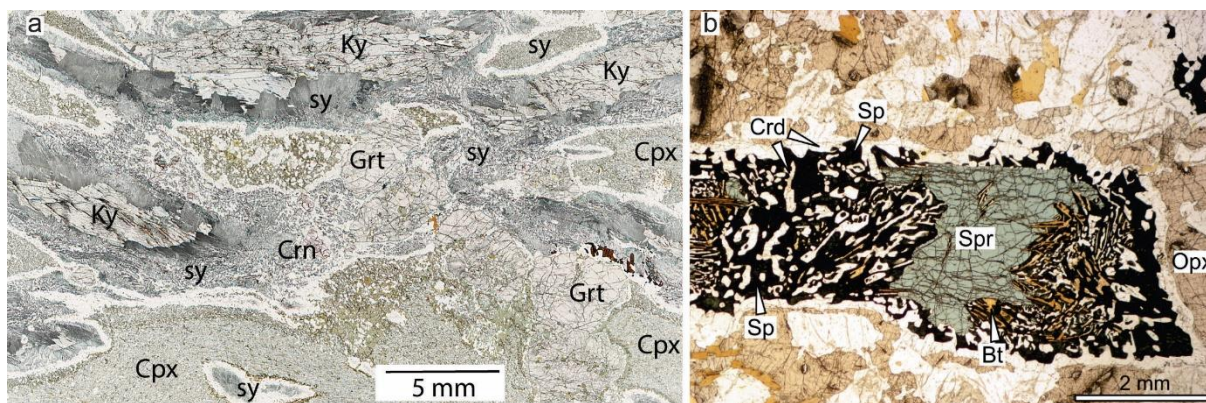
373    -------------------

**Figure 9.** Microphotographs of thin sections showing the contrast between high-pressure (eclogite-facies) and ultrahigh temperature (granulite-facies) metamorphism, east and west of the Sveconorwegian orogen, respectively, at c. 1000 Ma. (a) Kyanite-bearing (retro)eclogite from the eclogite-bearing nappe in the Eastern Segment (Möller and Andersson, 2018). The thin section shows a partly preserved peak eclogite-facies assemblage of garnet (Grt) + omphacite (Cpx) + kyanite (Ky) + amphibole + rutile (1.8 GPa - 870°C - 988 ± 6 Ma) breaking down into a symplectitic (sy) assemblage during isothermal decompression. Symplectites (sy) include a sapphirine + corundum + anorthite reaction rim around kyanite, an orthopyroxene + plagioclase + amphibole reaction rim around clinopyroxene, and plagioclase expulsion symplectite in former omphacite (Cpx). Garnet preserves a prograde (pre-eclogite-facies) zoning, and the rock shows evidence for a hairpin P-T path (Tual et al., 2017). (b) Sapphirine + orthopyroxene granulite from the Ivesdal locality, in the ultra-high temperature (UHT) zone of Rogaland, in the Telemarkia lithotectonic unit (Laurent et al., 2018b). The thin section shows the peak assemblage of sapphirine (Spr) mantled by orthopyroxene (Opx) (0.6 GPa - 920°C - 1029 ± 9 to 1006 ± 8 Ma) breaking down into an assemblage of cordierite (Crd) + hercynite (Sp) with additional biotite (Bt) (4.5 GPa – 900°C) giving evidence for a clockwise P-T path.

--------------------

### 3.2   *Eastern Segment*

394     *3.2.1    Svecokarelian and post-Svecokarelian evolution*

395     The Eastern Segment is a 60 to 120 km wide, N–S trending lithotectonic unit mainly

396     consisting of granitic to quartz-monzonitic orthogneiss (Fig. 2) (Berthelsen, 1980; Möller and

397     Andersson, 2018; Stephens and Wahlgren, 2020a). The protoliths formed between c. 1900

398     and 1660 Ma, with a strong frequency maximum of crystallization ages between 1710 and

399     1660 Ma (Fig. 7). They have an alkali-calcic geochemical composition and are characterized

400     by a mildly positive $\varepsilon_{Hf}$ and $\varepsilon_{Nd}$ isotopic signature (average $\varepsilon_{Hf} = + 3.0$ at 1700 Ma; Fig. 8)

401     (Appelquist et al., 2011; Appelquist et al., 2008; Brander et al., 2012; Gorbatschev and

402     Bogdanova, 2006; Petersson et al., 2015a; Söderlund et al., 1999; Söderlund et al., 2002;

403     Stephens and Wahlgren, 2020a). They represent the western continuation of the

404     Paleoproterozoic crust exposed in the foreland of the Sveconorwegian orogen, especially the

405     post-Svecokarelian, 1710–1680 Ma, magmatic rocks exposed just east of the Sveconorwegian

406     front (Petersson et al., 2015a; Ripa and Stephens, 2020a; Stephens and Wahlgren, 2020a).

407     They were presumably formed in the same geodynamic setting along the same active

408     continental margin.

409     *3.2.2    Hallandian and pre-Sveconorwegian evolution*

410     After an event of mafic magmatism around 1565 Ma (Beckman et al., 2017; Söderlund et al.,

411     2004; Söderlund et al., 2005), the southern part of the Eastern Segment and the

412     Sveconorwegian foreland were together affected by the Hallandian orogeny (Fig. 6; Fig. 7).

413     The Hallandian orogeny involved low-pressure amphibolite- to granulite-facies

414     metamorphism, migmatitization and deformation between c. 1465 and 1385 Ma (Brander et

415     al., 2012; Möller et al., 2007; Piñán-Llamas et al., 2015; Söderlund et al., 2002; Ulmius et al.,

416     2015), and was accompanied by magmatism during the same time interval (Fig. 7) (Åhäll et

417     al., 1997; Andersson et al., 1999; Brander and Söderlund, 2009; Cecys et al., 2002;

418     Christoffel et al., 1999; Möller et al., 2015; Ulmius et al., 2015). The final stage of Hallandian

419 magmatism includes a suite of charnockite-mangerite, granite and anorthosite plutons formed

420 between c. 1400 and 1380 Ma (Åhäll et al., 1997; Christoffel et al., 1999; Harlov et al., 2013;

421 Möller et al., 2015). The Hallandian orogeny may have involved subduction along the

422 southern margin of Baltica and may record a change in the configuration of subduction zones

423 around Baltica, from E-dipping before 1480 Ma to N-dipping after 1465 Ma (Pisarevsky et

424 al., 2014; Roberts and Slagstad, 2015; Stephens and Wahlgren, 2020b; Ulmius et al., 2015).

425 Post-Hallandian bimodal plutonism took place between 1225 and 1180 Ma, including

426 dolerites (Protogine zone dolerites) and syenitic to granitic plutons (e.g. the Vaggeryd syenite;

427 Fig. 6) (Larsson and Söderlund, 2005; Petersson et al., 2015a; Söderlund and Ask, 2006;

428 Söderlund et al., 2005). These rocks are characterized by a supra-chondritic (radiogenic) $\varepsilon_{Hf}$

429 isotopic signature ($+1.2 < \varepsilon_{Hf} < +6.6$) implying an influx of depleted mantle derived magmas

430 along the Sveconorwegian front (Fig. 8) (Petersson et al., 2015a; Söderlund et al., 2005).

431 *3.2.3 Sveconorwegian orogeny*

432 The Sveconorwegian metamorphic grade in the Eastern Segment increases towards the WSW

433 (Fig. 5) (Johansson et al., 1991; Möller and Andersson, 2018; Möller et al., 2015; Piñán-

434 Llamas et al., 2015). Four zones of distinct metamorphic and structural reworking can be

435 defined from east to west: (i) a frontal wedge, (ii) a transitional section, (iii) an internal

436 section and (iv) an eclogite-bearing ductile nappe (Möller and Andersson, 2018; Möller et al.,

437 2015).

438 The frontal wedge (i) is a zone of non-penetrative Sveconorwegian deformation forming a

439 steep or fan-shaped structure in cross section that narrows and steepens towards the south

440 (Möller and Andersson, 2018; Stephens and Wahlgren, 2020a; Wahlgren et al., 1994). The

441 zone comprises a network of thin (<100 m), N–S trending, steeply dipping, greenschist- to

442 amphibolite-facies ductile shear zones with mainly western-block-up kinematics (Andréasson

443 and Dallmeyer, 1995; Brander et al., 2012; Gorbatschev and Bogdanova, 2006; Söderlund et

444    al., 2004; Wahlgren et al., 1994). The frontal wedge is bound in the east by the

445    Sveconorwegian front, which in the north is a system of discontinuous west dipping shear

446    zones with reverse top-to-east sense of shear (Wahlgren et al., 1994). In the northernmost part

447    of the Eastern Segment in Norway, the frontal wedge is poorly documented.

448        The transitional section (ii) exhibits a near-penetrative amphibolite-facies overprint, with

449    little evidence for partial melting (Beckman et al., 2017; Möller and Andersson, 2018;

450    Söderlund et al., 1999). The internal section (iii) is characterized by upper-amphibolite-facies

451    conditions increasing westwards to high-pressure granulite-facies conditions (1.1 GPa -

452    850°C; Fig. 5). This metamorphic evolution caused widespread migmatitization, transposition

453    leading to mafic and felsic gneissic layering (banding), dynamic recrystallization of original

454    magmatic textures, as well as reworking of previous Hallandian structures, where present

455    (Andersson et al., 1999; Connelly et al., 1996; Hansen et al., 2015; Möller et al., 2015; Möller

456    et al., 2007; Piñán-Llamas et al., 2015). The regional aeromagnetic map (Geological Survey

457    of Sweden) unveils prominent, regional scale fold interference patterns, with E-W trending

458    and gently-plunging fold axes and trains of N–S trending folds (Möller et al., 2007; Stephens

459    and Wahlgren, 2020a; Viola et al., 2011). Several generations of folds can be recognised (F1

460    to F4), including km-scale asymmetric to recumbent folds and late upright folds (Möller and

461    Andersson, 2018; Möller et al., 2015 ; Piñán-Llamas et al., 2015; Tual et al., 2015). These

462    different generations record continued deformation under high-grade metamorphic conditions.

463        The eclogite-bearing ductile nappe (iv) is hosted in the innermost section of the Eastern

464    Segment as an E-vergent ductile nappe, folded into a c. 50 x 75 km large recumbent fold (Fig.

465    5) (Möller et al., 2015; Tual et al., 2015). It is well defined on the regional aeromagnetic map

466    and bordered (on the southern and eastern flanks) by a sheet of c. 1380 Ma granite (Fig. 6).

467    The ductile nappe hosts retro-eclogite bodies up to 2 km in length (Möller, 1998, 1999;

468    Möller and Andersson, 2018; Möller et al., 2015; Tual et al., 2015). The retro-eclogite bodies

469    are layered mafic rocks, including two characteristic varieties, a Mg-Al-rich kyanite-bearing

470    variety and a Fe-Ti-rich variety. Retro-eclogites preserve prograde growth zoning of garnet

471    and show widespread retrogression of omphacite and kyanite into granulite-facies

472    symplectites (clinopyroxene + plagioclase, orthopyroxene + plagioclase, and anorthite +

473    sapphirine + corundum) (Fig. 9 a). They constrain a narrow (hairpin) clockwise pressure-

474    temperature path at high temperature. Eclogite-facies peak conditions of 1.65–1.9 GPa and

475    850–900°C were followed by near-isothermal decompression (Tual et al., 2017). Eclogite

476    boudins are hosted in strongly deformed, partly migmatitic, gneisses characterized by a

477    pervasive foliation, E–W stretching lineation, and S- to E-vergent folds (Möller et al., 2015;

478    Tual et al., 2015). Two post-eclogite-facies deformation phases (D1-D2) are described as

479    successively documenting an early stage of exhumation and east-directed transport of the

480    ductile nappe, lubricated by partial melts.

481       A zircon U–Pb age determination from an eclogite sample defines a maximum age for

482    eclogite-facies metamorphism of 988 ± 6 Ma (Möller et al., 2015). Zircon in felsic and mafic

483    gneiss, migmatite and syn-kinematic granite in the entire Eastern Segment, including the

484    eclogite-bearing nappe, yields a consistent age interval between 978 ± 7 and 961 ± 6 Ma for

485    amphibolite- to granulite-facies metamorphism, deformation and partial melting (Andersson

486    et al., 2002a; Beckman et al., 2017; Hansen et al., 2015; Möller et al., 2015; Möller et al.,

487    2007; Piñán-Llamas et al., 2015; Söderlund et al., 2002). Cross-cutting pegmatite dykes

488    intruded between 961 ± 13 and 934 ± 6 Ma (Andersson et al., 1999; Möller et al., 2007;

489    Möller and Söderlund, 1997; Söderlund et al., 2008b; Söderlund et al., 2002). Titanite U–Pb

490    ages range from c. 976 ± 4 to 923 ± 3 Ma, with the oldest age recorded in the northern part of

491    the transitional section and the youngest ages in the internal section (Connelly et al., 1996;

492    Johansson et al., 2001; Söderlund et al., 1999; Wang et al., 1998). Hornblende and biotite

493    $^{40}Ar/^{39}Ar$ plateau ages in the internal section are interpreted to date regional cooling between

494  c. 530 and 330°C between c. 901 ± 2 and 893 ± 3 Ma (Ulmius et al., 2018). Biotite and

495  muscovite $^{40}$Ar/$^{39}$Ar plateau ages collected in the frontal wedge range from 930 ± 6 to 882 ± 2

496  Ma (Andréasson and Dallmeyer, 1995; Page et al., 1996a; Ulmius et al., 2018). The youngest

497  ages are recorded in the southernmost exposed section of the orogen. These ages either record

498  discrete events of (re)crystallization or cooling after deformation by shear zones at the front of

499  the orogen (Andréasson and Dallmeyer, 1995; Page et al., 1996a; Ulmius et al., 2018).

500  --------------------

501
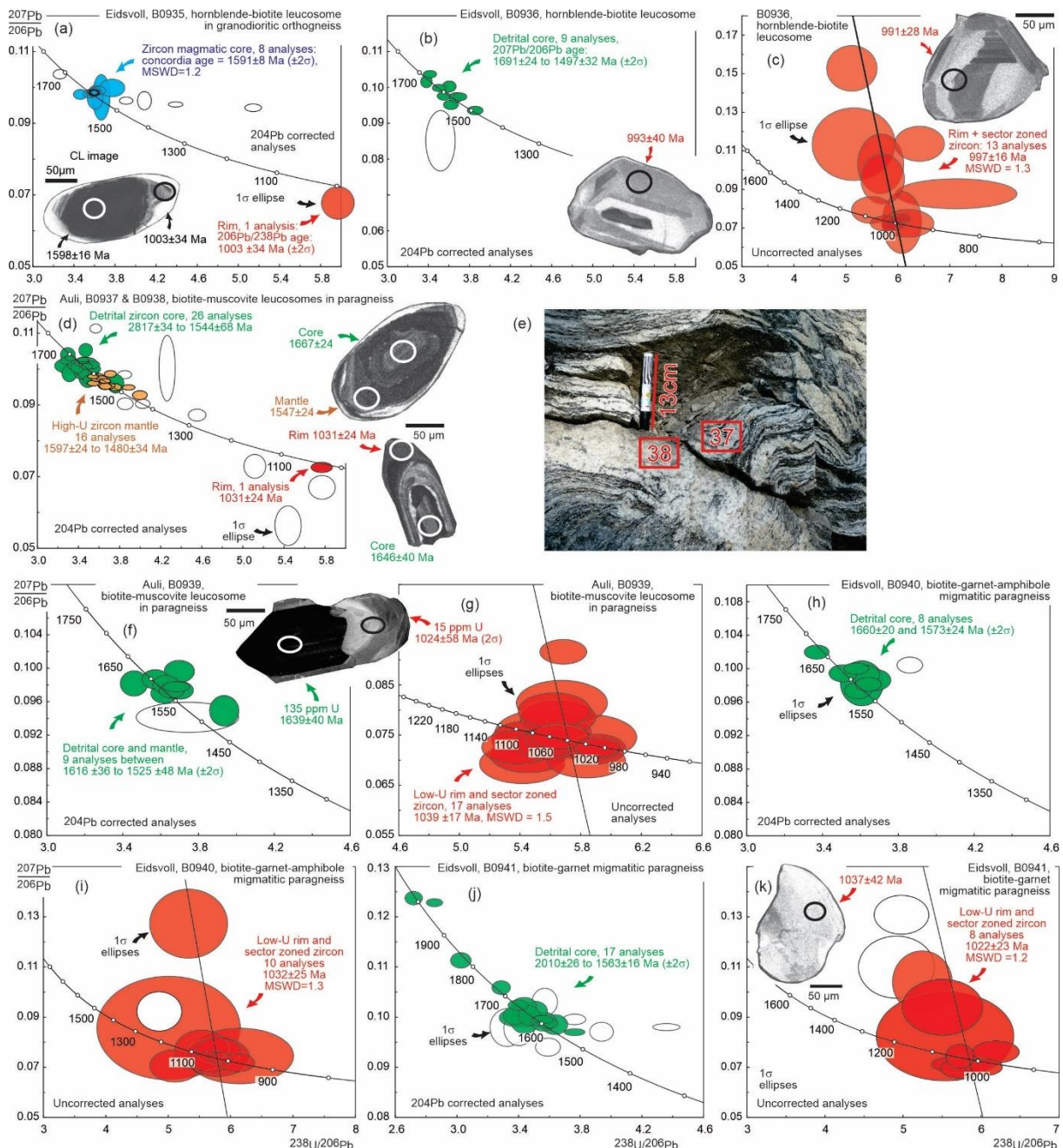
502 **Figure 10**. New geochronological data of migmatitic gneisses in the Eidsvoll-Auli area,

503 Idefjorden lithotectonic unit (Fig. 5). (a–k) Tera-Wasserburg concordia diagrams with zircon

504 SIMS U–Pb analyses and a selection of CL images of zircon with position of analyses. Blue

505 ellipses for magmatic zircon cores, green ellipses for detrital zircon cores, and red ellipses for

506 low-U sector zoned zircon and zircon rims attributed to migmatitization. One sigma error

507 ellipses. (e) Photo of outcrop where two samples represent two generations of leucosomes,

508 with B0938 crosscutting B0937. Interpretation: migmatites from the five studied localities are

509 characterized by abundant, interconnected leucosomes (stromatic texture) parallel to the

510 gneissic foliation. Zircon contains an inherited core (magmatic or detrital), a CL-dark mantle

511 and a CL-bright rim. Analyses of the mantle overlap with those of the core and define a

512 significant spread in each sample. The spread of apparent ages can be interpreted to represent

513 partial recrystallization of the core during partial melting. Newly formed CL-bright rims or

514 large crystals with oscillatory to weakly sector zoning reflect crystallization of zircon related

515 to migmatitization (Harley et al., 2007; Kelsey et al., 2008; Rubatto et al., 2009) between

516 $1039 \pm 17$ and $997 \pm 16$ Ma (a, c, g, i, k). In this c. 40 Myr time interval, the biotite-muscovite

517 and biotite-garnet leucosomes range from $1039 \pm 17$ to $1022 \pm 23$ Ma (d, g, i, k), while the

518 hornblende-biotite-bearing leucosomes are marginally to significantly younger with ages of

519 $1003 \pm 34$ and $997 \pm 16$ Ma (a, c). This difference suggests that muscovite and biotite

520 dehydration melting took place before amphibole dehydration melting, in what can be

521 interpreted as reflecting increasing temperature or isothermal decompression.

522 --------------------

523 **Table 2.** Summary of sampling and zircon U-Pb data for migmatitic gneisses, Eidsvoll-Auli

524 area, Idefjorden lithotectonic unit.

525 --------------------

526 *3.3   Idefjorden lithotectonic unit*

527    The Idefjorden lithotectonic unit is a c. 140 km wide unit exposed west of the Eastern

528    Segment on either side of the Permian Oslo Rift (Fig. 2, Fig. 5) (Åhäll and Connelly, 2008;

529    Åhäll and Gower, 1997; Bergström et al., 2020; Bingen et al., 2001; Park et al., 1991; Viola et

530    al., 2011). It is bounded in the east by the 450 km long, west dipping, Mylonite Zone.

531    *3.3.1    Gothian and pre-Sveconorwegian evolution*

532    The Idefjorden lithotectonic unit is made up of plutonic and volcanic rocks formed during the

533    Gothian accretionary orogeny mainly between 1660 and 1520 Ma and associated with

534    metasedimentary rocks (Fig. 7) (Åhäll and Connelly, 2008; Åhäll and Larson, 2000; Ahlin et

535    al., 2006; Andersen et al., 2004a; Bergström et al., 2020; Bingen et al., 2005; Brewer et al.,

536    1998; Graversen and Pedersen, 1999). From east to west, three complexes (called formations

537    or belts in the literature) are described as younging towards the west (Åhäll and Connelly,

538    2008; Brewer et al., 1998): (i) the 1660–1640 Ma metavolcanic Horred Complex, (ii) the

539    1630–1590 Ma metavolcanic and metasedimentary Åmål Complex associated with the

540    Göteborg granite suite, and (iii) the 1590–1520 Ma metasedimentary and metavolcanic Stora

541    Le-Marstrand Complex, associated with the 1580–1520 Ma plutonic Hisingen Suite. The

542    Stora Le-Marstrand Complex, exposed east of the Oslo Rift, correlates with the Veme

543    Complex west of the Oslo Rift (Fig. 6) (Bingen et al., 2001). The Stora Le-Marstrand and

544    Veme complexes comprise several metasedimentary successions (Åhäll and Connelly, 2008),

545    consisting of thick packages of turbiditic psammite and greywacke metamorphosed under

546    amphibolite-facies conditions (Bingen et al., 2001). Sedimentation started before c. 1585 Ma

547    (metagreywacke xenoliths in a 1584 ± 7 Ma granite pluton) and continued to after c. 1500 Ma

548    (detrital zircon geochronology in 12 samples) (Åhäll and Connelly, 2008; Åhäll et al., 1998;

549    Andersen et al., 2004a; Bingen et al., 2001; Bingen and Viola, 2018). The paragneisses

550    analysed in this study just east of the Oslo Rift (Eidsvoll and Auli; Fig. 5; Fig. 6; Fig. 10) are

551    attributed to the Stora Le-Marstrand Complex.

552    The c. 1660–1520 Ma (Gothian) magmatic suites (Fig. 7) are characterized by low- to

553    medium-K calc-alkaline geochemical compositions, with supra-chondritic Hf and Nd isotopic

554    signature (average $\varepsilon_{Hf} = + 4.8$ in the Idefjorden lithotectonic unit at 1570 Ma; Fig. 8),

555    reflecting continental and oceanic volcanic arc magmatism (Andersen et al., 2004a; Andersen

556    et al., 2002b; Bergström et al., 2020; Brewer et al., 1998; Petersson et al., 2015b). Metabasalts

557    interlayered in the Stora Le-Marstrand rocks are tholeiitic and interpreted as oceanic back-arc

558    magmatism (Brewer et al., 1998).

559    The c. 1660–1520 Ma rocks were assembled during the Gothian accretionary orogenic

560    event (Åhäll and Connelly, 2008; Andersen et al., 2004a; Petersson et al., 2015b; Roberts and

561    Slagstad, 2015). Convincing evidence for Gothian regional deformation and metamorphism

562    includes crosscutting relationships (folded xenoliths in a 1584 ± 7 Ma pluton) and U–Pb

563    geochronological data in zircon and monazite ranging from 1546 ± 5 to 1539 ± 8 Ma from a

564    few localities in the Veme and Stora Le-Marstrand complexes (Åhäll and Connelly, 1998,

565    2008; Bingen et al., 2008b; Bingen and Viola, 2018; Connelly and Åhäll, 1996).

566    The 1660–1520 Ma rocks are intruded by the 1457 ± 6 Ma, N–S trending Orust tholeiitic

567    dolerite dykes (Åhäll and Connelly, 1998), and the 1340–1305 Ma bimodal Kungsbacka suite

568    (Fig. 6) (Austin Hegardt et al., 2007). The Dal Group (or Dalsland Group) is a c. 2 km thick

569    succession of low-grade clastic sedimentary rocks and tholeiitic basalt, exposed in a syncline

570    structure, overlying (and therefore younger than) the Kungsbacka suite (Fig. 6) (Brewer et al.,

571    2002). The Dal Group is poorly characterized. However, it may provide critical evidence for

572    the tectonic evolution of the Idefjorden lithotectonic unit before the Sveconorwegian orogeny

573    (Brewer et al., 2002) and therefore would warrant new investigations.

574    *3.3.2   Sveconorwegian orogeny*

575    In the Idefjorden lithotectonic unit, the Sveconorwegian deformation is associated with a N–S

576    to NW–SE structural grain and has variable strain intensity. Several shear zones, including the

577     prominent Ørje and Göta Älv shear zones (Fig. 2), are parallel to this structural grain

578     (Bergström et al., 2020; Park et al., 1991; Viola et al., 2011; Wahlgren et al., 2015).

579     Metamorphism ranges from greenschist- to granulite-facies. The low-grade rocks are exposed

580     in syncline structures (Fig. 4). For example, between the Göta Älv shear zone and the

581     Mylonite Zone, the Gillberga syncline hosts the Glaskogen low-grade complex, bounded by

582     low-angle shear zones (Lindh et al., 1998), and the Åmal volcanic rocks (1614 ± 7 Ma),

583     known for good preservation of primary volcanic structures (Lundqvist and Skiöld, 1993). In

584     the amphibolite-facies gneiss complexes east and west of the Göta-Älv shear zone, garnet

585     amphibolites provide pressure-temperatures estimates of 0.9 to 1.2 GPa – 730 to 790 °C (3

586     samples; Austin Hegardt, 2010). High-pressure garnet–clinopyroxene-bearing granulite-facies

587     assemblages are reported from metadolerite dykes hosted in amphibolite-facies gneisses from

588     several localities east of the Göta-Älv shear zone (Trollhättan, Fig. 5) (Söderlund et al.,

589     2008a). Geothermobarometry coupled with zircon U–Pb data and mineral isochron data from

590     two dykes indicate conditions of c. 1.5 GPa – 740 °C at 1046 ± 6 Ma and c. 1.0 GPa – 700 °C

591     at 1026 ± 5 Ma (Söderlund et al., 2008a). In the Veme Complex, west of the Oslo rift in

592     Norway, a kyanite-garnet-rutile paragneiss hosting clinopyroxene-garnet-plagioclase-rutile

593     mafic boudins also records high-pressure granulite-facies conditions, with pressure-

594     temperature estimates of 1.2 GPa – 780 °C (Hensmoen, Fig. 5) (Bingen et al., 2008b).

595     Monazite in the kyanite-rutile-gneiss records peak metamorphism at 1052 ± 4 Ma (Bingen et

596     al., 2008b).

597         East of the Oslo rift in Norway, amphibolite-facies metamorphism is associated with a

598     foliation dipping unimodally to the NE and with folds verging to the W to SW (Viola et al.,

599     2011). The timing of this metamorphism is provided by the new U–Pb data from zircon rims

600     in migmatitic samples (Eidsvoll–Auli area, Fig. 5, Fig. 10, Table 2). The dates range from

601     1039 ± 17 to 997 ± 16 Ma, in seven samples affected by both muscovite- biotite- and

602   amphibole-dehydration melting. The dates are interpreted to record crystallization of the

603   leucosomes. This interval overlaps with published zircon and titanite U–Pb data and a Sm-Nd

604   mineral isochron interpreted to record high-grade metamorphism between $1043 \pm 11$ Ma and

605   $1024 \pm 9$ (7 samples ; Åhäll et al., 1998; Austin Hegardt, 2010; Austin Hegardt et al., 2007;

606   Bingen et al., 2008b), and also with intrusion of rare-mineral pegmatites between $1041 \pm 2$

607   and $984 \pm 6$ Ma (Romer and Smeds, 1996).

608   Several mafic to felsic magmatic intrusions, with a consistent WNW–ESE trend and dated

609   between $951 \pm 7$ and $915 \pm 1$ Ma, crosscut the regional amphibolite-facies ductile fabric in the

610   coastal area of Sweden (Årebäck et al., 2008; Hellström et al., 2004; Scherstén et al., 2000;

611   Wahlgren et al., 2015). These include a lamprophyre dyke ($915 \pm 1$ Ma) (Wahlgren et al.,

612   2015) and the small Hakefjorden norite-anorthosite complex ($916 \pm 11$ Ma), carrying

613   evidence for extensive fractional crystallization (Årebäck and Stigh, 2000). The Flå and

614   Bohus biotite-muscovite granite plutons intruded between $932 \pm 8$ and $922 \pm 3$ Ma, as large

615   tabular bodies, in pressure conditions of c. 0.4 GPa (Fig. 5) (Eliasson et al., 2003; Eliasson

616   and Schöberg, 1991; Lamminen et al., 2011). A final batch of rare-mineral pegmatite formed

617   between $909 \pm 1$ and $906 \pm 6$ Ma (Müller et al., 2017).

618   *3.3.3   The Mylonite Zone*

619   The Mylonite Zone is a generally west dipping shear zone juxtaposing the Eastern Segment

620   and Idefjorden lithotectonic unit. It is several km thick, continuous for some 450 km and

621   characterized by a widespread greenschist- to upper amphibolite-facies mylonitic fabric (Fig.

622   2, Fig. 5) (Andersson et al., 2002a; Bergström et al., 2020; Möller et al., 2015; Park et al.,

623   1991; Stephens et al., 1996; Viola and Henderson, 2010; Viola et al., 2011). It possibly roots

624   in the mantle (EUGENO-S-working-group, 1988).

625   The Mylonite Zone is interpreted as a Sveconorwegian mid-crustal thrust zone placing the

626   Idefjorden lithotectonic unit on top of the Eastern Segment, with an overall southeastward

627    transport direction oblique to the orogen (Stephens et al., 1996; Viola and Henderson, 2010;

628    Viola et al., 2011). Shear zones inside the Idefjorden lithotectonic unit, including the Ørje and

629    Göta Älv shear zones (Fig. 2) are similarly interpreted as transpressional thrust zones (Park et

630    al., 1991; Viola et al., 2011; Wahlgren et al., 2015).

631    In the north (in Norway), the Mylonite Zone trends NW–SE and has a steep attitude with

632    sinistral strike-slip kinematics. This segment has been interpreted as the sinistral lateral ramp

633    to the thrust frontal ramp farther to the southeast. The frontal ramp dips gently to moderately

634    to the west and bears a NW plunging stretching lineation associated with dominant top-to-

635    southeast reverse displacement. In the southernmost part, the shear zone turns quite abruptly

636    E–W, dipping gently to the north, and accommodating a dominant component of dextral

637    strike-slip shearing. This part is interpreted as a dextral lateral ramp of the thrust zone (Viola

638    and Henderson, 2010; Viola et al., 2011). The importance of the southernmost dextral lateral

639    ramp is downplayed by Bergström et al. (2020), who interpret the Mylonite Zone, as a whole,

640    as a sinistral transpressional thrust zone. Zircon U–Pb data in the Mylonite Zone and close

641    hanging wall and footwall record amphibolite-facies migmatitization and associated ductile

642    deformation between $980 \pm 13$ and $969 \pm 13$ Ma (Andersson et al., 2002a).

643    The Mylonite Zone was reactivated in extension with top-to-the-west kinematics along a

644    network of localized shear zones, contributing to exhumation of the Eastern Segment in the

645    footwall (Viola and Henderson, 2010; Viola et al., 2011). Muscovite and biotite $^{40}$Ar/$^{39}$Ar

646    data suggest that this deformation took place between $923 \pm 4$ and $861 \pm 5$ Ma (Viola et al.,

647    2011).

648    **3.4   Kongsberg and Bamble lithotectonic units**

649    The Bamble and Kongsberg lithotectonic units are two narrow c. 25 km wide units situated in

650    the center of the exposed Sveconorwegian orogen (Fig. 2). Kongsberg trends N–S while

651    Bamble trends NE–SW. These two lithotectonic units share a number of features, including

652    evidence for early-Sveconorwegian metamorphism (1150-1120 Ma) (Bingen et al., 2008b;

653    Bingen and Viola, 2018; Engvik et al., 2016; Knudsen et al., 1997; Nijland et al., 2014;

654    Starmer, 1985; Viola et al., 2016).

655    *3.4.1   Gothian–Telemarkian evolution*

656    Two main lithological complexes are present in the Bamble and Kongsberg lithotectonic

657    units, (i) an orthogneiss complex, referred to as Kongsberg Complex in Kongsberg and

658    Bamble Complex in Bamble, and (ii) a quartzite-dominated metasedimentary complex, called

659    Modum Complex in Kongsberg and Nidelva and Kragerø Complexes in Bamble (Fig. 6). (i)

660    The orthogneiss complex consists of penetratively deformed orthogneisses with composition

661    ranging from dioritic to tonalitic, to granitic, and more competent gabbro plutons (Holleia and

662    Blengsvatn ; Bingen and Viola, 2018; Nijland et al., 2000). The orthogneisses are interlayered

663    with comparatively heterogeneous layered gneisses (referred to as banded gneiss in the field),

664    commonly migmatitic, and generally fine-grained. The layered gneisses derive probably from

665    both volcanic and sedimentary protoliths. Thin sulfide-rich or graphite-rich schistose layers

666    are common (falhbands) (Broekmans et al., 1994; Gammon, 1966). The protoliths of the

667    orthogneisses range in age from $1575 \pm 44$ to $1460 \pm 21$ Ma, with two frequency maxima

668    around 1545 and 1505 Ma (Fig. 7) (Andersen et al., 2004a; Bingen and Viola, 2018; Engvik

669    et al., 2016). The orthogneisses have tholeiitic to low-K calc-alkaline geochemical signature,

670    typical of volcanic arc magmatism (Andersen et al., 2004a). Their Hf isotopic signature is

671    very radiogenic, with an average $\varepsilon_{Hf} = + 8.8$ ($+7 < \varepsilon_{Hf} < +11$), approaching the depleted

672    mantle reservoir at 1550 Ma (Fig. 8) (Andersen et al., 2002b). (ii) The metasedimentary

673    complexes (Fig. 6) consist of coarse quartzite, interlayered with mica schist, sillimanite gneiss

674    and sulfide-rich schist (Morton, 1971; Nijland et al., 2014; Nijland et al., 1993). They host

675    metasomatic rocks such as orthoamphibole-cordierite gneiss, talc schist, albitite, scapolitite

676    and dolomite, generally located at the interface with gabbro bodies (Dahlgren et al., 1993;

677    Engvik et al., 2014; Munz, 1990; Munz et al., 1994). Deposition of the sedimentary protoliths

678    took place after 1467 ± 33 Ma (detrital zircon U–Pb data in quartzite samples), implying that

679    they represent part of a cover to the orthogneiss basement (Åhäll et al., 1998; Bingen et al.,

680    2001).

681    *3.4.2   Pre- to early-Sveconorwegian plutonism*

682    The orthogneiss and quartzite-rich metasedimentary complexes are intruded by variably sized,

683    gabbroic plutons. These plutons are commonly zoned, with (sub)ophitic picritic gabbro in the

684    core and garnet amphibolite along the margin (Munz and Morvik, 1991). Two such gabbro

685    plutons have been dated by the Sm-Nd method at 1224 ± 15 and 1207 ± 14 Ma (Morud and

686    Vestre Dale gabbro, not represented in Fig. 7 ; deHaas et al., 2002b; Munz and Morvik,

687    1991), and two have been dated with the U–Pb method at 1164 ± 12 and 1149 ± 7 Ma

688    (Vinoren and Ringsjø; Bingen and Viola, 2018; Engvik et al., 2011). Felsic intrusive rocks are

689    quite common. They include thin gneissic units ranging in age from 1178 ± 9 to 1149 ± 8 Ma

690    (Andersen et al., 2004b; Bingen and Viola, 2018; Engvik et al., 2016), and also, in Bamble,

691    larger plutons ranging in age from 1152 ± 11 to 1140 ± 13 Ma (Gjeving, Ubergsmoen,

692    Hovdefjell-Vegårshei plutons, Fig. 6) (Bingen and Viola, 2018). These metaplutons are

693    characterized by a weakly foliated magmatic charnockite facies in the centre and a garnet-

694    bearing augen gneiss facies at the margin (Touret, 1971a, b), and therefore place a maximum

695    age bracket for the high-grade deformation and metamorphism in Bamble.

696    *3.4.3   Sveconorwegian orogeny*

697    The Sveconorwegian overprint in the Bamble and Kongsberg lithotectonic units is typified by

698    a steep to subvertical foliation, isoclinal and highly transposed folds and a penetrative tectonic

699    layering (Bingen and Viola, 2018; Slagstad et al., 2020; Starmer, 1985, 1991). These features

700    are interpreted as evidence for roughly orthogonal, syn-metamorphic shortening, oriented E–

701    W for Kongsberg and NW–SE for Bamble (Bingen and Viola, 2018). A steep stretching

702    lineation on the steep foliation planes suggests a component of near-vertical stretching. Inside

703    the Kongsberg lithotectonic unit, the N–S trending Hokksund-Solumsmo shear zone (Starmer,

704    1985) is characterized by a component of sinistral strike-slip shearing that overprinted and

705    thus postdates the orthogonal shortening (Scheiber et al., 2015).

706       Metamorphic grade increases across strike, northeastwards in Kongsberg and

707    southeastwards in Bamble. In Kongsberg, it increases from epidote-amphibolite facies to

708    upper amphibolite-facies conditions, with local occurrences of granulite-facies rocks towards

709    the northeast (Fig. 6). In Bamble, the grade increases from amphibolite-facies to granulite-

710    facies conditions towards the southeast, i.e. towards the coast (Tromøy and Hisøy islands;

711    Fig. 6) (Clough and Field, 1980; Harlov, 2000; Knudsen, 1996; Nijland et al., 2014; Nijland

712    and Maijer, 1993; Touret, 1971a). However, patches of granulite facies rocks are scattered

713    throughout the amphibolite-facies domain of Bamble (Mosleiken granulite; Fig. 6),

714    underscoring the importance of fluid activity on mineral parageneses (Engvik et al., 2016;

715    Nijland et al., 1998). The granulite-facies rocks record peak pressure-temperature values of

716    1.15 GPa and 850 °C, followed by hydration and decompression to 0.8 GPa – 740 °C (Engvik

717    et al., 2016).

718      Zircon and monazite U–Pb data constrain the peak of amphibolite- and granulite-facies

719    metamorphism between 1147 ±12 and 1122 ± 8 Ma in both the Bamble and Kongsberg

720    lithotectonic units (Bingen et al., 2008b; Bingen and Viola, 2018; Cosca et al., 1998; Engvik

721    et al., 2016; Knudsen et al., 1997). In coastal Bamble, the granulite-facies Tromøy complex

722    (Fig. 6) consists of low-K calc-alkaline enderbitic gneisses depleted in large ion-lithophile

723    elements (LILE) (Cooper and Field, 1977; Field et al., 1980; Knudsen and Andersen, 1999).

724    Zircon U–Pb data demonstrate that the protoliths formed between 1575 ± 44 and 1544 ± 14

725    Ma while the granulite facies overprint took place between 1147 ± 12 and 1132 ± 6 Ma

726    (Bingen and Viola, 2018). These data show that the volcanic arc magmatism belongs to the

727    Gothian orogenic cycle, while the granulite-facies metamorphism is early-Sveconorwegian in

728    age (Andersen et al., 2004a; Bingen et al., 2008c; Field et al., 1985).

729       Titanite U–Pb dates and a trail of monazite dates in gneisses range from 1107 ± 9 to 1091

730    ± 2 Ma (Bingen et al., 2008b; Cosca et al., 1998; deHaas et al., 2002a) while hornblende

731    $^{40}Ar/^{39}Ar$ plateau ages range from 1099 ± 3 to 1079 ± 5 Ma (Cosca et al., 1998; Cosca and

732    O'Nions, 1994). These dates are related to regional cooling and exhumation. Monazite, titanite

733    and rutile in albitite record at least two phases of fluid-rock interaction below 550 °C

734    (metasomatism), between 1104 ± 5 and 1078 ± 3 Ma (Engvik et al., 2017; Engvik et al., 2011;

735    Munz et al., 1994), while gadolinite-columbite data in pegmatite record intrusion of a small

736    batches of fluid-rich melt between 1094 ± 11 and 1082 ± 5 Ma (Müller et al., 2017; Scherer et

737    al., 2001). These data imply regional scale fluid mobility after the peak of metamorphism and

738    deformation.

739       Rare lamprophyre dykes with near vertical attitude and non-foliated chilled margins

740    crosscut at high angle the regional foliation of the host gneiss. One such dyke yields an

741    intrusion age of 1033 ± 12 Ma and thus provides both a minimum bracket for the steep, high-

742    grade fabric of the host gneiss and the age of a batch of ultrapotassic mafic magmatism

743    (Bingen and Viola, 2018). The large non-foliated Herefoss granite pluton formed at 920 +16/-

744    27 Ma (Fig. 5) (Andersen et al., 2002a).

745    *3.4.4   Kongsberg–Idefjorden boundary zone*

746    The Kongsberg–Idefjorden boundary zone is marked by a c. 500 m thick amphibolite-facies

747    shear zone made of banded gneiss of mafic composition, characterized by steeply dipping

748    foliation bearing a moderately to steeply plunging lineation (Bingen and Viola, 2018). It

749    follows the lithological contact between metagreywackes of the Veme Complex and

750    orthogneisses of the Kongsberg Complex (Viola et al., 2016).

751  *3.4.5  Kongsberg–Telemarkia boundary zone*

752  The Sokna-Saggrenda Shear Zone (Fig. 2) (Starmer, 1985) is a N–S trending, east-dipping, up

753  to 2 km thick multiphase shear zone. It is largely hosted within and along the eastern margin

754  of a > 100 km long belt of foliated granite, dated between 1170 ± 11 and 1146 ± 5 Ma (Fig. 6)

755  (Scheiber et al., 2015). This granite constitutes the footwall of the shear zone and is part the

756  Telemarkia lithotectonic unit. Three post-1170 Ma ductile deformation phases have been

757  identified in the shear zone (Scheiber et al., 2015). (i) The earliest structures accommodate

758  top-to-the-west kinematics and relate to thrusting of Kongsberg over Telemarkia. (ii) These

759  are selectively reactivated in a sinistral fashion along mylonitic to ultramylonitic shear zones.

760  The sinistral shear zones possibly record the same deformation as the N–S trending, steeply

761  dipping Hokksund-Solumsmo mylonite zones inside the Kongsberg lithotectonic unit,

762  showing evidence for sinistral transpressive shearing. (iii) Extensional top-to-the-east sense of

763  shear. A brittle zone overprinting this long-lived ductile deformation zone and traditionally

764  referred to as the "Great Friction Breccia" (Starmer, 1985) probably represents a normal fault

765  of Permian age (Larsen et al., 2008; Scheiber et al., 2015).

766  *3.4.6  Bamble–Telemarkia boundary zone*

767  The Kristiansand–Porsgrunn Shear Zone (Fig. 2) is a c. 1–2 km thick ductile to brittle shear

768  zone juxtaposing the Bamble and Telemarkia lithotectonic units. It dips moderately to the

769  southeast and is possibly connected with an offset of the Moho under the Skagerrak sea

770  (Andersson et al., 1996). The shear zone is interpreted as a top-to-the-northwest thrust, later

771  reactivated coaxially as an extensional shear zone (Henderson and Ihlen, 2004; Mulch et al.,

772  2005; Starmer, 1991). Upper greenschist- to amphibolite-facies thrust-related structures are

773  invariably northwest vergent. These structures are associated with tabular pegmatite bodies

774  (Henderson and Ihlen, 2004). The shear zone overprints the 1132 ± 3 Ma Morkheia

775  monzonite suite exposed in the Telemarkia footwall (Heaman and Smalley, 1994; Milne and

776 Starmer, 1982), and the 1140 ± 13 Ma Hovdefjell-Vegårshei metapluton exposed on the

777 Bamble hangingwall (Bingen and Viola, 2018; Touret, 1987), implying that thrusting is

778 younger than 1132 ± 3 Ma. Extension was accommodated by thin greenschist-facies shear

779 zones with syn-kinematic muscovite porphyroblasts constraining the top-to-the-southeast

780 deformation between 891 ± 3 and 880 ± 3 Ma ($^{40}$Ar/$^{39}$Ar data) (Mulch et al., 2005). The

781 contrast in titanite U–Pb ages between the Telemarkia footwall (c. 913 to 901 Ma) and

782 Bamble hanging wall (c. 1107 to 1091 Ma) (Bingen et al., 1998; Cosca et al., 1998; deHaas et

783 al., 2002a; Heaman and Smalley, 1994) underscores the importance of normal movement

784 along the shear zone. A narrow, fully brittle, Permian, normal fault zone locally reactivates

785 the Sveconorwegian ductile precursors.
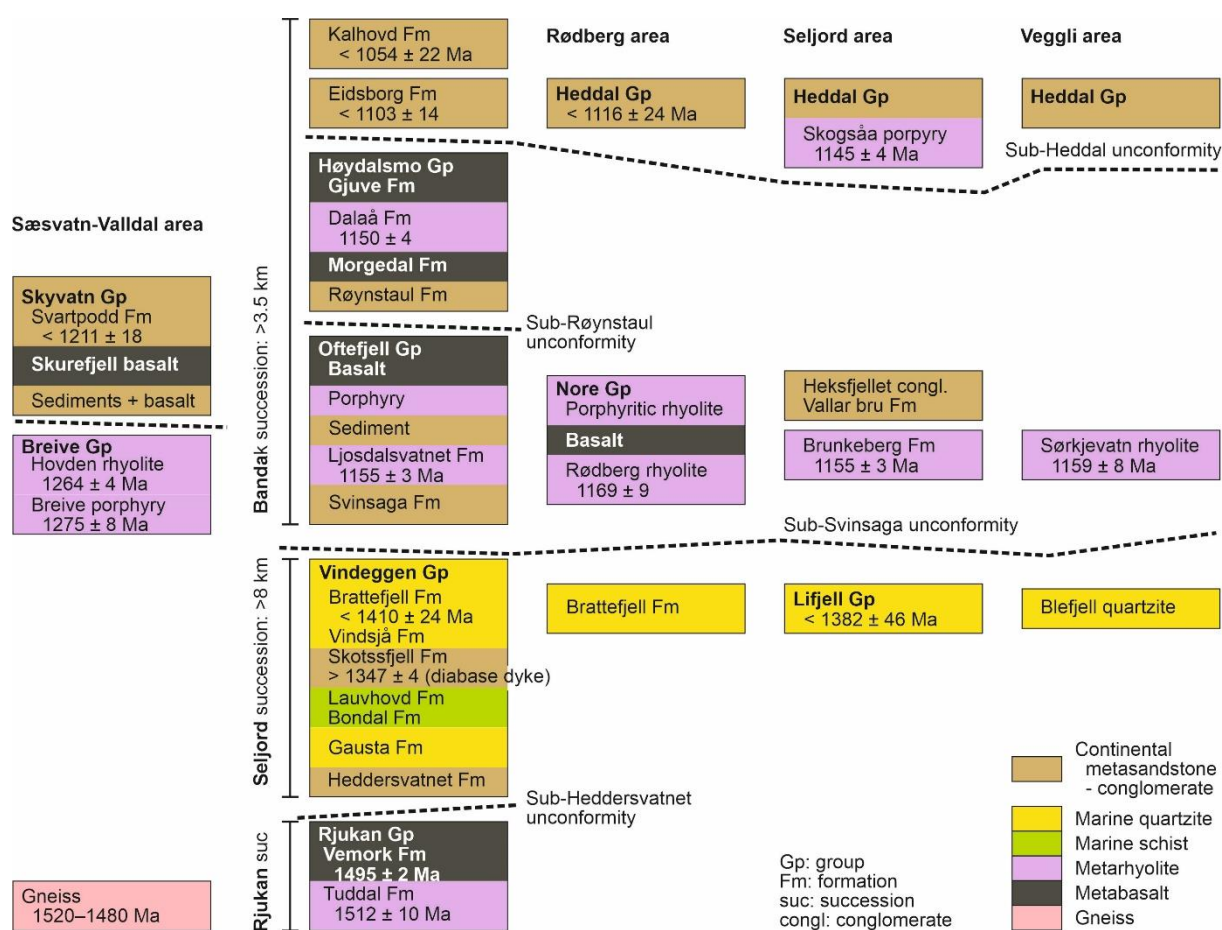
786 --------------------

787

788 **Figure 11.** Generalized stratigraphic columns for the Telemark supracrustal rocks in central

789 Telemark and supracrustal rocks in the Sæsvatn-Valldal area. These columns follow the

790 archetypal subdivision into the Rjukan, Seljord and Bandak successions (Dons, 1960; Dons

791 and Jorde, 1978; Sigmond, 1978), and integrate results of later mapping. Main sources of

792 stratigraphic and geochronological data: Bingen et al. (2002), Bingen et al. (2003), Corfu and

793 Laajoki (2008), Dons (1960; 1978), Laajoki et al. (2002), Laajoki and Corfu (2007), Köykkä

794 and Lammingen (2011), Lamminen and Köykkä (2010), Lamminen (2011), Nordgulen

795 (1999), Sigmond (1975, 1978, 1998), and Spencer et al. (2014).
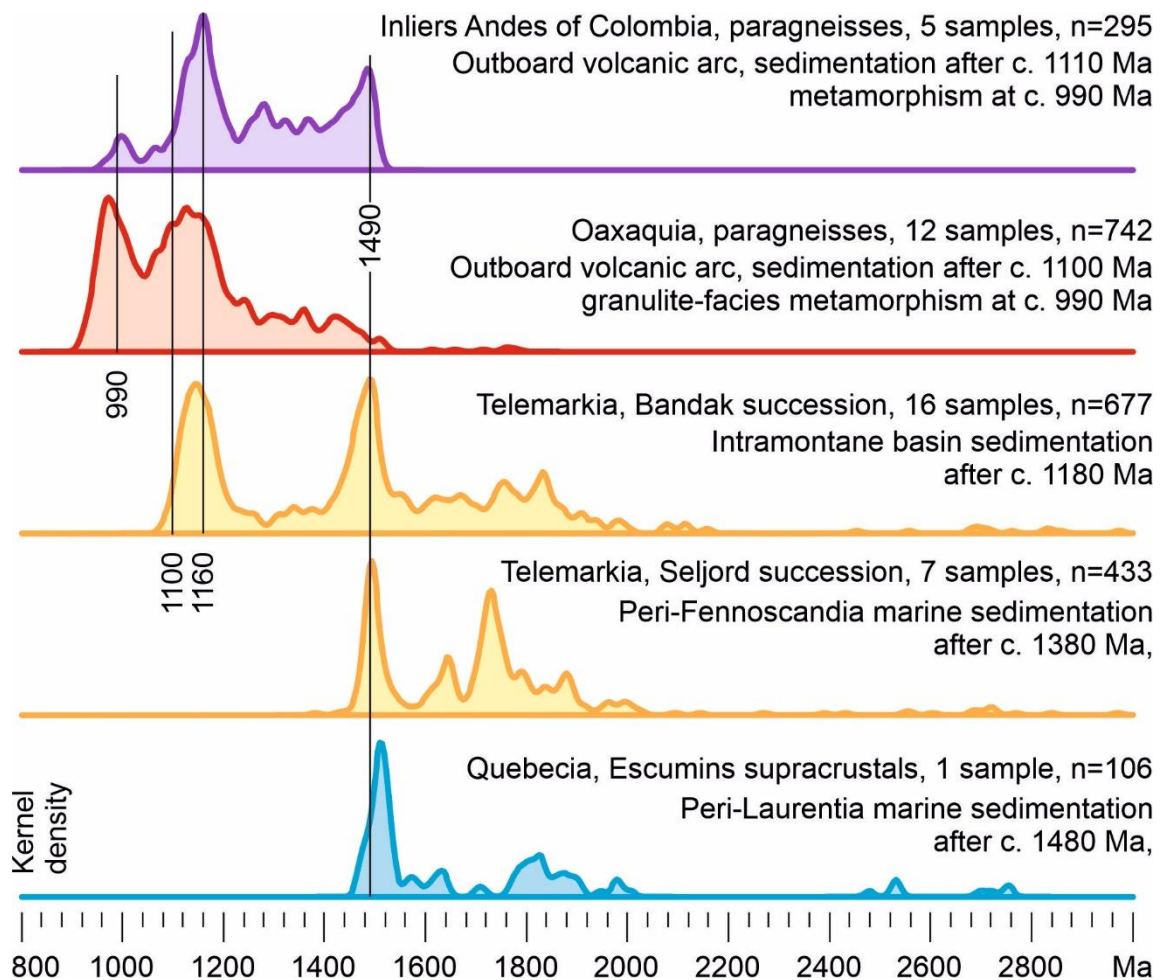
796 --------------------



797

798 **Figure 12.** Kernel density estimators of detrital zircon ages in metasediments of the

799 Telemarkia lithotectonic unit compared with paragneisses and metasediments in Quebecia,

800 Oaxaquia, and inliers in the Andes of Colombia. The Seljord succession in Telemarkia and

801    the Port au Quilles formation in the Escumins supracrustals record marine peri-Baltica and

802    peri-Laurentia sedimentation, respectively, after the 1520–1480 Ma continental generation.

803    The main peak reflects sourcing in the juvenile c. 1520-1480 Ma volcanic arcs, while the

804    diversity of older detrital zircons reflects sourcing from continental sources. The Bandak

805    succession in Telemarkia deposited after c. 1180 Ma (Eidsborg Formation after c. 1100 Ma)

806    and involved important recycling of the Seljord succession and younger magmatic rocks in

807    continental intramontane environment. Contrasting with this situation, the Oaxaquia

808    lithotectonic unit and the Inliers in the Andes of Colombia are interpreted as outboard

809    volcanic arcs formed in the ocean between Laurentia, Amazonia and Baltica after c. 1460 Ma,

810    and isolated almost entirely from continental sediment sources older than c. 1500 Ma. The

811    plots are generated with "DensityPlotter" by (Vermeesch, 2012) with a bandwidth of 10 Ma.

812    Data sources : Telemarkia, Bandak and Seljord successions: Bingen et al. (2001), de Haas et

813    al. (1999), Lamminen (2011) and Spencer et al. (2014); Quebecia: Escumins supracrustal

814    rocks, Port aux Quilles formation, Groulier et al. (2018b); Oaxaquia: granulite-facies

815    paragneisses, Solari et al. (2014); inliers in the Andes of Colombia: parageneisses, Cardona et

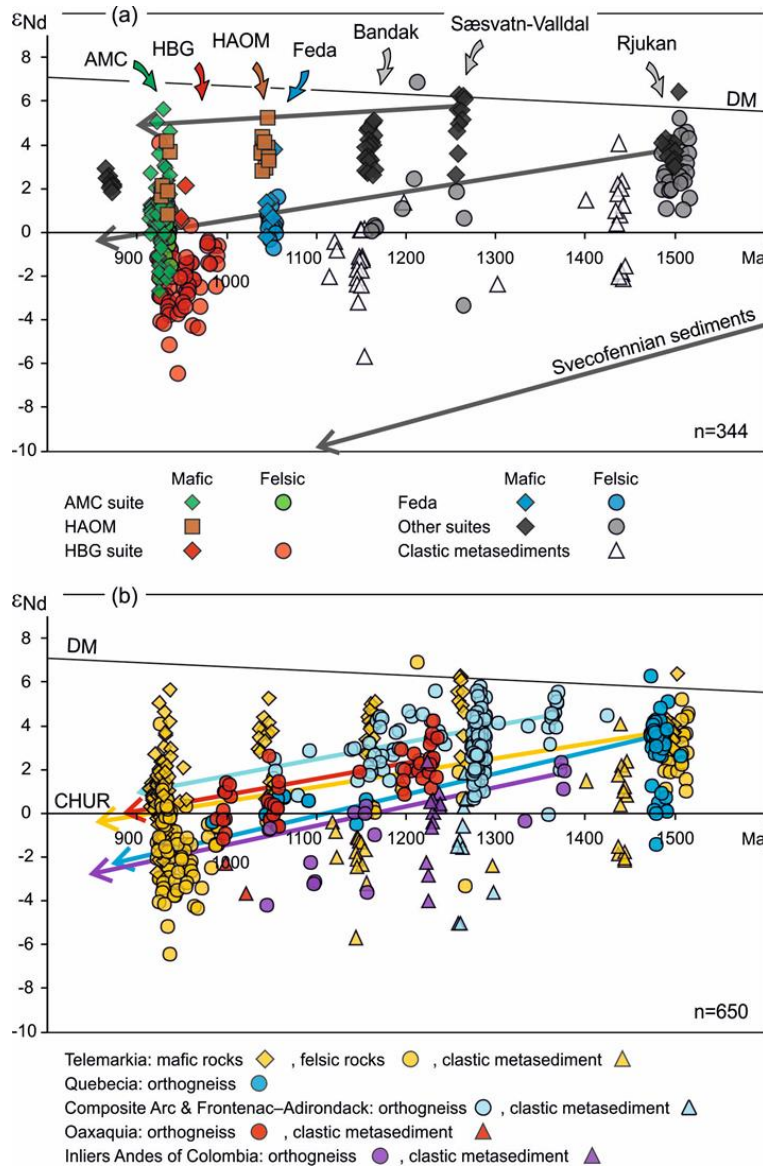816    al. (2010) and Ibanez-Mejia et al. (2011).

817    --------------------

**Figure 13.** Neodymium isotopic composition of rock suites in the Telemarkia lithotectonic unit, expressed as $\varepsilon_{Nd}$ (initial value) as a function of time. Each symbol represents one sample. Magmatic rocks are represented at their probable time of crystallization and metasedimentary rocks at their probable time of deposition (to improve legibility, each symbol is assigned a random scatter lower than ± 8 Ma along the time axis). Interpretations of the distribution of data are discussed in the text. (a) Rock suites in the Telemarkia lithotectonic unit. (b) Comparison between Telemarkia, Quebecia (Grenville orogen, Canada), the Composite Arc and Frontenac–Adirondack belt (Grenville orogen, Canada, USA), the Oaxaquia lithotectonic units (Mexico), and the inliers in the Andes of Colombia. These five lithotectonic units have

828    similar crustal evolution vectors. Sources of data: Hunnedalen dolerites at c. 870 Ma: (Maijer

829    and Verschure, 1998); Rogaland AMC suite at 930 Ma: (Barling et al., 2000; Bolle et al.,

830    2003a; Demaiffe et al., 1986; Menuge, 1988; Nielsen et al., 1996; Robins et al., 1997;

831    Schiellerup et al., 2000); high-alumina orthopyroxene megacrysts (HAOM) in anorthosite

832    plutons, 1040–930 Ma: (Bybee et al., 2014; Demaiffe et al., 1986); HBG granitoids, 985–925

833    Ma: (Andersen et al., 2001; Bogaerts et al., 2003; Demaiffe et al., 1990; Menuge, 1985, 1988;

834    Vander Auwera et al., 2003; Vander Auwera et al., 2014a); Feda suite at 1050 Ma: (Bingen et

835    al., 1993; Menuge, 1988; Vander Auwera et al., 2011); other magmatic rocks in Telemarkia:

836    (Andersen et al., 2001; Brewer et al., 2002; Brewer et al., 2004; Brewer and Menuge, 1998;

837    Menuge, 1985, 1988; Vander Auwera et al., 2003); metasedimentary rocks: (Andersen and

838    Laajoki, 2003; deHaas et al., 1999); Oaxaquia: (Lawlor et al., 1999; Ruiz et al., 1988; Weber

839    and Köhler, 1999) ; Inliers in the Andes of Colombia: (Cordani et al., 2005; Ibanez-Mejia et

840    al., 2015); Quebecia: (Dickin, 2000; Dickin and Higgins, 1992; Groulier et al., 2018a;

841    Groulier et al., 2018b); Composite Arc and Frontenac–Adirondack belt: (Chiarenzelli et al.,

842    2010; Daly and McLelland, 1991; Dickin et al., 2010; Marcantonio et al., 1990; McLelland et

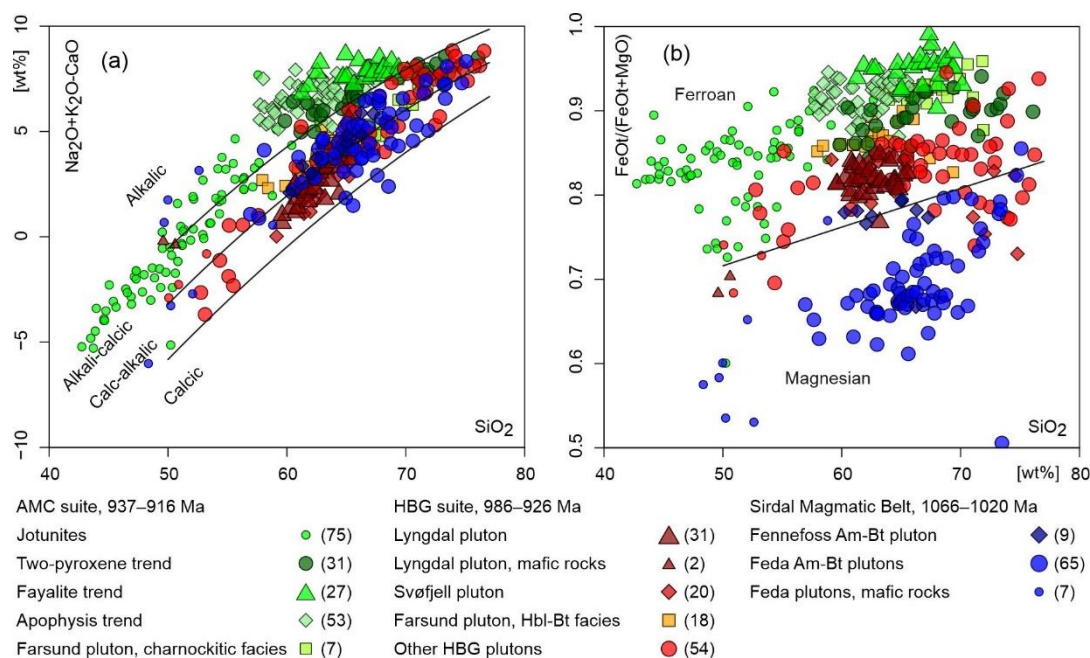843    al., 1993; Valentino et al., 2019).

844    --------------------

AMC suite, 937–916 Ma

| | | HBG suite, 986–926 Ma | | | Sirdal Magmatic Belt, 1066–1020 Ma | | |
|---|---|---|---|---|---|---|---|
| Jotunites | ● (75) | Lyngdal pluton | ▲ (31) | | Fennefoss Am-Bt pluton | ◆ (9) |
| Two-pyroxene trend | ● (31) | Lyngdal pluton, mafic rocks | ▲ (2) | | Feda Am-Bt plutons | ● (65) |
| Fayalite trend | ▲ (27) | Svøfjell pluton | ◆ (20) | | Feda plutons, mafic rocks | ● (7) |
| Apophysis trend | ◇ (53) | Farsund pluton, Hbl-Bt facies | ■ (18) | | | |
| Farsund pluton, charnockitic facies | □ (7) | Other HBG plutons | ● (54) | | | |

**Figure 14.** Comparison of the geochemical signature between three diagnostic magmatic suites intruded between 1066 and 916 Ma in the Telemarkia lithotectonic unit: c. 1050 Ma high-K calc-alkalic Feda plutonic suite of the Sirdal magmatic belt and 1030 Ma Fennefoss pluton (Bingen, 1989; Pedersen, 1981; Vander Auwera et al., 2011), 986–926 Ma hornblende-biotite granite (HBG) suite with ferro-potassic calc-alkalic to alkali-calcic signature (Bogaerts et al., 2003; Vander Auwera et al., 2003; Vander Auwera et al., 2014a) and the 937–916 Ma anorthosite-mangerite-charnockite (AMC) suite with ferro-potassic alkalic signature (Bolle and Duchesne, 2007; Charlier et al., 2010; Duchesne and Wilmart, 1997; Vander Auwera et al., 2014a; Vander Auwera et al., 1998; Wilmart et al., 1989). For the AMC suite, 3 different trends are recognized based on the mineralogy (two-pyroxene and fayalite trends) or their belonging to a specific intrusion (apophysis of the Bjerkreim-Sokndal intrusion).

### 3.5 Telemarkia lithotectonic unit

The western part of the Sveconorwegian orogen can be considered as one single lithotectonic unit, c. 230 x 300 km long, named Telemarkia (Fig. 2) (Bingen et al., 2005). The Telemarkia lithotectonic unit comprises low-grade supracrustal rocks preserved in several syncline structures, structurally overlying amphibolite- to granulite-facies gneiss complexes, and hosts

862    voluminous plutons (Fig. 4; Fig. 5.; Fig. 6). The gneiss complexes comprise orthogneisses

863    with subordinate paragneisses. The largest and most complete tract of supracrustal rocks,

864    called the Telemark supracrustal rocks, is exposed in a 60 km wide area in central Telemark

865    (Fig. 4; Fig. 6). Original mapping showed that stratigraphic relationships and deposition

866    structures are well preserved in the Telemark supracrustal rocks, and defined three groups or

867    successions separated by unconformities, which are, from bottom to top, the Rjukan, Seljord

868    and Bandak successions (Fig. 11, Fig. 12) (Dons, 1960; Dons and Jorde, 1978; Sigmond,

869    1978). Other supracrustal sequences are described in several other syncline structures, less

870    than 25 km wide, in the Ullensvang, Sauda, Grjotdokki-Nesflaten, Sæsvatn-Valldal and

871    Nissedal areas (Fig. 4).

872    *3.5.1    Telemarkian evolution*

873    Rapid generation of juvenile continental crust is recorded by voluminous magmatism between

874    $1521 \pm 6$ and $1476 \pm 13$ Ma, hosted in both the low-grade successions and in the gneiss

875    complexes (Fig. 7) (Bingen et al., 2008a; Bingen et al., 2005; Laajoki and Corfu, 2007;

876    Pedersen et al., 2009; Roberts et al., 2013). This event is called the Telemarkian accretionary

877    orogeny and it is geographically zoned.

878        In the west, in the Suldal area, gneisses and granitoids are characterized by a calc-alkaline

879    geochemical signature, with s supra-chondritic Hf isotopic signature at 1500 Ma (average $\varepsilon_{Hf}$

880    $= + 5.7$; Fig. 8) (Pedersen et al., 2009; Roberts et al., 2013). These are interpreted to reflect

881    volcanic arc magmatism (the Suldal arc; Roberts et al., 2013).

882        In the east, in the Telemark area, magmatism is bimodal and typified by the Rjukan

883    bimodal metavolcanic rocks at the base of the Telemark supracrustal rocks (Vemork basalt vs.

884    Tuddal rhyolite dated between $1512 \pm 10$ and $1495 \pm 2$ Ma, Fig. 11) and coeval plutonism

885    (Bingen et al., 2005; Laajoki and Corfu, 2007). This magmatism is characterized by a within-

886    plate geochemical signature and moderately supra-chondritic Nd isotopic signatures ($+1.1 <$

887    $\varepsilon_{Nd(1500\ Ma)} < +4.3$) (Fig. 13). It is interpreted to reflect back-arc rifting (the Rjukan rift basin),

888    continentwards of the active arc (Brewer and Menuge, 1998; Köykkä and Lamminen, 2011;

889    Lamminen and Köykkä, 2010; Roberts et al., 2013).

890        The Telemarkian orogenic event cannot be demonstrated to be associated with high-grade

891    metamorphism. The Seljord succession overlying the Rjukan succession is a c. 8 km thick,

892    shallow marine sedimentary succession, dominated by quartzite (Fig. 11, Fig. 12) (Köykkä

893    and Lamminen, 2011). The Seljord succession was deposited during a transgressive cycle,

894    interpreted as reflecting thermal subsidence after magmatism, between $1410 \pm 24$ Ma (detrital

895    zircon U–Pb data) and $1347 \pm 4$ Ma (U–Pb age of intrusive dolerite dyke ; Corfu and Laajoki,

896    2008; Köykkä and Lamminen, 2011; Lamminen and Köykkä, 2010).

897    *3.5.2   Pre- to early-Sveconorwegian evolution*

898    The Telemarkia lithotectonic unit hosts several generations of gneissic plutonic rocks in the

899    1280–1240, 1220–1180 and 1180–1145 Ma time intervals, with frequency maxima at c. 1280,

900    1260, 1210, 1170 and 1150 Ma (Fig. 6, Fig. 7) (Andersen et al., 2007; Bingen et al., 2003;

901    Corfu and Laajoki, 2008; Heaman and Smalley, 1994; Pedersen et al., 2009; Scheiber et al.,

902    2015).

903        In the southeast of the Telemarkia lithotectonic unit, a voluminous c. 60 x 120 km gneiss

904    complex consists of amphibolite-facies, NE–SW trending, moderately to weakly foliated

905    granitic gneiss and granitoids, named in different areas Drivheia gneiss (Heaman and

906    Smalley, 1994) and Vråvatn complex (Fig. 6) (Andersen et al., 2007). This complex is

907    dominated by c. 1220–1190 Ma plutonic rocks with a within-plate geochemical signature

908    (Andersen et al., 2007; Bingen and Viola, 2018; Heaman and Smalley, 1994) and a supra-

909    chondritic (radiogenic) Hf isotopic signature ($+9 < \varepsilon_{Hf} < +10$, in zircon from 4 samples, Fig.

910    8) approaching the depleted mantle reservoir value at 1210 Ma ($\varepsilon_{Hf} = +12$) (Andersen et al.,

911    2007).

912      The Sæsvatn–Valldal and Nissedal supracrustal rocks are two low-grade basalt-dominated

913    successions (Fig. 6, Fig. 11), exposed in two c. 15 km wide syncline. Basalt is interlayered

914    with felsic volcanic and clastic sedimentary rocks and intruded by fine-grained granite sills

915    and dykes (Dons and Jorde, 1978; Sigmond, 1975). In the Sæsvatn–Valldal succession, the

916    basalts are overlying rhyolites and porphyries dated to between $1275 \pm 8$ and $1259 \pm 2$ Ma,

917    themselves unconformably overlying the 1520–1480 Ma gneissic basement (Bingen et al.,

918    2002; Brewer et al., 2004). In the Nissedal succession, the basalts overly the $1219 \pm 8$ to 1202

919    $\pm 9$ Ma Vråvatn complex and host fine-grained granite sheets, one of which yields an

920    intrusion age of $1196 \pm 6$ Ma (Bingen and Viola, 2018). The Nissedal and Sæsvatn-Valldal

921    successions are interpreted as near-coeval bimodal (mafic dominated) continental successions

922    with an age close to 1210 Ma, coeval with the Drivheia and Vråvatn gneisses in the

923    underlying gneiss complex (Andersen et al., 2007; Heaman and Smalley, 1994).

924      In the Telemark supracrustal rocks, the c. 3.5 km thick Bandak succession rests over both

925    the Rjukan and Seljord successions (Köykkä, 2011; Laajoki et al., 2002), above a first order

926    unconformity locally decorated by a regolith (Köykkä and Laajoki, 2009) (Fig. 6, Fig. 11, Fig.

927    12). The succession includes at least two internal unconformities, implying active tectonism

928    during sedimentation (Laajoki, 2002; Laajoki et al., 2002). The lower part of the Bandak

929    succession consists of bimodal volcanic rocks interlayered with sediments (Köykkä, 2011).

930    The mafic rocks (Morgedal and Gjuve metabasalts) have a within-plate geochemical signature

931    (Brewer et al., 2002; Spencer et al., 2014). The felsic volcanic rocks range in age from $1169 \pm$

932    9 to $1145 \pm 4$ Ma (Bingen et al., 2003; Laajoki et al., 2002). The upper part of the Bandak

933    succession consists of exclusively sedimentary rocks. These are the Heddal Group, Eidsborg

934    Formation and Kalhovd Formation, deposited after $1116 \pm 24$, $1103 \pm 14$ and $1054 \pm 22$ Ma

935    respectively (Fig. 5, Fig. 11) (detrital zircon U–Pb data ; Bingen et al., 2003; deHaas et al.,

936    1999; Lamminen, 2011; Spencer et al., 2014).

937     The sedimentary rocks of the entire Bandak succession are generally immature, coarse-

938     grained to conglomeratic, and of limited lateral extent. They are interpreted as alluvial fan-,

939     braided fluvial- and locally eolian deposits, accumulated in continental fault-bounded

940     intermontane extensional basins (Bingen et al., 2003; Köykkä, 2011; Lamminen, 2011;

941     Spencer et al., 2014). Syn-sedimentary normal faults are well documented (Lamminen, 2011).

942     *3.5.3   Sveconorwegian magmatism*

943     After 70 Myr of quiescence, magmatism resumed at c. 1065 Ma with formation of the c. 50

944     km wide – 170 km long, orogen-parallel, NNW-SSE trending, Sirdal magmatic belt in the

945     Agder area (Fig. 5) (Bingen et al., 2015; Coint et al., 2015; Granseth et al., 2020; Slagstad et

946     al., 2013). This belt is a composite granitoid batholith, comprising mainly elongate and

947     variably foliated plutons of granodiorite, granite and leucogranite. Slivers of heterogeneous

948     gneiss interleaved within granitoid plutons are interpreted as xenoliths or panels of wall-rocks

949     (Coint et al., 2015). The granitoids intruded under pressure conditions of 0.38–0.48 GPa

950     (Coint et al., 2015) between $1066 \pm 10$ and $1020 \pm 15$ Ma (Bingen et al., 2015; Bingen and

951     van Breemen, 1998a; Coint et al., 2015; Möller et al., 2002; Slagstad et al., 2018; Slagstad et

952     al., 2013). A large portion of the belt comprises silica-rich biotite granite and leucogranite.

953     Foliated plutons of biotite + amphibole K-feldspar-phyric quartz-monzonite to granodiorite

954     are specifically called the Feda suite ($1050 \pm 8$ Ma) and Fennefoss augen gneiss ($1031 \pm 2$

955     Ma) (Fig. 5) (Bingen and van Breemen, 1998a). These are characterized by a magnesian,

956     high-K, high-Sr-Ba, calc-alkaline geochemical signature and locally host ultrapotassic

957     (lamprophyre) mafic layers and enclaves (Fig. 14) (Bingen et al., 1993; Bingen and van

958     Breemen, 1998a).

959     After 985 Ma, large plutons with a distinctly ferroan geochemical signature were emplaced

960     (Fig. 5, Fig. 14) (Andersen et al., 2001; Granseth et al., 2020; Vander Auwera et al., 2011).

961     These plutons are weakly- to non-foliated, have sharp contacts to their wall-rock and are well

962    defined on aeromagnetic maps by positive anomalies (Slagstad et al., 2018). Two main

963    ferroan suites are defined: a ferro-potassic hornblende–biotite–granitoid (HBG) suite and an

964    orthopyroxene-bearing anorthosite–mangerite–charnockite (AMC) suite (Fig. 5, Fig. 14)

965    (Bogaerts et al., 2003; Duchesne and Wilmart, 1997; Vander Auwera et al., 2003; Vander

966    Auwera et al., 2011; Vander Auwera et al., 2014a). The HBG suite formed between $986 \pm 2$

967    and $926 \pm 4$ Ma and is exposed in the area of the Sirdal magmatic belt and eastwards

968    (Andersen et al., 2001; Andersen et al., 2007; Granseth et al., 2020; Jensen and Corfu, 2016;

969    Sigmond, 1985; Slagstad et al., 2018; Vander Auwera et al., 2011; Vander Auwera et al.,

970    2014a). The AMC suite formed between $937 \pm 1$ and $916 \pm 9$ Ma and is restricted to the

971    southwestern end of the Telemarkia lithotectonic unit (Fig. 5) (Bolle et al., 2018; Schärer et

972    al., 1996; Vander Auwera et al., 2011; Vander Auwera et al., 2014a). A few plutons (Farsund

973    and Kleivan plutons, $931 \pm 2$ and $936 \pm 1$ Ma) are composite HBG–AMC plutons, with

974    charnockitic and non-charnockitic facies, reflecting tapping of distinct sources into one pluton

975    (Vander Auwera et al., 2014a).

976    The Rogaland AMC suite (Fig. 5) consists of three large anorthosite plutons (Egersund-

977    Ogna, Håland-Helleren, Åna-Sira anorthosites), two satellite leuconorite plutons (Hidra and

978    Garsaknatt leuconorites), a layered intrusion (Bjerkreim-Sokndal layered intrusion), and

979    volumetrically minor sills and dykes of jotunite and ilmenite-norite, all emplaced during a

980    short lived magmatic event between c. 932 and 916 Ma (Charlier et al., 2006; Duchesne et al.,

981    1985; Duchesne et al., 1989; Schärer et al., 1996; Vander Auwera et al., 2011).

982    The Egersund-Ogna anorthosite pluton exhibits an isotropic core and a foliated margin,

983    characterized by a syn-magmatic fabric parallel to the contact. The centre of the pluton is

984    made up of anorthosite and leuconorite with a granulated matrix of plagioclase ($An_{40}$–$An_{50}$),

985    hosting 1–3 m large aggregates of plagioclase (up to $An_{55}$) and high-alumina orthopyroxene

986    megacrysts (HAOM, $En_{75}$) (Charlier et al., 2010). The high aluminium and chromium

987   contents (up to 8.5 wt% $Al_2O_3$ and 1500 ppm Cr) of the orthopyroxene megacrysts indicate a

988   pressure of crystallization of c. 1.1 GPa for the megacrysts, contrasting with the ambient

989   pressure of 0.5 GPa for the matrix minerals (2-3 wt% $Al_2O_3$ in matrix orthopyroxene). The

990   anorthosite plutons intruded as a plagioclase-dominated crystal mush lubricated by melt, from

991   the base of the crust (1.1 GPa) to the middle of the crust (0.5 GPa) (Barnichon et al., 1999;

992   Charlier et al., 2010; Duchesne et al., 1999). The orthopyroxene megacrysts with the highest

993   aluminum content (> 8 wt% $Al_2O_3$) define a Sm–Nd isochron with an age of 1041 ± 17 Ma

994   (Bybee et al., 2014), pointing either to inheritance (Vander Auwera et al., 2014b) or

995   protracted ponding of mafic magma at the base of the crust (Bybee et al., 2014).

996     The Bjerkreim-Sokndal layered intrusion (931 ± 7 Ma) can be subdivided into a layered

997   lower part and a non-layered upper part. The lower part comprises five macrocyclic units of

998   cumulates (Barling et al., 2000; Duchesne, 1972; Nielsen et al., 1996; Robins et al., 1997).

999   The upper part comprises, fractionated and wall-rock-contaminated, mangerite and

1000  charnockite (Duchesne and Wilmart, 1997; Nielsen et al., 1996). The Bjerkreim-Sokndal

1001  intrusion intruded at pressure conditions of ≤ 0.5 GPa (Vander Auwera and Longhi, 1994). It

1002  forms a syncline (lopolith), the formation of which is attributed to gravity-driven subsidence

1003  of the central part of the intrusion (Bolle et al., 2000; Bolle et al., 2002; Paludan et al., 1994).

1004    Undeformed pegmatites intruded between c. 914 and 900 Ma. They include the Evje-

1005  Iveland rare-mineral pegmatite field (Müller et al., 2017; Pasteels et al., 1979; Scherer et al.,

1006  2001; Seydoux-Guillaume et al., 2012).

1007  *3.5.4   Sveconorwegian metamorphism*

1008  As outlined above, the supracrustal rocks in the centre of the Telemarkia lithotectonic unit

1009  were affected by greenschist to epidote-amphibolite facies metamorphism and deformed by

1010  open to tight folding. Basalt in the Sæsvatn-Valldal succession (Fig. 6) was deformed under

1011    epidote-amphibolite facies conditions at c. 1032 ± 2 Ma and faulted at 1017 ± 2 Ma

1012    (molybdenite Re-Os data; Stein and Bingen, 2002).

1013    In the gneiss complexes, the metamorphic grade typically reached upper amphibolite-

1014    facies conditions, with widespread migmatitization between 1026 ± 14 and 1005 ± 7 Ma

1015    (zircon and monazite U–Pb data; Bingen et al., 2008b; Coint et al., 2015). Granitoids of the

1016    Sirdal magmatic belt (c. 1065–1020 Ma) are commonly moderately deformed (Coint et al.,

1017    2015). Locally, they contain zircons with rims recording a hydrothermal to metamorphic

1018    overprint at c. 1016 Ma (Knaben Mo district ; Bingen et al., 2015).

1019    The metamorphic grade increases southwestwards towards the Rogaland AMC complex,

1020    structurally downwards, across to the N–S trending and E-dipping regional fabric (Fig. 5)

1021    (Bingen and van Breemen, 1998b; Maijer, 1987; Slagstad et al., 2018; Tobi et al., 1985).

1022    Metamorphism was coeval with the formation of lithological banding, tight to isoclinal

1023    folding and migmatitization. Two concentric granulite facies zones are defined: the

1024    orthopyroxene zone and the osumilite zone close to the AMC complex (Fig. 5). Osumilite is

1025    diagnostic of water poor, low-pressure, ultrahigh temperature (UHT; T > 900 °C) granulite-

1026    facies conditions (Harley, 2008; Holland et al., 1996).

1027    Zircon and monazite U–Pb geochronology from a diversity of granulite-facies samples

1028    gave apparent ages spreading between c. 1045 and 900 Ma (Bingen et al., 2008b; Bingen and

1029    van Breemen, 1998b; Laurent et al., 2018a; Möller et al., 2002, 2003; Slagstad et al., 2018;

1030    Tomkins et al., 2005). Insight into the pressure-temperature-time evolution of this protracted

1031    metamorphism requires careful linkage of petrography, phase equilibrium modelling,

1032    geochronology and trace-element characterization of zircon and monazite. Typical samples

1033    inside the orthopyroxene zone reached peak conditions of 0.5 GPa – 880 °C between c. 1040

1034    and 1010 Ma (Laurent et al., 2018b). Rims of neocrystallized zircon in such samples spread

1035    from 1045 to 955 Ma, supporting 90 Myr of melt-present conditions (Laurent et al., 2018a).

1036   In the osumilite zone, the onset of migmatitization, associated with biotite and sulfide mineral

1037   breakdown, is recorded by sulfate-rich monazite cores in an osumilite-bearing paragneiss at

1038   1034 ± 6 Ma (Laurent et al., 2016). In a (quartz- and garnet-free) sapphirine + orthopyroxene

1039   sample (Fig. 9; Ivesdal locality), a Y-rich monazite (5–7 wt% $Y_2O_3$) further constrains

1040   temperature higher than 900°C between 1029 ± 9 and 1006 ± 8 Ma (Laurent et al., 2018b), in

1041   accordance with zircon data (1010 ± 7 to 1006 ± 4 Ma) (Drüppel et al., 2013). The breakdown

1042   of the peak sapphirine + orthopyroxene assemblage into a cordierite + hercynite assemblage

1043   implies a clockwise P-T path with a decompression between 0.6 GPa – 920 °C and 4.5 GPa –

1044   900°C (Fig. 9) (Blereau et al., 2017; Laurent et al., 2018b). This decompression is best

1045   captured by a garnet-bearing sample from the osumilite zone that contains Y-rich monazite

1046   recording garnet breakdown into cordierite  + hercynite + orthopyroxene, pinning a robust P-

1047   T-t point at 0.4 GPa – 910 °C – 930 ± 6 Ma (Laurent et al., 2018b). Together, the data give

1048   evidence for two events of low-pressure granulite-facies metamorphism peaking at UHT

1049   conditions, the first event (M1) between c. 1030 and 1005 Ma, and the second (M2) at c. 930

1050   Ma, associated with formation of osumilite (Blereau et al., 2017; Drüppel et al., 2013; Laurent

1051   et al., 2018b; Laurent et al., 2016). Minor exhumation (c. 6 km) took place between the two.

1052     These two events were penecontemporaneous with magmatic activity (Laurent et al.,

1053   2018b; Slagstad et al., 2018). The first M1 event started with dehydration melting (c. 1034

1054   Ma) coeval with intrusion of the Sirdal magmatic belt (c. 1065-1020 Ma) and associated

1055   underplating (c. 1040 Ma), and peaked at the end and after this magmatic event (1030–1005

1056   Ma). The second M2 event (c. 930 Ma) was coeval with intrusion of the AMC suite. This

1057   correlation strongly suggests that magmatism and metamorphism had a common heat source

1058   in the mantle. The lag between magmatism and peak metamorphism for M1 may reflect

1059   temperature buffering by melt until melt migration effectively took place.

1060    The M2 metamorphic event was followed by regional scale cooling, dated by titanite U–Pb

1061    data at 918 ± 2 Ma (Bingen and van Breemen, 1998b). Amphibole $^{40}Ar/^{39}Ar$ apparent ages

1062    scatter between 1059 ± 8 and 853 ± 3 Ma (Bingen et al., 1998). The main cluster at 871 ± 10

1063    Ma overlaps with biotite Rb–Sr ages (Verschure et al., 1980) and is interpreted as a cooling

1064    age.

1065    *3.5.5    The Mandal-Ustaoset fault and shear zone*

1066    The Mandal-Ustaoset fault and shear zone is a N–S trending structure inside the Telemarkia

1067    lithotectonic unit (Fig. 2). It includes a precursor ductile shear zone and a set of later brittle

1068    normal faults (Sigmond, 1985). In its northern segment, it is an east dipping (c. 45°) normal

1069    (extensional) shear zone, juxtaposing the amphibolite-facies Hardangervidda gneiss complex

1070    in the west against the low-grade intramontane basin hosting the Kalhovd Formation (≤ 1054

1071    ± 22 Ma) in the east (Sigmond and Ragnhildstveit, 2004). Towards the south, the Mandal-

1072    Ustaoset fault and shear zone merges into an amphibolite-facies N–S trending banded gneiss

1073    unit on the eastern side of an elongate pluton of the Feda suite (1049 ± 8 Ma, Mandal augen

1074    gneiss; Bingen and van Breemen, 1998a). The Mandal-Ustaoset fault and shear zone still

1075    requires detailed kinematic and geochronological characterization.

1076    **4    Discussion**

1077    ***4.1    U–Pb and Lu–Hf evidence for continental growth at the margin of Fennoscandia***

1078    The continental crust exposed in the Sveconorwegian orogen was formed after 1900 Ma

1079    (Åhäll and Connelly, 2008; Andersen et al., 2004a; Bingen et al., 2005; Bingen and Viola,

1080    2018; Petersson et al., 2015b; Roberts and Slagstad, 2015; Roberts et al., 2013). The age of

1081    the dominant magmatic suites in the different lithotectonic units decreases towards the west

1082    (Fig. 7). The oldest major magmatic suites in each lithotectonic unit are dated between 1710

1083    and 1660 Ma in the Eastern Segment, 1660 and 1520 Ma in the Idefjorden lithotectonic unit,

1084    1575 and 1480 Ma in the Bamble and Kongsberg lithotectonic units, and 1520 and 1480 Ma

1085    in the Telemarkia lithotectonic unit. The Lu–Hf isotopic signature of igneous zircon in these

1086    magmatic suites (Fig. 8) becomes more radiogenic (more positive $\varepsilon_{Hf}$ values) westward in the

1087    orogenic belt, with average initial $\varepsilon_{Hf}$ values increasing from +3.0 in the Eastern Segment

1088    (1700 Ma) to +8.8 in the Bamble-Kongsberg lithotectonic units (1550 Ma), and back to +5.7

1089    in the Telemarkia lithotectonic unit (1500 Ma; Fig. 8) (Andersen et al., 2002b; Pedersen et al.,

1090    2009; Petersson et al., 2015a; Petersson et al., 2015b; Roberts et al., 2013). The geochemical

1091    signature of these different magmatic suites generally ranges from calc-alkalic to alkali-calcic

1092    (references above), suggesting that the continental lithosphere was generated dominantly in a

1093    supra-subduction (accretionary) geodynamic setting between 1710 and 1480 Ma (Åhäll and

1094    Connelly, 2008; Andersen et al., 2004a; Petersson et al., 2015a; Petersson et al., 2015b;

1095    Roberts et al., 2013).

1096        The weakly positive initial $\varepsilon_{Hf}$ values in the Eastern Segment (Fig. 8) imply significant

1097    recycling of older Paleoproterozoic (Svecokarelian) continental crust in the genesis of the

1098    1710–1660 Ma magmatic suites (Petersson et al., 2015a). The more positive initial $\varepsilon_{Hf}$ values

1099    westwards imply, instead, that the four lithotectonic units to the west of the Mylonite Zone

1100    were generated in more juvenile volcanic arc and back arc environment, away from old

1101    Paleoproterozoic continental lithosphere (Andersen et al., 2002b; Petersson et al., 2015b;

1102    Roberts et al., 2013). The variability within and between these units can be accounted for by a

1103    change from an advancing to a retreating subduction system or, alternatively, a variable

1104    contribution of metasedimentary components incorporated in the subduction system along the

1105    oceanic lower plate (Andersen et al., 2002b; Petersson et al., 2015b; Roberts et al., 2013).

1106        The age and isotopic trends of magmatism in the 1710–1480 Ma interval (Fig. 7, Fig. 8)

1107    are compatible with incremental westward growth of the continental lithosphere at the margin

1108    of Fennoscandia. This is compatible with any orogenic model interpreting the lithotectonic

1109    units as endemic to the margin of Fennoscandia (Fig. 3 b, d, e, f).
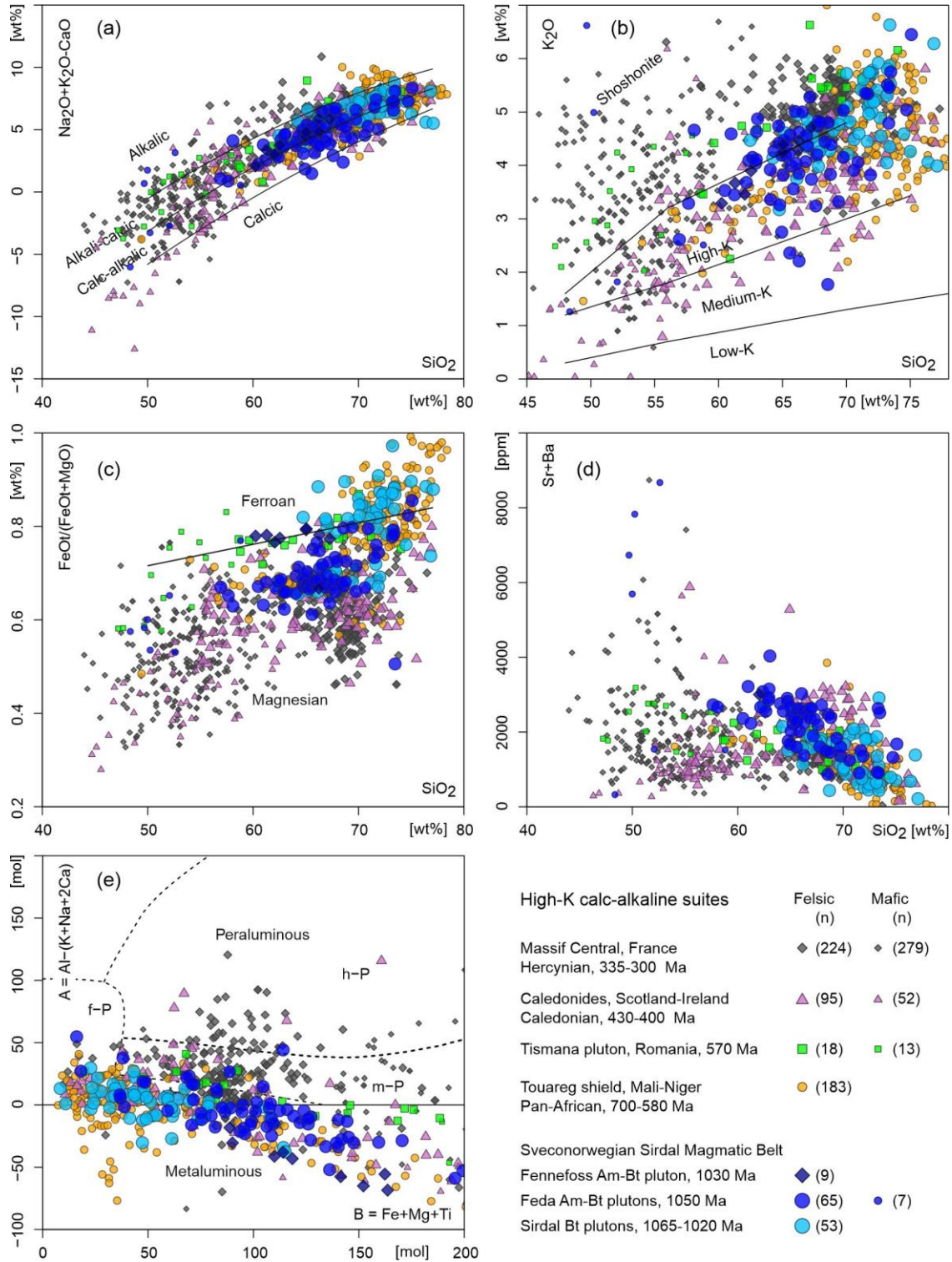
1110    ------------------------



1111

1112 **Figure 15.** Comparison of the geochemical signature of the Sirdal magmatic belt (c. 1065–

1113 1020 Ma) in the Telemarkia lithotectonic unit, and syn-collisional high-K calc-alkaline

1114 magmatic suites in younger collision orogenic belts. Large symbols represent granitoids while

1115 small symbols represent associated minor mafic sills, dykes and enclaves. The Sirdal

1116 magmatic belt is divided into the magnesian amphibole-biotite Feda plutonic suite hosting

1117 minor volume of ultrapotassic enclaves, the ferroan amphibole-biotite-bearing Fennefoss

1118 pluton and more silica-rich biotite-bearing foliated plutons (Bingen, 1989; Pedersen, 1981;

1119 Slagstad et al., 2013; Vander Auwera et al., 2011). For comparison, the Hercynian high-K

1120 calc-alkaline plutons of the Massif Central in France associated with "vaugnerites"

1121 (compilation: Moyen et al., 2017), the Caledonian high-K, high Ba-Sr plutons of Scotland and

1122 Ireland associated with "appinites" (Clemens et al., 2009; Ghani and Atherton, 2006), the

1123 Neoproterozoic shoshonitic Tismana pluton in the Carpathians of Romania (Duchesne et al.,

1124 1998), and the Neoproterozoic high-K calc-alkalines suites of the Touareg Shield in Mali and

1125 Niger (Liégeois et al., 1998). The figure shows a broad overlap of the geochemistry between

1126 these different suites. (a) $SiO_2$ vs. $Na_2O+K_2O-CaO$ diagram (Frost et al., 2001). (b) $SiO_2$ vs.

1127 $K_2O$ diagram (Peccerillo and Taylor, 1976). (c) $SiO_2$ vs. $FeO_{tot} / (FeO_{tot}+MgO)$ (Frost et al.,

1128 2001). (d) $SiO_2$ vs. Sr+Ba diagram showing the high Sr+Ba signature of high-K calc-alkaline

1129 suites, including the Feda plutons and their ultrapotassic mafic enclaves. (e) B-A diagram (B

1130 = Fe+Mg+Ti, A = Al-(K+Na+2Ca) (expressed in gram-atoms of each element in 100 gr of

1131 material) (Debon and Le Fort, 1983; Villaseca et al., 1998) (h-P: highly peraluminous, m-P:

1132 moderately peraluminous, l-P: low peraluminous, f-P: felsic peraluminous).

1133 *4.2   Significance of high-K calc-alkaline granite plutonism*

1134 Tracing past subduction systems largely relies on tracing a subduction-related geochemical

1135 signature in magmatic rocks. In the Telemarkia lithotectonic unit, a significant component of

1136 the large (50 x 170 km) orogen-parallel Sirdal magmatic belt (c. 1065–1020 Ma) has a calc-

1137    alkaline geochemical signature (Bingen et al., 2015; Coint et al., 2015; Granseth et al., 2020;

1138    Slagstad et al., 2018; Slagstad et al., 2013). More specifically, the biotite + amphibole K-

1139    feldspar-phyric quartz-monzonite–granodiorite foliated plutons of the Feda suite are

1140    characterized by a high-K, high-Sr-Ba, magnesian, calc-alkalic geochemical trend (Fig. 14)

1141    (Bingen et al., 1993; Bingen and van Breemen, 1998a). They are associated with a small

1142    volume of ultrapotassic rocks. Calc-alkaline rocks are typically observed in active supra-

1143    subduction environment (Bateman and Chappell, 1979; Hervé et al., 2007; Pearce et al.,

1144    1984). However, high-K calc-alkaline suites are also typically representative of syn- to late-

1145    collision plutons and batholiths in collisional orogens (Fig. 15). They are well described in the

1146    Caledonian orogen (Bruand et al., 2014; Clemens et al., 2009; Ghani and Atherton, 2006;

1147    Neilson et al., 2009), the Hercynian orogen (Couzinié et al., 2016; Laurent et al., 2014;

1148    Laurent et al., 2017; Moyen et al., 2017) and the Pan-African orogens (Janoušek et al., 2010;

1149    Liégeois et al., 1998). These plutons are commonly associated with minor volumes of

1150    ultrapotassic rocks such as lamprophyre, appinite or vaugnerite (Fig. 15 b). The Sirdal

1151    magmatic belt and more specifically the Feda suite exhibits a complete overlap in major and

1152    trace element geochemical composition with syn- to late-collision high-K calc-alkaline

1153    plutons in collisional orogens (Fig. 15). Therefore, the belt could be reasonably interpreted as

1154    well as the product of syn- to late-collision magmatism.

1155        To sum up, the geochemical signature of the Sirdal magmatic belt is not fully diagnostic of

1156    a geodynamic environment. There are two alternatives. (i) It records supra-subduction

1157    magmatism as part of an active subduction system in the 1065–1020 Ma time interval. This

1158    subduction was either dipping eastwards in the context of the models of protracted Andean

1159    margin (Fig. 3 e, f) (Slagstad et al., 2020; Slagstad et al., 2017; Slagstad et al., 2013) or was

1160    dipping westwards in the model of suturing along the Mylonite Zone at c. 990 Ma (Fig. 3 c)

1161    (Brueckner, 2009; Möller and Andersson, 2018; Petersson et al., 2015b). (ii) The Sirdal

1162     magmatic belt represents syn-collision magmatism, therefore recording ongoing continent-

1163     continent collision between 1065 and 1020 Ma (Fig. 3 d).

1164     *4.3    Significance of massif-type anorthosite plutonism*

1165     Massif-type anorthosite plutons formed on Earth only in the Proterozoic. This peculiarity is

1166     inferred to relate directly or indirectly to the secular evolution of the temperature of the

1167     asthenosphere (Ashwal, 1993). The geodynamic context and petrogenesis of AMC plutonism

1168     remain controversial (Ashwal, 1993; Bédard, 2010; Duchesne et al., 1985; Emslie, 1985;

1169     Vander Auwera et al., 2011).

1170         Petrologically, the AMC suite of Rogaland (Fig. 5; Fig. 14) can be accounted for by

1171     differentiation of several parental magmas ranging in composition from high-alumina basalt

1172     (anorthosite plutons) to ferro-basalt (Bjerkreim-Sokndal intrusion and jotunites) in anhydrous

1173     and reduced (QFM to QFM-1) conditions (Charlier et al., 2010; Duchesne and Wilmart, 1997;

1174     Duchesne et al., 1989; Robins et al., 1997; Vander Auwera and Longhi, 1994).

1175         Here, we draw the attention to the fact that the AMC complex is almost entirely devoid of

1176     water-bearing minerals (Duchesne and Charlier, 2005; Longhi et al., 1999). Amphibole

1177     appears only very locally as a late-stage replacement mineral. The dry nature of the magmas

1178     as well as the water-poor to water-absent assemblages of the granulite-facies wall rock of the

1179     AMC plutons (Blereau et al., 2017; Drüppel et al., 2013; Laurent et al., 2018b) are objectively

1180     irreconcilable with the definition of magmatism in a supra-subduction setting (Grove et al.,

1181     2006). Supra-subduction magmatism is induced by fluids released from and fluxing above a

1182     subducting oceanic plate. It typically contains 1–6 wt % $H_2O$ (Plank et al., 2013; Sobolev and

1183     Chaussidon, 1996; Wallace, 2005) and produces hornblende-bearing cumulates (Jagoutz and

1184     Schmidt, 2013). Therefore, in our opinion, models framing AMC magmatism in a supra-

1185     subduction setting (Fig. 3 e, f) (Bybee et al., 2014; Slagstad et al., 2013) are not realistic.

1186     *4.4    Sveconorwegian orogenic plateau*

1187     Evidence for the presence of a past orogenic plateau in Proterozoic orogens is largely indirect

1188     (Jamieson and Beaumont, 2013; Rey et al., 2001; Rivers, 2008, 2012; Vanderhaeghe, 2012).

1189     Today, following extension (collapse), exhumation and erosion, the Sveconorwegian orogen

1190     exposes widespread gneiss complexes characterized by ductile deformation accompanied by

1191     partial melting, compressional structures, and protracted upper amphibolite- to granulite-

1192     facies metamorphism, structurally overlain by discontinuous exposures of low-grade

1193     supracrustal rocks (Fig. 4). The supracrustal rocks are greenschist- to epidote-amphibolite-

1194     facies metavolcanic and metasedimentary sequences, exhibiting partially preserved primary

1195     structures and stratigraphic relationships. The age distribution of rocks in the supracrustal

1196     complexes matches that in the gneiss complexes. Transition between high-grade and low-

1197     grade rock occurs over short distances.

1198         We interpret the gneiss complexes and supracrustal complexes as remnants of the

1199     infrastructure and superstructure of an orogenic plateau, respectively, now tectonically

1200     juxtaposed along extensional shear zones. Characterization of the geometry, kinematics and

1201     geochronology of these shear zones is still very fragmentary today. However, recent data

1202     support diffuse late-Sveconorwegian extensional tectonics (Persson-Nilsson and Lundqvist,

1203     2014; Torgersen et al., 2018; Viola et al., 2011).

1204         The sedimentary rocks in the supracrustal complexes offer a window into the surface

1205     environment at the time of deposition. As reviewed above, the supracrustal rocks deposited

1206     between 1280 and 1050 Ma reflect continental (above sea level) conditions, with evidence for

1207     sediment accumulation in fault-bounded intermontane extensional basins (Bingen et al., 2003;

1208     Köykkä, 2011; Lamminen, 2011; Spencer et al., 2014). Gneiss complexes in the Bamble and

1209     Kongsberg lithotectonic units were exhumed to upper-crustal level after the early-

1210     Sveconorwegian orogenic phase (1150–1120 Ma) and, therefore, they can be regarded as part

1211     of the orogenic superstructure during the main Sveconorwegian orogeny (after 1065 Ma).

1212    Plutons, produced by partial melting of the lower and middle crust, can be anticipated to

1213    accumulate mainly at the transition between ductile and brittle crust (Brown, 2013). In an

1214    orogenic plateau, they will accumulate between the infrastructure and superstructure. The

1215    Sveconorwegian orogen exposes Sveconorwegian plutons increasing in abundance westwards

1216    and mainly hosted in gneiss complexes (Fig. 5). Plutons intruded between 1065 and 920 Ma,

1217    define a consistent pressure of intrusion of 0.4–0.5 GPa (Table 1). This suggests a rather

1218    constant depth of c. 16 km for the boundary between the infrastructure and superstructure,

1219    through time during the main Sveconorwegian orogeny. Additionally, this is consistent with a

1220    model of stable orogenic plateau extending over large areas in the orogen.

1221    *4.5    End of convergence and collapse of the orogenic plateau*

1222    The switch between plate convergence and plate divergence is a fundamental parameter of

1223    orogeny. However, it is not trivial to constrain in time, because evidence for compression or

1224    extension are distinct in the infrastructure and superstructure of an orogenic plateau. The last

1225    undisputable evidence for convergence in the Sveconorwegian orogen corresponds to eclogite

1226    facies metamorphism dated at 988 ± 6 Ma in the Eastern Segment (Möller et al., 2015).

1227    Several observations, however, indicate that compression continued after this point in the

1228    middle crust (infrastructure), probably to at least c. 930 Ma. (i) In the Eastern Segment, the

1229    internal section and the eclogite-bearing ductile nappe are folded by east-verging to

1230    recumbent folds and later upright folds, recording continued high-grade E–W contraction

1231    (Möller and Andersson, 2018; Möller et al., 2015; Piñán-Llamas et al., 2015; Tual et al.,

1232    2015). Zircon carries a record of these events between c. 978 and 961 Ma. (ii) In the

1233    Telemarkia lithotectonic unit, plutons of the HBG suite exhibit a petrofabric, which is largely

1234    controlled by wall-rock ductile deformation during emplacement (Bolle et al., 2018). A study

1235    of the anomaly of magnetic susceptibility (AMS) of the Holum, Kleivan, and Sjelset plutons

1236    in the Agder area provided evidence for regional E–W compression during intrusion, at 957 ±

1237　7, 936 ± 1 and 932 ± 1 Ma respectively (Fig. 5) (Bolle et al., 2010; Bolle et al., 2003b; Bolle

1238　et al., 2018). (iii) In the frontal wedge of the orogen, dykes attributed to the c. 980–945 Ma

1239　Blekinge-Dalarna dolerite swarm (Fig. 5) are known to be displaced along discrete ductile

1240　shear zones with top-to-east reverse sense of shear. This suggests that thrusting along the

1241　Sveconorwegian front took place as late as after c. 945 Ma (Stephens and Wahlgren, 2020a;

1242　Wahlgren et al., 1994).

1243　　In contrast with this evidence, dykes and sills intruded along brittle structures suggest

1244　coeval extension in the upper crust (superstructure). (i) In the Idefjorden lithotectonic unit,

1245　WNW–ESE trending mafic to felsic intrusions suggest a phase of NNE-SSW extension

1246　between c. 951 and 915 Ma (Fig. 5) (Årebäck et al., 2008; Hellström et al., 2004; Scherstén et

1247　al., 2000; Wahlgren et al., 2015). (ii) In the internal section of the Eastern Segment, pegmatite

1248　dykes crosscutting the gneiss fabric suggest relaxation between c. 961 and 934 Ma

1249　(Andersson et al., 1999; Möller et al., 2007; Möller and Söderlund, 1997; Söderlund et al.,

1250　2008b; Söderlund et al., 2002) (iii) In the frontal wedge and the foreland of the orogen, the N-

1251　S trending Blekinge-Dalarna dolerites document a phase of E–W extension between c. 978

1252　and 946 Ma (Fig. 5) (Gong et al., 2018; Ripa and Stephens, 2020d; Söderlund et al., 2005).

1253　　This cumulatively suggests that the Sveconorwegian orogenic plateau was sustained and

1254　grew eastwards until c. 930 Ma, in an overall convergent orogen. Evidence of compression in

1255　the ductile middle crust (infrastructure) to c. 930 Ma contrasts with evidence for extension in

1256　the same time interval in the brittle upper crust (superstructure), and in the brittle foreland of

1257　the orogen.

1258　**5　Review of Sveconorwegian orogenic models**

1259　In light of the evidence summarised and discussed above, we now review and discuss the

1260　orogenic models sketched in Fig. 3 are discussed in more detail in the following.

1261  ***5.1   Early-Sveconorwegian collision-accretion with suture in Bamble-Kongsberg***

1262  The oldest known Sveconorwegian high-grade metamorphism (1150–1120 Ma) is recorded in

1263  the Kongsberg and Bamble lithotectonic units, in the centre of the Sveconorwegian orogen.

1264  This metamorphism could be interpreted to reflect crustal thickening during an early-

1265  Sveconorwegian collision. This interpretation leads to the conceptual model of Fig. 3 a

1266  involving collision or accretion of an exotic Telemarkia microcontinent to the Idefjorden

1267  lithotectonic unit between 1150 and 1120 Ma, closing an intervening ocean and forming the

1268  Bamble-Kongsberg orogenic wedge (Bingen et al., 2008c; Bingen et al., 2005). At least two

1269  arguments rule out the closure of an oceanic realm. (i) The Mesoproterozoic magmatism

1270  exhibits a significant age overlap between the Bamble–Kongsberg, Telemarkia and Idefjorden

1271  lithotectonic units. Specifically, the 1520–1480 Ma magmatic suites, which are prominant in

1272  the Telemarkia lithotectonic unit, extend well into the Bamble, Kongsberg and Idefjorden

1273  lithotectonic units, thus representing a stitching element of these units around c. 1500 Ma

1274  (Fig. 7). (ii) The granulite-facies low-K calc-alkaline Tromøy Complex in Bamble was

1275  formerly interpreted as an early-Sveconorwegian, c. 1200 Ma old, oceanic volcanic arc

1276  (Andersen et al., 2004a; Andersen et al., 2002b; Knudsen and Andersen, 1999). However,

1277  new data demonstrate that the magmatic protolith of the Tromøy Complex is Gothian (1575 ±

1278  44 to 1544 ± 14 Ma) (Bingen and Viola, 2018), meaning that no evidence for remnants of

1279  early-Sveconorwegian oceanic lithosphere is known in the Bamble lithotectonic unit. There is

1280  therefore no actual geological support for the conceptual model sketched in Fig. 3 a.

1281  ***5.2   Early-Sveconorwegian wrench tectonics***

1282  The Bamble and Kongsberg lithotectonic units have been referred to as shear belts in the

1283  literature mostly because of widespread, steep shear foliation zones and penetrative

1284  lithological banding (Starmer, 1991). This intense deformation has inspired tectonic models

1285  (Fig. 3 b) involving long distance early-Sveconorwegian strike-slip transport of the

1286    Telemarkia lithotectonic unit relative to the Idefjorden lithotectonic unit, at the margin of

1287    Fennoscandia, generating a Bamble–Kongsberg transpressional shear belt (Andersen et al.,

1288    2004a; Bingen et al., 2008c; deHaas et al., 1999; Lamminen and Köykkä, 2010). However,

1289    recent field data from the tectonic boundaries between the Bamble, Kongsberg, Telemarkia

1290    and Idefjorden lithotectonic units, and from the centre of the Bamble and Kongsberg

1291    lithotectonic units (Bingen and Viola, 2018; Henderson and Ihlen, 2004; Scheiber et al., 2015)

1292    highlight orthogonal compression and rule out significant wrench tectonics, thus excluding

1293    orogen-scale strike-slip transport. A component of sinistral strike-slip shearing is indeed

1294    recorded by some of the mylonite zones within the Kongsberg lithotectonic unit (Scheiber et

1295    al., 2015). These are, however, compatible with transpressional deformation ensuing only

1296    after the peak of orthogonal deformation and high-grade metamorphism (1150–1120 Ma).

1297    *5.3    Collisional orogeny with suture along the Mylonite Zone*

1298    The Mylonite Zone is a major Sveconorwegian east-southeastward-verging shear zone,

1299    juxtaposing the Eastern Segment beneath the Idefjorden lithotectonic unit. The geological

1300    records of these two units are significantly distinct and, as a consequence, several authors

1301    have argued that the Mylonite Zone may represent a suture zone. An oceanic domain would

1302    have closed at c. 990 Ma between the Eastern Segment, representing the Fennoscandia

1303    continent as lower plate, and distal terranes formed outboard of the Fennoscandia margin in

1304    the west as upper plate (the four western lithotectonic units of the orogen named together

1305    'Sveconorwegia'; Fig. 3 c) (Andersson et al., 2002a; Austin Hegardt et al., 2005; Brueckner,

1306    2009; Cornell et al., 2000; Möller and Andersson, 2018; Möller et al., 2015; Petersson et al.,

1307    2015b). This model envisions the pre-990 Ma (pre-collision) magmatism and metamorphism

1308    west of the Mylonite Zone as formed in a supra-subduction setting, above a west-dipping

1309    subduction zone. At least four arguments support this model. (i) The magmatic records in the

1310    Eastern Segment and in the Idefjorden lithotectonic unit are distinct (Fig. 7). Magmatic suites

1311    do not extend across the Mylonite Zone. (ii) Hallandian metamorphism between 1465 and

1312    1385 Ma is documented only east of the Mylonite Zone (Fig. 6) (Söderlund et al., 2002;

1313    Ulmius et al., 2015). (iii) The Sveconorwegian metamorphism in the Eastern Segment reached

1314    eclogite-facies conditions at c. 990 Ma (Möller et al., 2015), significantly after granulite-

1315    facies metamorphism in the Idefjorden hanging wall at c. 1050 Ma (Söderlund et al., 2008a).

1316    Eclogite-facies metamorphism could record continental burial after closure of an ocean basin

1317    (Möller and Andersson, 2018; Möller et al., 2015). (iv) The Lu–Hf isotopic signature of

1318    magmatic rocks in the 1780–1480 Ma interval documents a geochemical disconnect across

1319    the Mylonite Zone, with an average $\varepsilon_{Hf} = +3.0$ in the Eastern Segment at 1700 Ma against

1320    +4.8 in the Idefjorden lithotectonic unit at 1570 Ma (Petersson et al., 2015a; Petersson et al.,

1321    2015b) (Fig. 8). This difference implies a lower contribution of old continental crust in the

1322    genesis of the magmatic rocks in the Idefjorden lithotectonic unit.

1323    These four pro-arguments, however, are balanced by counterarguments. Specifically (i) the

1324    Orust dolerites (1457 ± 6 Ma) in the Idefjorden lithotectonic unit (Åhäll and Connelly, 1998)

1325    overlap in age with 1465–1385 Ma Hallandian granitic to charnockitic plutonism in the

1326    Eastern Segment. (ii) The Lu–Hf isotopic signature of early-Sveconorwegian magmatism

1327    between 1225 and 1180 Ma is distinctly supra-chondritic in both the Eastern Segment

1328    (bimodal magmatism along the Sveconorwegian front; $+1.2 < \varepsilon_{Hf} < +6.6$) and the Telemarkia

1329    lithotectonic unit (Vråvatn Complex; $+9 < \varepsilon_{Hf} < +10$; Fig. 8) (Andersen et al., 2007;

1330    Petersson et al., 2015a; Söderlund et al., 2005). This signature attests to coeval depleted

1331    mantle derived magmatism on both side of the Mylonite Zone before the presumed ocean

1332    closure at 990 Ma. (iii) The Mylonite Zone (or geological units in its direct proximity) does

1333    not contain any remnants or slivers of pre- to early-Sveconorwegian (1340–1080 Ma) marine

1334    sedimentary sequences, oceanic lithosphere, oceanic volcanic arc, or ultramafic rocks, such

1335    that no suture zone can be directly constrained.

1336      To conclude, closure of an oceanic basin along the Mylonite Zone at c. 990 Ma represents

1337    a plausible model (Fig. 3 c) (Möller and Andersson, 2018). However, the evidence is not

1338    conclusive at this point of research. In the following text, we do not select this model as the

1339    most probable.

1340    *5.4   Non-collisional (Andean type) orogeny*

1341    In the non-collisional (Andean type) orogenic models (Fig. 3 e, f), the Sveconorwegian

1342    orogen represents an active margin of Fennoscandia, evolving from at least 1280 Ma to after

1343    900 Ma, above an oceanic plate subducting to the east into a trench situated to the west of the

1344    exposed orogen (Falkum and Petersen, 1980; Slagstad et al., 2013). The geological record in

1345    the Sveconorwegian orogen is explained by changes in the conditions of subduction, such as

1346    trench position, subduction angle, convergence rate, convergence direction and age of the

1347    oceanic lithosphere. This model is an adaptation of the tectonic switching model (Collins,

1348    2002; Haschke et al., 2002), which is based on the observation that a retreating or steepening

1349    oceanic subduction is associated with an extensional tectonic regime and abundant

1350    magmatism in the (supra-subduction) upper plate, while an advancing or flattening subduction

1351    is associated with compression, metamorphism and magmatic quiescence.

1352      Different versions of the non-collisional (Andean type) model have been proposed by

1353    Slagstad et al. (2020; 2018; 2017; 2013) and Granseth et al. (2020). These models offer an

1354    elegant and flexible framework for the orogeny. However, we think that they are

1355    irreconcilable with a number of key features and concepts. (i) In its simple expression, the

1356    tectonic switching model predicts either extension or compression in the upper (supra-

1357    subduction) plate. During the main Sveconorwegian orogeny, voluminous magmatism (mafic

1358    and felsic) in the Telemarkia lithotectonic unit would indicate a retreating subduction trench

1359    between 1065 and 1020 Ma, while HP granulite facies metamorphism in the Idefjorden

1360    lithotectonic unit (Söderlund et al., 2008a) would indicate an advancing trench in the same

1361    time interval, in contradiction with the model. (ii) Conceptually, an eastwards oceanic

1362    subduction to the west of the orogen can hardly represent the driving force for westwards

1363    underthrusting of the Eastern Segment at c. 990 Ma to eclogite-facies conditions. Considering

1364    the presumably weak rheology of the lithosphere in the Telemarkia lithotectonic unit around

1365    990 Ma, it is unlikely that compressive stresses from a plate subducting west of the orogen

1366    could be effectively transmitted at least 400 km to the east to the Eastern Segment. (iii) The

1367    Sveconorwegian magmatism (1065–915 Ma) does not represent typical volcanic arc

1368    magmatism. The geochemical signature and petrology of magmatic suites can be related to

1369    lower crustal sources and partial melting conditions (Granseth et al., 2020; Vander Auwera et

1370    al., 2008; Vander Auwera et al., 2011), rather than to an active subduction. The geochemical

1371    signature of the Sirdal magmatic belt (1065–1020 Ma) can be interpreted in both a collisional

1372    setting or a supra-subduction setting (see above). The magmatism between 985 and 915 Ma

1373    lacks a subduction signature and the dry nature of AMC magmatism is not compatible with a

1374    supra-subduction setting (see above). The magmatism between 935 and 915 Ma is exposed

1375    over a zone at least 350 km wide, much larger than a typical volcanic arc. The geographical

1376    polarity of the magmatism in the 935–915 Ma time interval, involving dry plutonism of the

1377    AMC suite in the west and water-bearing plutonism of the HBG suite in the east is opposite to

1378    what should be expected from an east dipping subduction system.

1379        For these different reasons, we remain sceptical that an oceanic subduction in the

1380    hinterland of the orogen could have steered tectonic forces and magmatism inside the orogen

1381    during the main Sveconorwegian orogeny (1065–900 Ma). The non-collisional models

1382    proposed by Slagstad et al. (2020; 2018) omit to propose specific tectonic driving forces,

1383    either oceanic subduction or continental subduction-delamination inside the orogen, to explain

1384    the metamorphism with high-pressure signature in the Bamble–Kongsberg lithotectonic units

1385    (1150–1120 Ma), Idefjorden lithotectonic unit (c. 1050 Ma) and Eastern Segment (c. 990 Ma).

1386    In a recent version of the non-collisional model (Slagstad et al., 2020), the margin of

1387    Fennoscandia is proposed to have been fragmented (into micro-continents) by extension

1388    before c. 1150 Ma and re-amalgamated during the Sveconorwegian orogeny between c. 1150

1389    and 980 Ma to form the Sveconorwegian orogen. However, as discussed previously in this

1390    chapter, there is no evidence between the lithotectonic units for (i) marine sediment sequences

1391    that could represent marine basins, (ii) ophiolites or oceanic volcanic arcs that could represent

1392    oceanic basins, or (iii) ultramafic bodies that could represent exhumed hyperextended

1393    domains. As noted earlier, the low-K calc-alkaline Tromøy Complex in Bamble (Andersen et

1394    al., 2004a) should not be interpreted as an early-Sveconorwegian oceanic volcanic arc

1395    (Bingen and Viola, 2018).

1396    *5.5    Collisional orogeny with suture west of the orogen*

1397    The Grenville orogen is the archetypal example of a large (> 600 km wide) and hot

1398    Mesoproterozoic collisional orogen (Fig. 1) (Gower et al., 2008; Jamieson and Beaumont,

1399    2013; Rivers, 2008, 2012). The Grenville orogeny was long lived (> 110 Myr). It propagated

1400    from a weak Proterozoic lithosphere into the cratonic Archean foreland, with thrusting along

1401    two orogen parallel, continuous, crustal-scale shear zones (the Allochthon Boundary Thrust

1402    and Grenville Front) and two main phases of orogenic convergence (the Ottawan, 1090–1020

1403    Ma, and Rigolet, 1010–980 Ma, phases; Fig. 1). Protracted high-temperature–low-pressure

1404    high-grade metamorphism in the hinterland, associated with both crustal- and mantle-derived

1405    magmatism, was coeval with comparatively short-lived high-pressure metamorphism in thick

1406    thrust slices towards the foreland (Groulier et al., 2018a; Indares, 2020; Rivers, 2008). The

1407    first order architecture of the Sveconorwegian orogen and its orogenic evolution are

1408    comparable to that of the Grenville orogen (Cawood and Pisarevsky, 2017; Gower, 1985;

1409    Gower et al., 2008; Hoffman, 1991; Rivers, 2008, 2012). An analogy in the geodynamic

1410    evolution is therefore natural.

1411    In the collisional models (Fig. 3 d), closure of (one or several) oceanic basin(s) to the west

1412    of the exposed orogen was followed by the collision of Baltica (Fennoscandia) with (one or

1413    several) continental plate(s) at and after 1065 Ma (Bingen et al., 2008c; Bogdanova et al.,

1414    2008; Cawood and Pisarevsky, 2017; Gower et al., 2008; Ibanez-Mejia et al., 2011; Li et al.,

1415    2008; Pisarevsky et al., 2014; Stephens and Wahlgren, 2020b; Weber et al., 2010).

1416    Consumption of these oceanic basins involved subduction and formation of volcanic arcs,

1417    either at the margin of Fennoscandia or in an outboard position prior to final collision. During

1418    collision, the Sveconorwegian orogen was situated in the upper plate position, on the

1419    Fennoscandia side of the main suture zone.

1420    Here are some key features supporting the collisional model for the main Sveconorwegian

1421    orogeny (1065–900 Ma). (i) The Sveconorwegian orogen is c. 550 km wide, i.e. wider than

1422    any present-day Andean orogen. It exhibits a c. 550 km wide zone of convergent tectonics

1423    (1065–930 Ma) and a c. 350 km wide zone of syn-orogenic magmatism (Fig. 5). (ii) The

1424    orogen has the structure of an extended (collapsed) orogenic plateau, with the juxtaposition of

1425    high-grade gneiss complexes representing a middle crustal infrastructure, against low-grade

1426    supracrustal rocks representing a brittle superstructure, and plutons representing the product

1427    of lower- to middle-crustal melting during orogeny (Fig. 4) (Andersen et al., 2001; Granseth

1428    et al., 2020; Vander Auwera et al., 2011). The gneiss complexes carry evidence for protracted

1429    (> 110 Myr) middle-crustal high-temperature-low-pressure metamorphism (Bingen et al.,

1430    2008b; Blereau et al., 2017; Laurent et al., 2018a; Laurent et al., 2018b; Slagstad et al., 2018).

1431    (iii) High pressure granulite- and eclogite-facies rocks attest to crustal thickening, up to c. 70

1432    km, between c. 1050 and 990 Ma (Möller and Andersson, 2018; Söderlund et al., 2008a).

1433    After peak metamorphism, these rocks were incorporated and overprinted into the middle-

1434    crustal infrastructure. They were probably more abundant in the orogen than what is apparent

1435    from their exposure. (iv) The orogenic zone grew towards the foreland, in a stepwise fashion

1436    with time. This process involved thrusting along crustal scale shear zones (Mylonite Zone and

1437    Sveconorwegian front). This pattern is typical of collision orogens (Royden et al., 2008). (v)

1438    The orogenic zone lacks evidence for syn-orogenic marine sedimentary sequences, in spite of

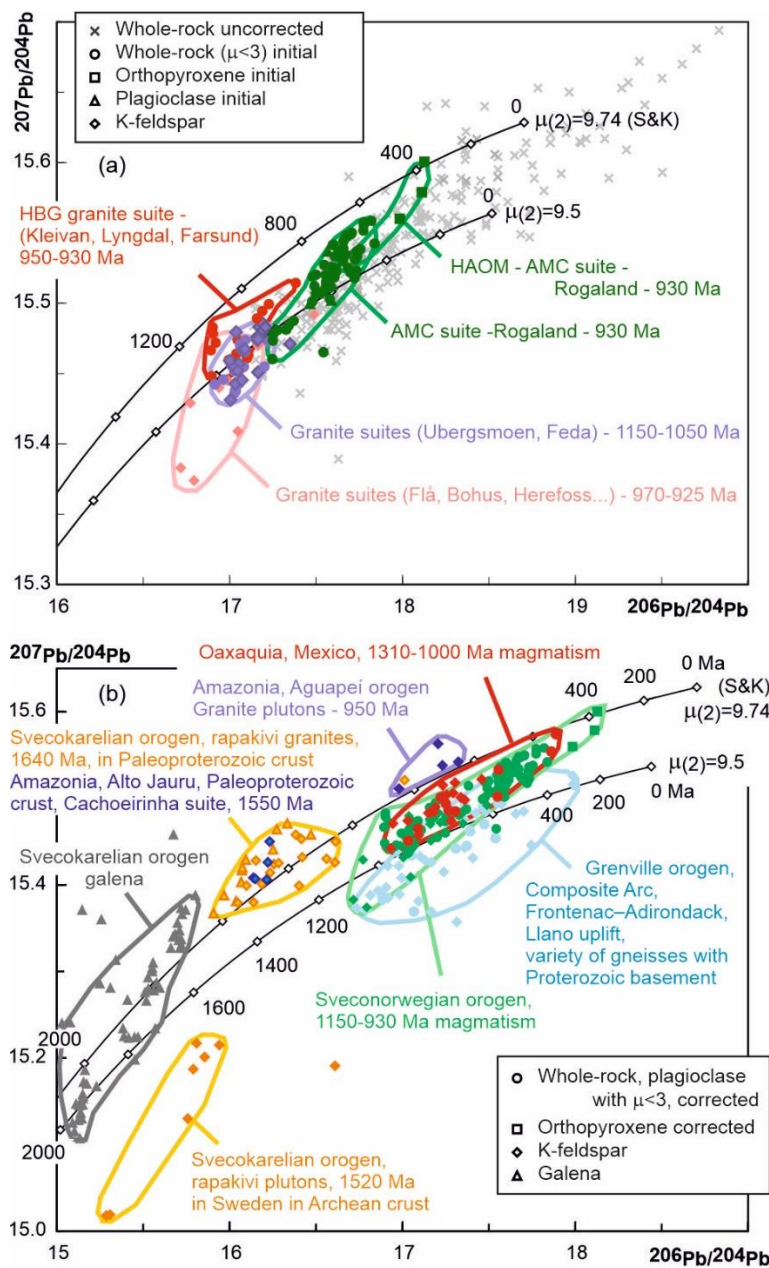1439    a largely exposed superstructure (Fig. 4), and therefore was above sea-level during the entire

1440    orogeny.

1441    -------------------



1443    **Figure 16.** Common Pb isotopic composition in the $^{206}Pb/^{204}Pb$ vs. $^{207}Pb/^{204}Pb$ diagram, with

1444    reference growth curves of terrestrial common Pb ($\mu_{(2)}$ = 9.74 (Stacey and Kramers, 1975) and

1445    $\mu_{(2)} = 9.5$, with $\mu = ^{238}U/^{204}Pb$). (a) Compilation of data from the Sveconorwegian orogen.

1446    Highlighted symbols represent initial ratio of plutonic suites dated between 1150 and 930 Ma.

1447    Initial ratio (ratio corrected for U decay since intrusion) is calculated for analyses of K-

1448    feldspar, plagioclase, orthopyroxene and whole-rock with $\mu < 3$. The initial ratio of plutonic

1449    rocks defines a short trend below the reference growth curve of Stacey and Kramers (1975).

1450    High alumina orthopyroxene megacrysts (HAOM) hosted in the anorthosite plutons are

1451    situated at the radiogenic (upper-right) end of the trend. They are interpreted to represent a

1452    mafic, mantle-derived, underplate, formed at c. 1040 Ma and remelted at c. 930 Ma. The

1453    granite plutons partly sourced from metasedimentary protoliths, like the Flå and Bohus

1454    muscovite-bearing plutons, are situated at the less radiogenic (lower-left) end of the trend.

1455    The hornblende-biotite granite plutons, ranging from c. 1150 to 930 Ma, sourced from

1456    metaigneous protoliths, cluster in the centre of the trend (Andersen, 1997; Andersen et al.,

1457    2001; Andersen et al., 1994; Andersen and Munz, 1995; Bingen et al., 1993; Vander Auwera

1458    et al., 2014a; Weis, 1986). (b) Compilation of initial isotopic compositions for Baltica

1459    (Fennoscandia) and selected late-Mesoproterozoic orogenic belts. Data for the

1460    Sveconorwegian orogen are copied from panel (a). A variety of ortho- and paragneisses from

1461    the hinterland of the Grenville orogen, including the Composite Arc (Ontario), Frontenac-

1462    Adirondack (Ontario) and Llano uplift (Texas) overlap with the data of the Sveconorwegian

1463    orogen, as well as orthogneisses from the Oaxaquia lithotectonic unit (Mexico) (Cameron et

1464    al., 2004; DeWolf and Mezger, 1994). Granite plutons (950 Ma) in the Aguapei Belt in

1465    Amazonia are characterized by a more radiogenic [207]Pb signature than coeval rocks in the

1466    Sveconorwegian orogen, consistent with involvement of an older Paleoproterozoic basement

1467    in this orogen (Geraldes et al., 2001). Data for rapakivi granite plutons from Fennoscandia on

1468    Paleoproterozoic and Archean basement, as well as Paleoproterozoic galena deposits from the

1469    Svecokarelian orogen are shown for reference (Andersson et al., 2002b; Rämö, 1991;

1470    Vaasjoki, 1981).

1471    *5.6    Conjugate margins in Rodinia*

1472    In classical Rodinia assembly models, Laurentia and Baltica were probably already

1473    contiguous at low latitudes at c. 1260 Ma as part of Nuna (Columbia), facing an ocean, the

1474    Mirovoio ocean (Buchan et al., 2000; Evans and Mitchell, 2011; Pisarevsky et al., 2014;

1475    Zhang et al., 2012). Opening of the Asgard sea (north of Baltica; Fig. 1), clockwise rotation

1476    and drift of Baltica relative to Laurentia, and consumption of the Mirovoio ocean (south of

1477    Baltica) led to collision of Amazonia with Laurentia and Baltica, involving three sequential

1478    tectonic phases (Bogdanova et al., 2008; Cawood and Pisarevsky, 2017; Gower et al., 2008;

1479    Hynes and Rivers, 2010; Ibanez-Mejia et al., 2011; Johansson, 2009; Li et al., 2008;

1480    Pisarevsky et al., 2014; Roberts, 2013; Tohver et al., 2004a; Weber et al., 2010). (i) Collision

1481    between Amazonia and the southwestern part of Laurentia starting at c. 1200 Ma and

1482    generating the Llano section of the Grenville orogen and the Sunsás orogen (Fig. 1). (ii)

1483    Sinistral transpression between Amazonia and Laurentia, between c. 1150 and 1050 Ma,

1484    generating the Grenville orogen. (iii) Collision between Amazonia and Baltica at c. 1060 Ma,

1485    following closure of the intervening oceans, producing the Sveconorwegian and Putumayo

1486    orogens (Fig. 1) (Boger et al., 2005; Ibanez-Mejia et al., 2011; Tohver et al., 2004b; Tohver et

1487    al., 2005).

1488    Following Cawood et al. (2010), a subduction system was initiated along the northern open

1489    margin of Rodinia (Asgard sea; Fig. 1) after the Amazonia–Laurentia–Baltica collision (i.e.

1490    after 1000 Ma). In this model, Tonian sediments sequences and volcanic and plutonic rocks

1491    hosted in variably far-travelled nappes of the Caledonides of NE Greenland, Scandinavia,

1492    Svalbard and Scotland (Augland et al., 2014; Cawood and Pisarevsky, 2017; Cawood et al.,

1493    2015; Corfu, 2019; Cutts et al., 2009; Kalsbeek et al., 2000; Kirkland et al., 2006, 2007) are

1494 interpreted as fragments of an accretionary orogen, the Valhalla orogen, at the margin of

1495 Rodinia (Fig. 1). An orogenic phase, including magmatism, metamorphism, and deformation

1496 (Renlandian) took place between 980 and 910 Ma (Cawood et al., 2010), therefore

1497 overlapping with metamorphism in the Sveconorwegian orogen (Table 1).

1498 Several Mesoproterozoic basement inliers in the Andes of Colombia (Garzón, Las Minas)

1499 and in Mexico (Oaxaquia lithotectonic unit) are characterized by high-grade metamorphism,

1500 dated consistently between 1000 and 980 Ma (Zapotecan-Putumayo orogenies). These

1501 lithotectonic units are interpreted as oceanic volcanic arcs formed in ocean tracts between

1502 Laurentia, Amazonia and Baltica (after c. 1460 Ma) (Fig. 12 a, b) and involved in the

1503 collision zone between these plates (Fig. 1) (Cardona et al., 2010; Cordani et al., 2005;

1504 Ibanez-Mejia et al., 2015; Ibanez-Mejia et al., 2011; Jiménez-Mejía et al., 2006; Keppie et al.,

1505 2003; Keppie and Ortega-Gutiérrez, 2010; Weber and Köhler, 1999; Weber et al., 2010).

1506 In archetypal Rodinia reconstructions (Fig. 1), the hinterland of the Sveconorwegian

1507 orogen is facing Mesoproterozoic basement inliers in the Andes of Colombia (Garzón, Las

1508 Minas) and in Mexico (Oaxaquia lithotectonic unit) and the hinterland of the Grenville

1509 orogen. The isotopic signature of these units is compared in a $\varepsilon$Nd vs. time diagram (Fig. 13

1510 b). The Quebecia and Telemarkia lithotectonic units, located in the hinterland of the exposed

1511 Grenville and Sveconorwegian orogens respectively, represent coeval continental growth

1512 zones generated by volcanic arc and back arc magmatism between c. 1520 and 1480 Ma

1513 (Pinwarian and Telemarkian phases; Table 1; Fig. 13 b) (Dickin and Higgins, 1992; Groulier

1514 et al., 2018b). These units are characterized by very similar isotopic evolution trends starting

1515 from close to the Depleted Mantle reservoir at and after 1520 Ma and decreasing along a

1516 continental recycling trend to near-chondritic value at c. 1000 Ma. The basement inliers in the

1517 Andes of Colombia (Garzón, Las Minas) and in Mexico (Oaxaquia lithotectonic unit) define

1518 evolution trends starting at c. 1380 Ma and 1300 Ma, respectively, that overlap with the

1519    Telemarkia trend (Ibanez-Mejia et al., 2015; Lawlor et al., 1999; Weber and Köhler, 1999). In

1520    the hinterland of the Grenville Belt, the Composite Arc and Frontenac–Adirondack

1521    lithotectonic units define the most juvenile trend, starting at c. 1380 Ma (Fig. 13 b) (Daly and

1522    McLelland, 1991; Dickin et al., 2010; Marcantonio et al., 1990). These units are interpreted as

1523    marginal or outboard volcanic arcs, back-arcs and microcontinents assembled (or

1524    reassembled) to Laurentia early during the Grenvillian orogeny (Shawinigan phase, 1190–

1525    1140 Ma) (Carr et al., 2000; Hanmer et al., 2000; Rivers, 2008). Interestingly, the 1280-1200

1526    Ma magmatism in the Composite Arc (Elzevirian) has a Nd isotopic signature approaching

1527    that of the Depleted Mantle reservoir (Carr et al., 2000; Corfu and Easton, 1995; Corriveau

1528    and van Breemen, 2000; Dickin and McNutt, 2007), very similar to the one of coeval 1280–

1529    1200 Ma continental magmatism in the Sveconorwegian orogen (Sæsvatn–Valldal bimodal

1530    volcanism) (Brewer et al., 2004).

1531        In the $^{206}Pb/^{204}Pb$ vs. $^{207}Pb/^{204}Pb$ diagram (Fig. 16), the initial isotopic composition of

1532    Sveconorwegian plutonic rocks intruded between 1150 and 930 Ma defines a short trend

1533    below the evolution curve of terrestrial common Pb of Stacey and Kramers (1975) ($\mu_{(2)}$ =

1534    9.74). Ortho- and paragneisses from the hinterland of the Grenville Belt, including the

1535    Composite Arc (Ontario), Frontenac-Adirondack (Ontario) and Llano uplift (Texas) and

1536    orthogneisses from the Oaxaquia lithotectonic unit (Mexico) overlap with the data of the

1537    Sveconorwegian orogen (Cameron et al., 2004; DeWolf and Mezger, 1994).

1538        To summarize, Nd and Pb isotopic data (Fig. 13; Fig. 16) and detrital zircon data (Fig. 12)

1539    underscore the existence of juvenile lithotectonic units generated at and after c. 1520 Ma

1540    exposed in the hinterland of the Grenville and Sveconorwegian orogens and the basement

1541    inliers in the Andes of Colombia (Garzón, Las Minas) and in Mexico (Oaxaquia lithotectonic

1542    unit). These isotopic data therefore support to join these lithotectonic units in the core of the

1543    collision zone between Laurentia, Amazonia and Baltica, in a classical Rodinia reconstruction

1544    (Fig. 1). These data also suggest that, in the collision model of Fig. 3 d, the continental margin

1545    colliding with the Sveconorwegian orogen possessed a weak lithosphere similar to the one of

1546    the Telemarkia lithotectonic unit (as opposed to a stronger cratonic lithosphere).

1547    **6     Model of large, hot and long-duration continental collision**

1548    The previous discussion argues for a collisional model for the main Sveconorwegian orogeny.

1549    Here, we further develop a model of large, hot and long-duration continent-continent collision

1550    starting at c. 1065 Ma, wherein the five lithotectonic units of the orogen are endemic to

1551    Fennoscandia (Fig. 3 d). The plate tectonic interpretation of the pre-collision evolution

1552    between 1280 and 1080 Ma is still largely speculative. The model is fitted into a classical

1553    Rodinia assembly framework (Fig. 1), involving an Amazonia-Laurentia-Baltica collision, as

1554    discussed previously. However, the model is based upon evidence from within the exposed

1555    Sveconorwegian orogen (and its foreland) and therefore independent of Rodinia models.

1556    -------------------
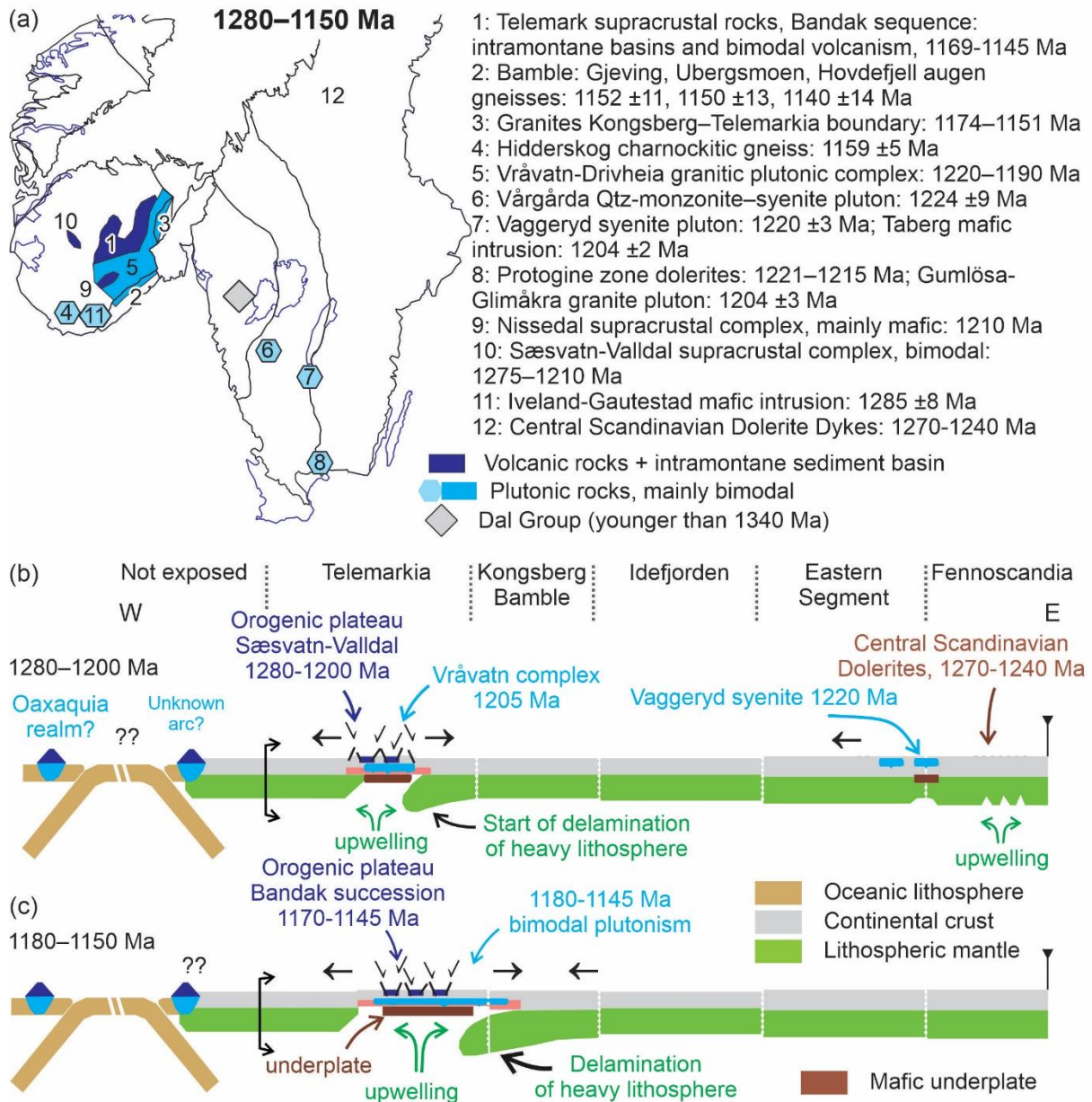
**Figure 17.** Schematic geodynamic model for the 1280–1150 Ma time interval. (a) Sketch map of the Sveconorwegian orogen, with position and list of plutonic and supracrustal complexes. (b, c) Interpretative E-W cross sections of the Sveconorwegian orogen and speculative linkage westwards. The exposed part of the orogen is limited by an arrowed bracket. The limit between lithotectonic units is schematically represented by a white vertical dashed line. References and explanations in the text.

--------------------
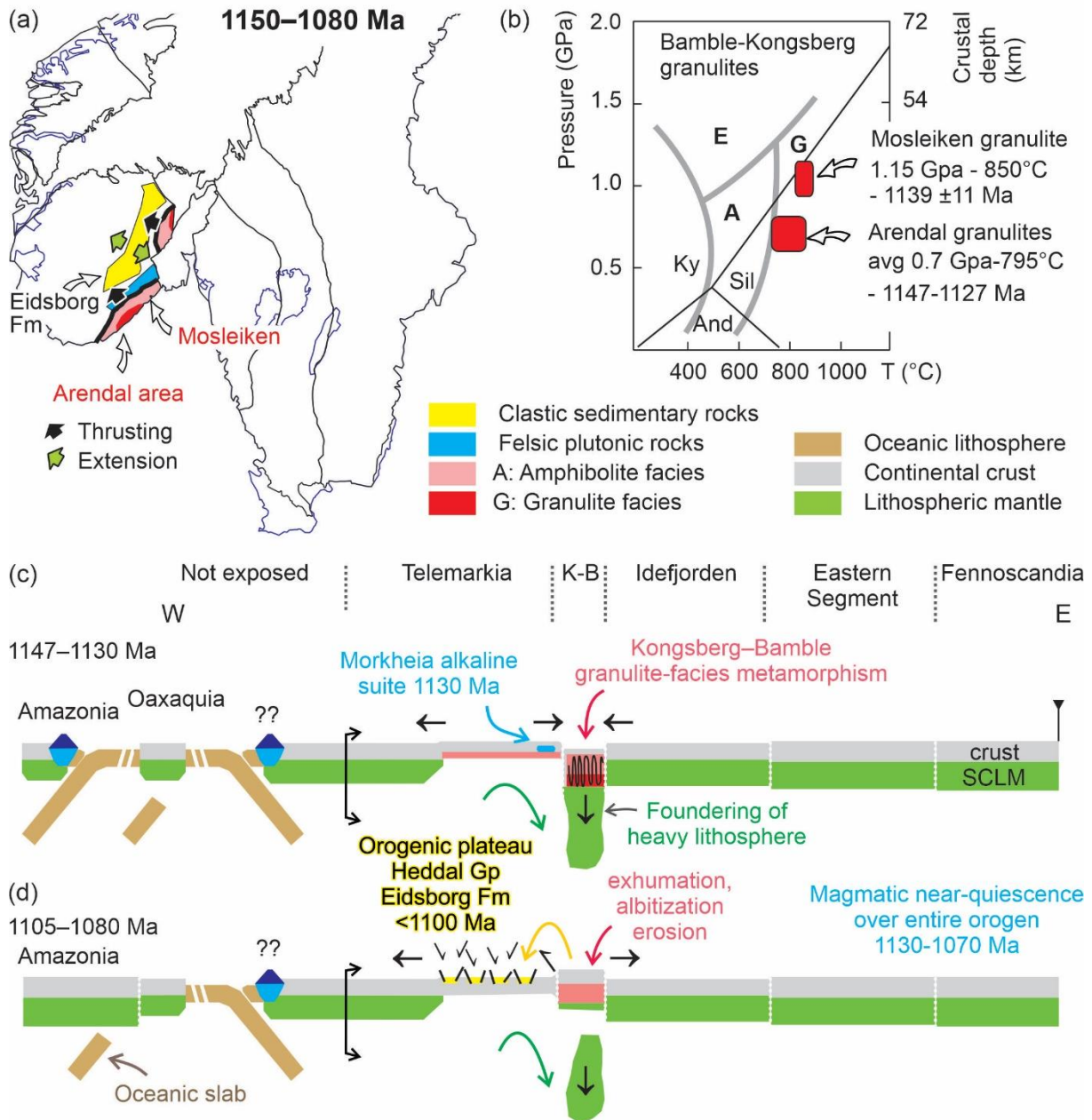
**Figure 18.** Schematic geodynamic model for the 1150–1080 Ma time interval. (a) Sketch map of the Sveconorwegian orogen, with distribution of metamorphism, magmatism and clastic sediment basins. (b) Pressure-temperature diagram with fields of the main metamorphic facies following Spear (1993): E: eclogite facies, G: granulite facies, A: amphibolite facies. (c, d) Interpretative E-W cross sections of the Sveconorwegian orogen and speculative linkage westwards. Explanations and references in the text.

--------------------

1573 ***6.1    1280–1080 Ma, pre-collision: lithospheric mantle delamination***

1574 The geological record for the pre- to early-Sveconorwegian 1280-1080 Ma time interval is

1575 very distinct in the Telemarkia, Kongsberg–Bamble and Idefjorden lithotectonic units.

1576 Abundant bimodal magmatism between 1280 and 1145 Ma, and protracted (upper) crustal

1577 extension in Telemarkia between 1280 and 1080 Ma (Fig. 17; Fig. 18) contrast with

1578 amphibolite- to granulite-facies metamorphism and shortening in the Kongsberg–Bamble

1579 lithotectonic units between 1150 and 1120 Ma (Fig. 18). Except for a few dolerite dykes, the

1580 Idefjorden lithotectonic unit is lacking evidence for magmatism, metamorphism and

1581 deformation between 1280 and 1080 Ma, and therefore it is regarded as having played the role

1582 of a passive buttress during this time interval. There is no evidence for closure of marine or

1583 oceanic basins between the Telemarkia, Kongsberg–Bamble and Idefjorden lithotectonic units

1584 (Scheiber et al., 2015). These different features cannot be explained by a simple model of

1585 regional scale inversion from extension to compression at c. 1150 Ma, as one would anticipate

1586 compression structures to be located in the weakest Telemarkia lithosphere, or distributed

1587 evenly throughout the Telemarkia, Bamble and Kongsberg lithotectonic units.

1588   In Fig. 17, we propose that upwelling of asthenosphere and development of an orogenic

1589 plateau started at c. 1280 Ma in the Telemarkia lithotectonic unit. Repeated pulses of bimodal

1590 magmatism between 1280 and 1145 Ma provide evidence for upwelling and decompression

1591 melting of asthenospheric mantle (Fig. 7). The most prominent mafic volcanic rocks (Fig. 11;

1592 Sæsvatn–Valldal, Nissedal, Morgedal and Gjuve metabasalts) exhibit a within-plate

1593 geochemical signature and supra-chondritic Nd isotopic signature ($+2.6 < \varepsilon_{Nd} < +6.3$)

1594 implying sourcing in the asthenosphere (Fig. 13 a) (Brewer et al., 2002; Brewer et al., 2004;

1595 Spencer et al., 2014). The voluminous felsic gneisses of the Vråvatn Complex (1220–1190

1596 Ma) have Hf isotopic signature of zircon ($+9 < \varepsilon_{Hf} < +10$) also close to the depleted mantle

1597 reservoir at 1210 Ma ($\varepsilon_{Hf} = +12$) (Fig. 8) (Andersen et al., 2007). These values indicate that

1598 the Vråvatn Complex was not produced principally by partial melting of the Telemarkian

1599 (1520–1480 Ma) crust. Rather, it was probably produced by partial melting of a mafic lower

1600 crust or mafic underplate, itself produced shortly before in the depleted mantle (a maximum

1601 of some 50 Mys before 1210 Ma; Andersen et al., 2007). The earliest magmatism between

1602 1280 and 1190 Ma occurred in the centre of the Telemarkia lithotectonic unit (Vråvatn,

1603 Nissedal, Sæsvatn–Valldal, Iveland-Gautestdad; Fig. 6; Fig. 17) while younger magmatism

1604 between 1170 and 1140 Ma is more abundant towards the periphery of the lithotectonic unit

1605 (mainly eastwards and southwards) and is well recorded into the Kongsberg and Bamble

1606 lithotectonic units. This geographic distribution suggests that mantle upwelling affected

1607 progressively a larger area between c. 1280 and 1145 Ma (Fig. 17).

1608 Upwelling of hot asthenosphere at c. 1280 Ma induced partial melting at the base of the

1609 crust. This weakening of the lower crust possibly initiated decoupling between the crust and

1610 the lithospheric mantle and progressive delamination of the lithospheric mantle between c.

1611 1280 and 1145 Ma. Alternatively, protracted upwelling of asthenosphere between 1280 and

1612 1145 Ma progressively induced convective removal (or displacement) of the continental

1613 lithospheric mantle. Both interpretations resulted in uplift, formation of a plateau and

1614 extension in the crust (Dewey, 1988; Li et al., 2016).

1615 Evidence for an orogenic plateau involving uplift and extension in the upper crust is

1616 provided by the sedimentology of low-grade sedimentary rocks deposited between 1260 and

1617 1080 Ma in Telemarkia. The sediments of the Bandak succession are high-energy immature

1618 deposits, accumulated in continental (above sea level) intermontane basins (Bingen et al.,

1619 2003; Köykkä, 2011; Lamminen, 2011; Spencer et al., 2014). The limited lateral extent of the

1620 basin infills, the existence of at least two major internal unconformities in the Bandak

1621 succession, and the direct evidence for normal syn-sedimentary growth faults, suggest active

1622 extension during accumulation (Fig. 11; Fig. 12) (Laajoki, 2002; Laajoki et al., 2002;

1623    Lamminen, 2011). This orogenic plateau does not satisfy to the definition of a Tibetan

1624    orogenic plateau, as evidence for crustal thickening and protracted metamorphism is lacking

1625    in the 1280–1080 Ma time interval inside the Telemarkia lithotectonic unit.

1626        Compression in the Kongsberg–Bamble lithotectonic units in the interval between 1150

1627    and 1120 Ma can be explained by compression at the margin of the plateau and foundering

1628    (subduction) below the Kongsberg–Bamble lithotectonic units of the lithospheric mantle slab

1629    delaminated below Telemarkia (Fig. 18). We suggest that the pull effect of foundering

1630    generated subsidence in the crust, high-grade metamorphism (up to 1.15 GPa) and

1631    deformation with lithological banding and commonly steep lineation in Kongsberg–Bamble

1632    between 1150 and 1120 Ma.

1633        Eventual breakoff of the mantle slab triggered exhumation of the Bamble and Kongsberg

1634    lithotectonic units after 1120 Ma (Fig. 18 d). The volumetrically minor alkaline Morkheia

1635    monzonite suite, located just north of the Bamble–Telemarkia boundary zone, may record this

1636    event with local melting of a sliver of lithospheric mantle at c. 1134–1130 Ma (Fig. 18 c)

1637    (Heaman and Smalley, 1994). Exhumation to upper crustal levels (1105–1080 Ma) was

1638    associated with northwestwards thrusting of Bamble and westwards thrusting of the

1639    Kongsberg onto Telemarkia and reworking of plutons emplaced shortly before the foundering

1640    process (Henderson and Ihlen, 2004; Scheiber et al., 2015). Exhumation of the Bamble and

1641    Kongsberg lithotectonic units after 1105 Ma was associated with fluid-rock interaction,

1642    albitization and scapolitization (Engvik et al., 2017). Erosion provided the clastic material

1643    stored in the Heddal Group and Eidsborg Formation in Telemarkia (Fig. 6; Fig. 11; Fig. 12;

1644    Fig. 18).

1645        The plate tectonic context and paleogeographic setting of this pre- to early-

1646    Sveconorwegian asthenosphere upwelling, plateau development and sub-continental

1647    lithospheric mantle delamination model is difficult to assess. The asthenosphere upwelling

1648    could be related to a deep mantle plume, similar to the ones that generated the four mafic

1649    dyke swarms of the Central Scandinavian dolerites in the cratonic center of Fennoscandia

1650    between c. 1271 and 1246 Ma (Brander et al., 2011; Söderlund et al., 2006), and dolerites

1651    along the Sveconorwegian front (Protogine zone dolerites) between 1221 and 1215 Ma

1652    (Söderlund et al., 2005) (Fig. 17). Alternatively, in recent paleogeographic models (Cawood

1653    and Pisarevsky, 2017), the Sveconorwegian orogen (Telemarkia–Bamble–Kongsberg

1654    lithotectonic units) is located in a continent back-arc position on the Fennoscandia side of an

1655    active volcanic arc, in the 1280–1080 Ma interval, during consumption of the oceans between

1656    Baltica, Amazonia and Laurentia (Fig. 17; Fig. 18) (Bingen et al., 2003; Brewer et al., 2002;

1657    Roberts and Slagstad, 2015; Slagstad et al., 2017; Spencer et al., 2014). This arc would be

1658    located to the west of the exposed orogenic belt and possibly disappeared by tectonic erosion

1659    (Spencer et al., 2014). A Cenozoic analogue to this Mesoproterozoic evolution would be

1660    plateau building and lithospheric delamination in the Colorado Plateau and the North

1661    American Cordillera (Bao et al., 2014; Levander et al., 2011).

1662    -------------------
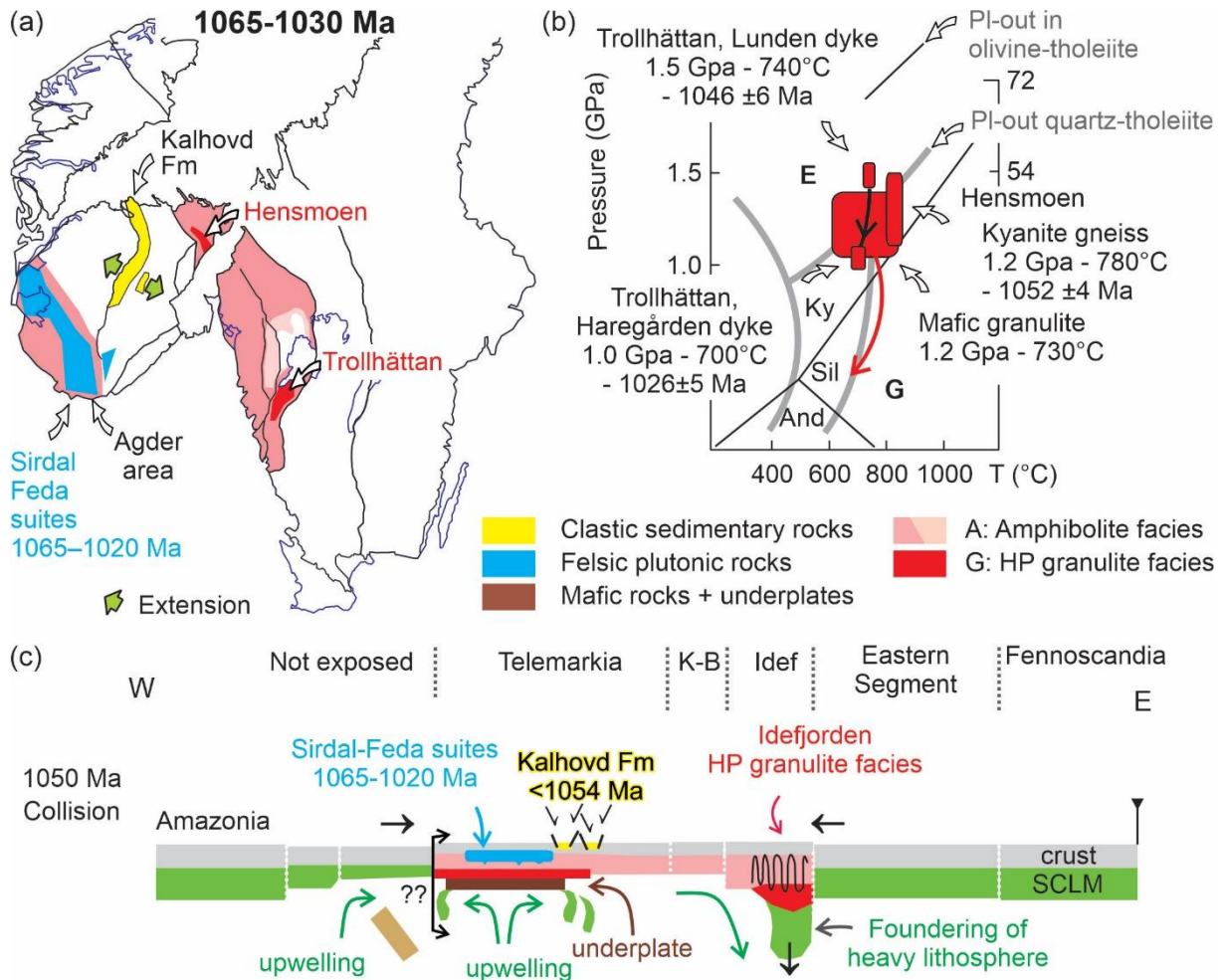
**Figure 19.** Schematic geodynamic model for the 1065–1030 Ma time interval. (a) Sketch map of the Sveconorwegian orogen, with distribution of metamorphism, magmatism and clastic sediment basins. (b) Pressure-temperature diagram. (c) Interpretative E-W cross section. Explanations and references in the text.
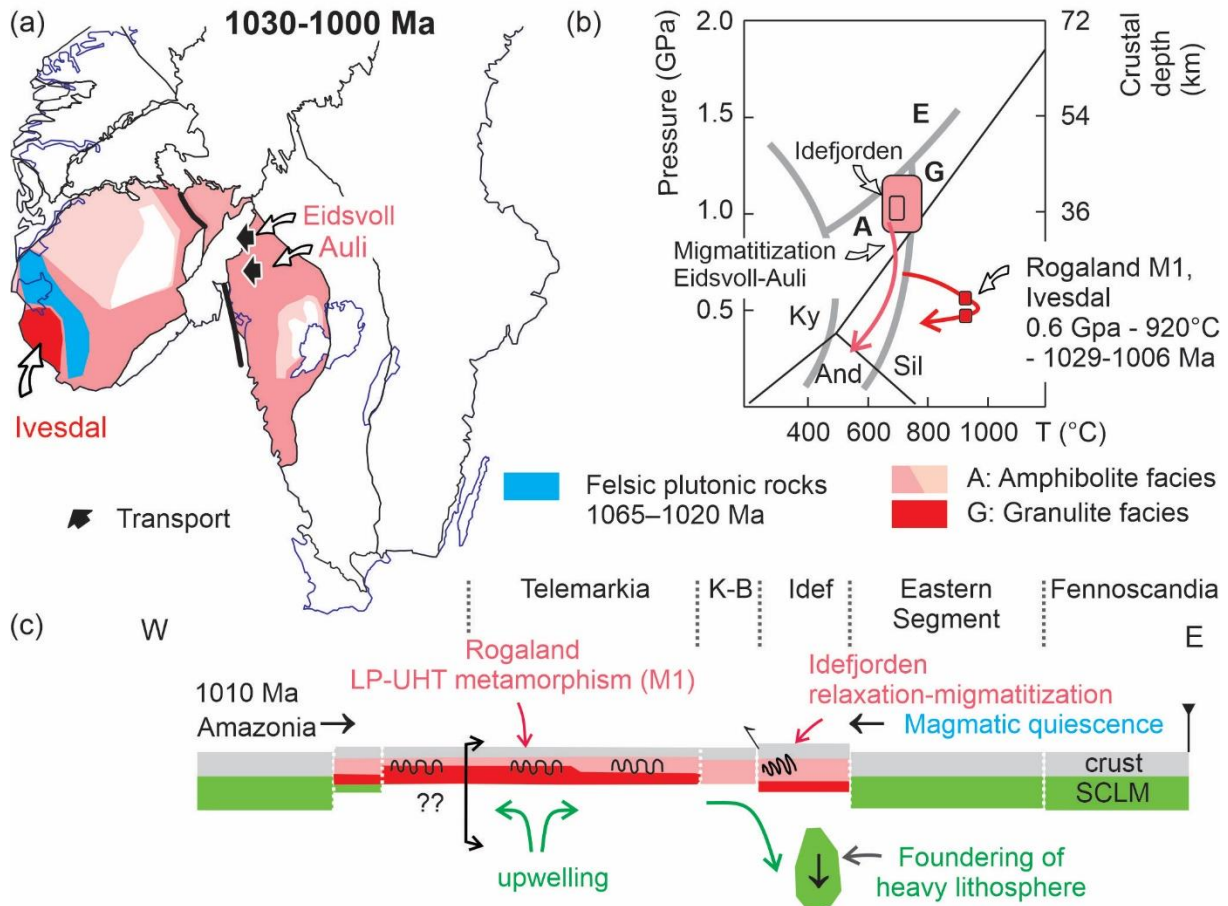
--------------------

**Figure 20.** Schematic geodynamic model for the 1030–1000 Ma interval. (a) Sketch map of the Sveconorwegian orogen, with distribution of metamorphism and magmatism. (b) Pressure-temperature diagram. (c) Interpretative E-W cross section. Explanations and references in the text.

--------------------

### 6.2   1065–1000 Ma: main Sveconorwegian continental collision

After a period of quiescence, the orogenic zone grew substantially around 1065 Ma, both eastwards (continentwards) and westwards, to include the entire Idefjorden and Telemarkia lithotectonic units (Fig. 19; Fig. 20). Widespread compressional deformation, high-grade metamorphism, partial melting and magmatism are recorded in these units between 1065 and 1000 Ma (Agder phase). Little is recorded in the Kongsberg–Bamble lithotectonic units, which were exhumed to high crustal levels (superstructure) and juxtaposed as reflected by

1682     their current position before 1080 Ma. High-pressure granulite facies metamorphism in the

1683     Idefjorden lithotectonic unit, dated to c. 1050 Ma, contrasts with the voluminous granite

1684     magmatism of the Sirdal magmatic belt (1065–1020 Ma) and low-pressure granulite-facies

1685     metamorphism (1045–990 Ma) culminating at UHT conditions (1030–1005 Ma) in the west

1686     of the Telemarkia lithotectonic unit (Fig. 5; Fig. 19; Fig. 20). The width of the orogenic zone

1687     (minimum of 460 km), the large volume of magmatism with syn- to late-collision

1688     geochemical signature (Sirdal magmatic belt), the paired belts of high-pressure (towards the

1689     foreland) vs. high-temperature (towards the hinterland) metamorphism, and the structural

1690     evidence for convergence suggests that the Sveconorwegian orogeny entered the main phase

1691     of continent-continent collision around 1065 Ma.

1692         In Fig. 19, we propose that collision resulted in the formation of a Tibetan-style orogenic

1693     plateau (Jamieson and Beaumont, 2013) extending from the Telemarkia to the Idefjorden

1694     lithotectonic units. The infrastructure of this orogenic plateau is defined by widespread gneiss

1695     complexes characterized by partial melting, compressive ductile deformation and

1696     amphibolite- to granulite-facies metamorphism between 1050 and 1000 Ma. Evidence from

1697     the superstructure of this plateau is scanty, simply because little upper crustal rocks younger

1698     than 1050 Ma are preserved. The N–S trending Kalhovd Formation consists of unconformable

1699     conglomerate and immature sandstone, deposited after c. 1054 Ma, in a continental (above sea

1700     level) intermontane basin (Fig. 5; Fig. 11; Fig. 19; Fig. 20). This basin was downfaulted along

1701     the Mandal-Ustaoset fault zone, possibly during deposition, recording extension after c. 1054

1702     Ma in the upper crust in the centre of the Telemarkia lithotectonic unit.

1703         Dynamic of the mantle in the collision zone would be simulated by a "pro-plate" (upper-

1704     plate) Tibetan-style delamination numerical models by Li et al. (2016). In Fig. 19, we propose

1705     that mantle upwelling under the Telemarkia lithotectonic unit was counterbalanced by mantle

1706     downwelling and lithospheric mantle delamination and foundering under the Idefjorden

1707    lithotectonic unit. In the Idefjorden lithotectonic unit, the crust was pulled down by a

1708    lithospheric mantle slab to reach peak high-pressure low-temperature granulite facies

1709    conditions (c. 1.2–1.5 GPa, 740–780 °C) between c. 1052 and 1046 Ma (Fig. 19) (Bingen et

1710    al., 2008b; Söderlund et al., 2008a). The crust in the Idefjorden lithotectonic unit was not

1711    affected by orogenic processes before 1050 Ma and therefore could reach high-pressure

1712    conditions before melting. Decoupling between the mantle slab and the crust (breakoff)

1713    probably took place when partial melting reactions were activated in the lower crust. During

1714    exhumation, widespread migmatitization (including muscovite-, biotite- and amphibole-

1715    dehydration melting) is observed at regional scale between c. 1040 and 1000 Ma in the

1716    Idefjorden lithotectonic unit (Fig. 10; Fig. 20; Table 2). Migmatitization took place in

1717    convergent setting; east of the Oslo rift, it is associated with a well-defined top-to-west

1718    direction of transport (Viola et al., 2011). Lamprophyre dykes, close to the boundary between

1719    the Kongsberg and Idefjorden lithotectonic units, attests to local melting of lithospheric

1720    mantle material at c. 1030 Ma (Bingen and Viola, 2018), and is consistent with a model of

1721    foundering of the lithospheric mantle around 1030 Ma.

1722       In the Telemarkia lithotectonic unit (Agder area), the NNW-SSE trending Sirdal magmatic

1723    belt attests to voluminous crustal melting between c. 1065 and 1020 Ma (Fig. 5; Fig. 19)

1724    (Bingen et al., 2015; Coint et al., 2015; Granseth et al., 2020; Slagstad et al., 2013). As

1725    discussed earlier, it contains high-K calc-alkaline quartz-monzonite–granodiorite plutons

1726    associated with minor ultrapotassic rocks (Fig. 7; Fig. 15) (Bingen et al., 1993; Bingen and

1727    van Breemen, 1998a). Such calc-alkaline granitoids can be derived by partial melting of lower

1728    crustal mafic metaigneous rocks. Enrichment in K and other large ion lithophile elements

1729    (LILE) implies either that this crustal source was previously enriched in LILE or that the

1730    melts were mixed with ultrapotassic lamprophyric melts, themselves generated from

1731    lithospheric mantle previously enriched in LILE. The most straightforward interpretation is

1732 that this lithospheric mantle source was part of a mantle wedge enriched in LILE by supra-

1733 subduction fluids between 1520 and 1480 Ma. It would then become part of a subcontinental

1734 lithospheric mantle after 1480 Ma, and finally, it would melt during collision between 1065

1735 and 1020 Ma, heated during orogeny. Two observations support this three stage model: i) the

1736 1065–1020 Ma Sirdal magmatic belt overlaps geographically with the 1520-1480 Ma Suldal

1737 magmatic arc (Roberts et al., 2013); ii) the near-chondritic Nd isotopic signature of the Feda

1738 suite granitoids (-1 < $\varepsilon_{Nd}$ < +1.5) and ultrapotassic enclaves (+1 < $\varepsilon_{Nd}$ < +1.5) are lying on the

1739 evolution vector of the crust generated at 1520-1480 Ma (Fig. 13 a). A similar interpretation is

1740 provided for near-coeval (1063 ± 3 Ma) high-Sr-Ba quartz-monzonite plutons in the Quebecia

1741 lithotectonic unit of the Grenville orogen (Michaud pluton hosted in the c. 1500 Ma Escumins

1742 supracrustal rocks)(Groulier et al., 2018a).

1743     Voluminous melting of the crust clearly requires an appropriate heat source. The high-

1744 alumina orthopyroxene megacrysts (HAOM) and plagioclase megacrysts hosted in the c. 930

1745 Ma anorthosite plutons constrain mafic magmatism at the base of the crust at 1041 ± 17 Ma

1746 coeval with formation of the Sirdal magmatic belt (Bybee et al., 2014; Slagstad et al., 2018;

1747 Vander Auwera et al., 2014b). The supra-chondritic Nd isotopic values for the megacrysts

1748 (+2.8 < $\varepsilon_{Nd(1041\ Ma)}$ < +5.3) trace the source of this magmatism to the asthenosphere (Fig. 13

1749 a). Here we suggest that upwelling of hot asthenosphere in the collision zone generated

1750 asthenospheric melts, produced underplates (with HAOM), reheated and destabilized the

1751 lithospheric mantle, and generated minor lamprophyre melts (from this lithospheric mantle)

1752 (Fig. 19; Fig. 20). Heating of the crust produced granitoids of the Sirdal magmatic belt. After

1753 extraction of these melts, protracted heating in the crust resulted in a first phase of granulite-

1754 facies metamorphism (M1), reaching ultra-high temperature conditions (0.7–0.5 GPa, 900–

1755 950 °C) between 1030 and 1005 Ma (Fig. 20) (Blereau et al., 2017; Drüppel et al., 2013;

1756 Laurent et al., 2018b).

1757    The HAOM hosted in the anorthosites record a pressure of crystallization of 1.1 GPa and

1758    an age of 1041 ± 17 Ma (Bybee et al., 2014; Charlier et al., 2010). These numbers imply a

1759    crustal thickness of at least 42 km around 1040 Ma, corresponding to a moderate crustal

1760    overthickening relative to the standard 30 km. The regional folding observed at various scales

1761    in the Telemarkia lithotectonic unit, also requires at least one phase of compression between

1762    1030 and 1000 Ma.

1763    In Fig. 17 to Fig. 20, the Oaxaquia and inliers of in the Andes of Columbia, which contain

1764    evidence of high-grade metamorphism between 1050 and 980 Ma, are represented

1765    speculatively as volcanic arcs in the ocean between, Amazonia Laurentia and Baltica (Fig. 8,

1766    Fig. 12; Fig. 13; Fig. 16). They were first accreted to Amazonia (Putumayo) before colliding

1767    with Baltica around 1050 Ma (Fig. 19; Fig. 20) (Ibanez-Mejia et al., 2011; Lawlor et al.,

1768    1999; Weber et al., 2010). In this framework, the Telemarkia–Kongsberg–Bamble units are

1769    indeed situated in a back-arc domain, in the time interval between 1280 and 1080 Ma, before

1770    closure of all oceans, and they ended-up in upper plate position at c. 1065 Ma during collision

1771    with Amazonia (Fig. 18; Fig. 19; Fig. 20). Upwelling of hot asthenosphere in the collision

1772    zone was possibly promoted by break-off all oceanic lithospheric plates to the west of the

1773    orogen when subductions ceased (Fig. 19).

1774    --------------------
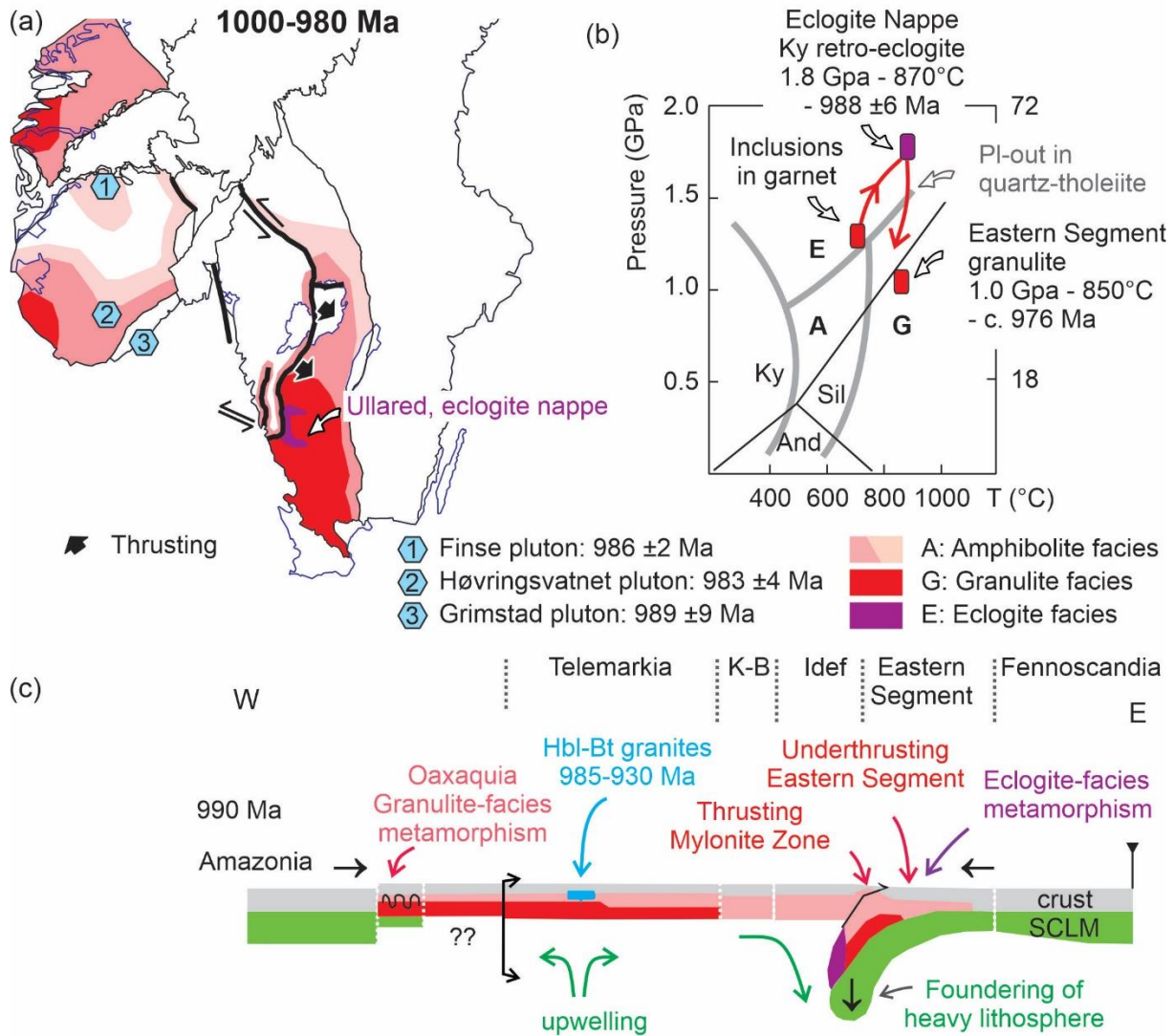
**Figure 21.** Schematic geodynamic model for the 1000–980 Ma time interval. (a) Sketch map of the Sveconorwegian orogen, with distribution of metamorphism and magmatism. (b) Pressure-temperature diagram. (c) Interpretative E-W cross section. Explanations and references in the text.

--------------------

### 6.3   1000–920 Ma: long-duration growth of the collision zone

At c. 1000 Ma, orogeny propagated to the east, all the way into the Eastern Segment. Continued high-temperature low-pressure metamorphism in the west of the collision zone and voluminous magmatism contrast with high pressure metamorphism in the east, suggesting that

1785     the western part was characterized by protracted mantle upwelling while the eastern part by

1786     underthrusting and mantle downwelling. In Fig. 21, Fig. 22 and Fig. 23, we propose that the

1787     Tibetan-style orogenic plateau grew towards the foreland to includes the Eastern Segment and

1788     covered the entire orogen. The Eastern Segment offers a nice example of how crust

1789     underthrust to high-pressure conditions is incorporated into a melt-lubricated middle-crustal

1790     infrastructure of an orogenic plateau. We suggest that the orogenic plateau was sustained to c.

1791     930 Ma before it collapsed.

1792     *6.3.1    Eastward growth of orogenic plateau*

1793     The Eastern Segment was a cold lithospheric segment of Fennoscandia foreland affinity,

1794     unaffected by Sveconorwegian orogenic processes before 1000 Ma. At this point in time, it

1795     was underthrust as a slab towards the west beneath the Mylonite Zone during convergence

1796     (Fig. 21) (Möller and Andersson, 2018; Möller et al., 2015). The deepest underthrust western

1797     part of the slab reached eclogite-facies conditions corresponding to a depth of c. 70 km (1.65–

1798     1.9 GPa, 850–900°C) at c. 990 Ma (Fig. 5; Fig. 21 b), while the adjacent part of the slab (now

1799     the internal section) reached high-pressure granulite-facies conditions (1.1 GPa, 850°C; Fig.

1800     21 b) (Möller et al., 2015; Piñán-Llamas et al., 2015; Tual et al., 2017). Preservation of

1801     prograde zoning in garnet in eclogites attests to faster-than-equilibration prograde

1802     metamorphism (Möller, 1998; Tual et al., 2017). In Fig. 21, we propose that this underthrust

1803     crustal slab was pulled down by foundering of the dense subcontinental lithospheric mantle.

1804     Breakoff of the lithospheric mantle slab triggered exhumation after c. 980 Ma (Fig. 22).

1805     Exhumation took place in two steps (Fig. 22). During the first step, the eclogitized

1806     westernmost part of the Eastern Segment was detached from the deepest part of the segment

1807     and exhumed with an overall eastward vergence, as a single and coherent (eclogite-bearing)

1808     ductile nappe to an intermediate depth of c. 35–40 km (1.1 GPa), where it was juxtaposed to

1809     the granulite-facies internal section. This process is interpreted as eastwards extrusion during

1810     overall E-W convergence (Möller and Andersson, 2018; Möller et al., 2015; Piñán-Llamas et

1811     al., 2015; Tual et al., 2015). During the second step, the eclogite-bearing nappe and the

1812     granulite-facies internal section were exhumed together, also with an overall eastwards

1813     vergence. Accurate geochronology of these two steps remains difficult to establish. Breakoff

1814     of the lithospheric mantle slab was probably facilitated by partial melting in the crust. East

1815     vergent exhumation was clearly lubricated by abundant partial melting. The crystallization of

1816     these leucosome melts is dated between c. 978 and 961 Ma inside the eclogite-bearing nappe

1817     (Andersson et al., 2002a; Möller et al., 2015) and between c. 976 and 965 Ma, i.e. in a coeval

1818     time interval, in the granulite-facies internal section (Andersson et al., 2002a; Hansen et al.,

1819     2015; Möller et al., 2007; Piñán-Llamas et al., 2015; Söderlund et al., 2002).

1820        The Blekinge-Dalarna dolerite dyke swarm intruded in the upper crust in the foreland of

1821     the orogen between c. 978 and 946 Ma (Gong et al., 2018; Ripa and Stephens, 2020d;

1822     Söderlund et al., 2005). This mafic magmatism is characterized by a within-plate geochemical

1823     signature and supra-chondritic Hf isotopic signature ($+1 < \varepsilon_{Hf} < +5$). It is evidence for

1824     asthenosphere upwelling and decompression melting under the cratonic lithosphere of the

1825     foreland (Gong et al., 2018; Ripa and Stephens, 2020d; Söderlund et al., 2005). The upwelling

1826     may represent a dynamic response in the asthenosphere of the breakoff and foundering of the

1827     lithospheric mantle slab under the Eastern Segment at and after c. 980 Ma (Fig. 22).

1828        Eastwards thrusting in the frontal wedge and along the Sveconorwegian front represents a

1829     final spasm of the orogeny. Both $^{40}Ar/^{39}Ar$ data and the observation that Blekinge-Dalarna

1830     dolerite dykes are sheared in the frontal wedge suggest that it took place after c. 945 Ma

1831     (Andréasson and Dallmeyer, 1995; Page et al., 1996a; Stephens and Wahlgren, 2020a; Ulmius

1832     et al., 2018).

1833     *6.3.2    Sustained orogenic plateau west of the Mylonite Zone*

1834     Little tectonic activity or metamorphism is dated in the central part of the orogen (western

1835     part of the Idefjorden lithotectonic unit, Kongsberg and Bamble lithotectonic units and eastern

1836     part of the Telemarkia lithotectonic unit) between c. 980 and 930 Ma, suggesting that this part

1837     of the orogen behaved passively during this time interval. In the west, in the orthopyroxene

1838     zone of Rogaland, a scatter of zircon rim U–Pb ages between 1045 and 955 Ma is interpreted

1839     as evidence for protracted high-grade metamorphism with melt-present conditions in the

1840     middle crust (0.45–0.55 GPa) (Fig. 22) (Blereau et al., 2017; Laurent et al., 2018a; Slagstad et

1841     al., 2018). In Fig. 22, we propose that the orogenic plateau formed between 1050 and 1000

1842     Ma west of the Mylonite Zone was sustained throughout the orogeny to c. 930 Ma.

1843     --------------------



1844
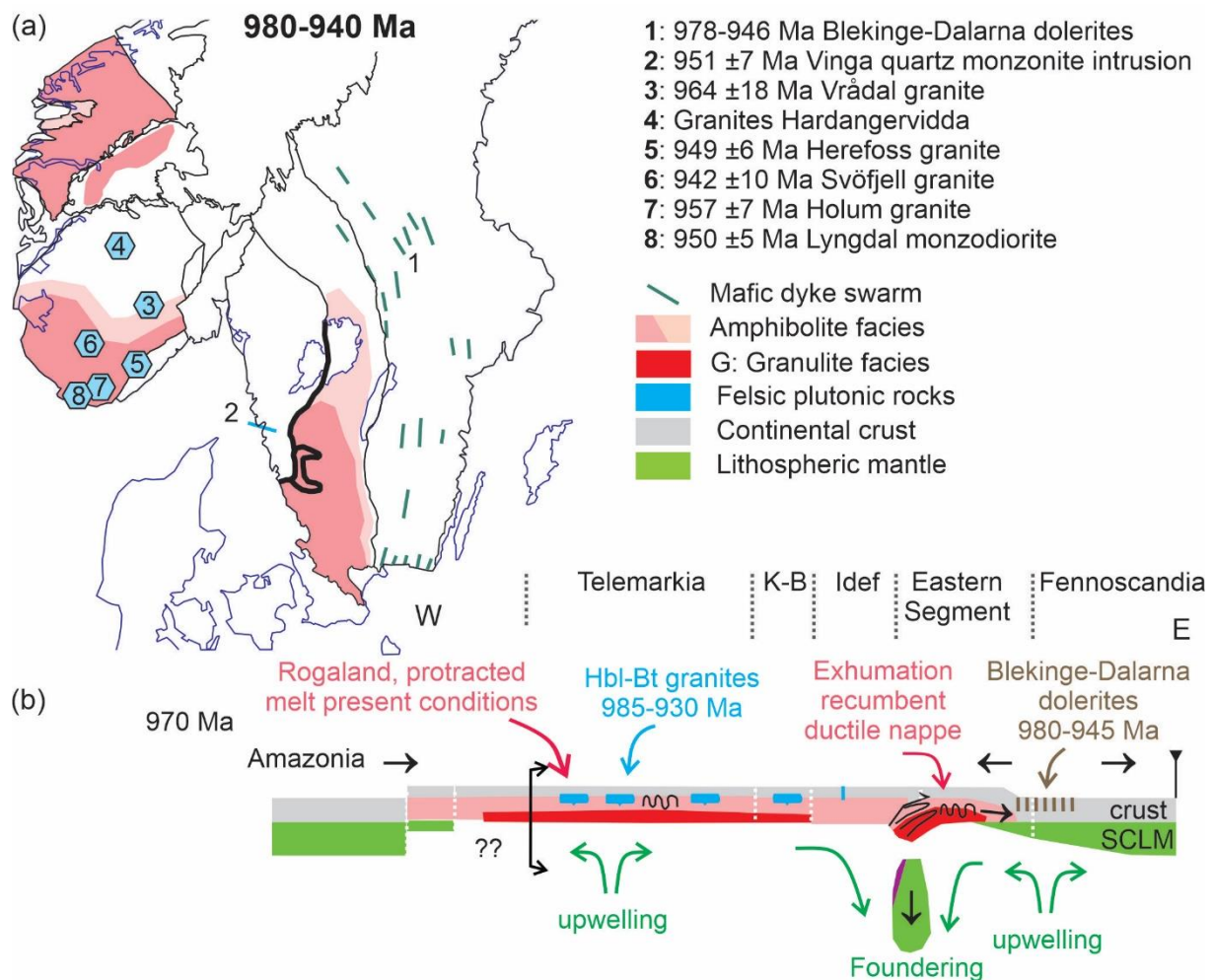
1845 **Figure 22.** Schematic geodynamic model for the 980–940 Ma time interval. (a) Sketch map

1846 of the Sveconorwegian orogen, with distribution of metamorphism and magmatism. (b)

1847 Interpretative E-W cross section. WGR: Western Gneiss Region. Explanations and references

1848 in the text.

1849 --------------------



1850
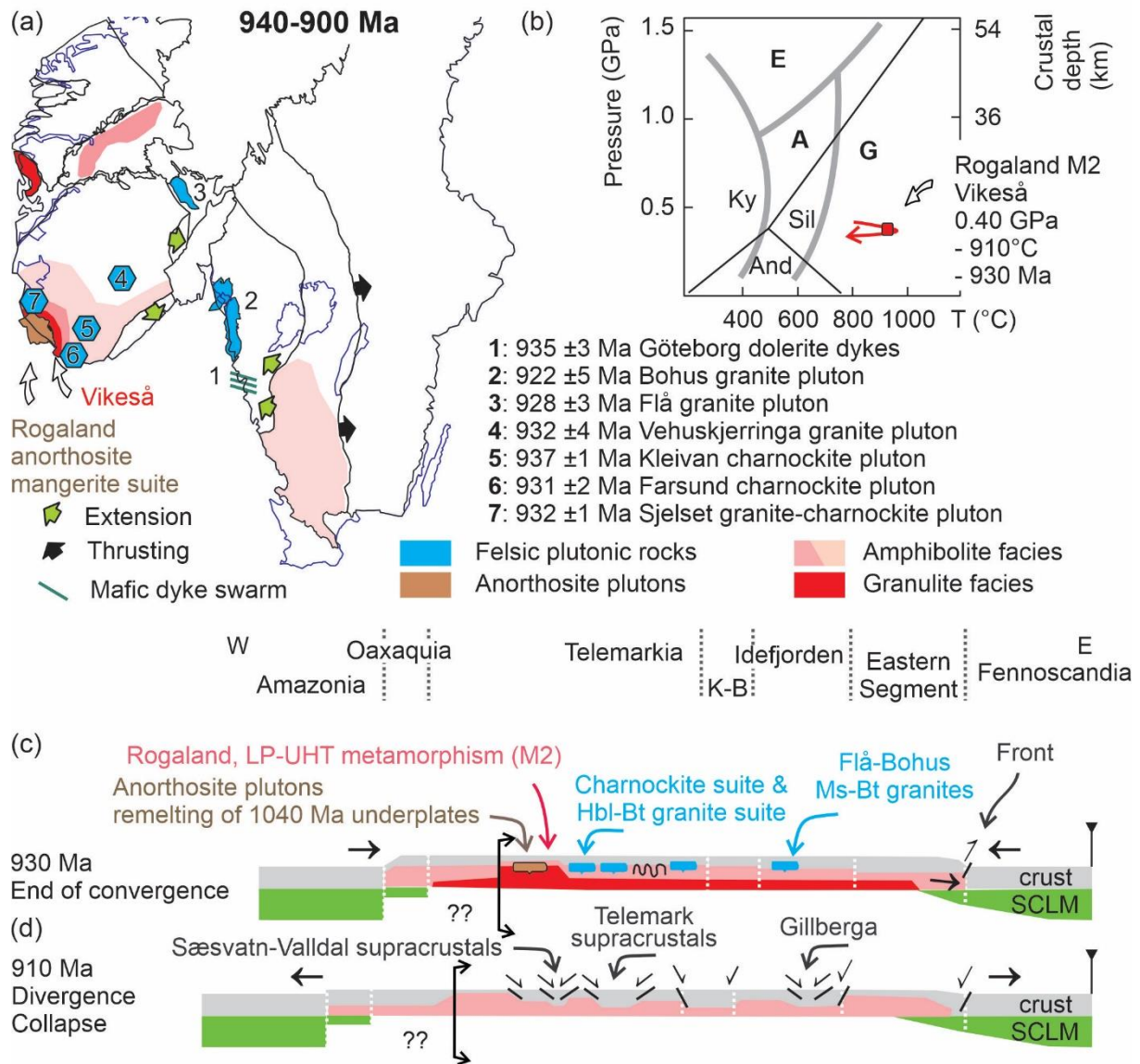
1851 **Figure 23.** Geodynamic model for the 940–900 Ma time interval. (a) Sketch map of the

1852 Sveconorwegian orogen, with distribution of metamorphism and magmatism. (b) Pressure-

1853 temperature diagram. (c, d) Interpretative E-W cross sections. Explanations and references in

1854 the text.

1855    --------------------

1856

1857    *6.3.3   Late-Sveconorwegian magmatism and associated metamorphism*

1858    The volume of late-Sveconorwegian magmatism increases dramatically westwards in the

1859    orogen (Fig. 5; Fig. 7; Fig. 22; Fig. 23). In the Eastern Segment, minor pegmatite and granite

1860    bodies formed between c. 961 and 935 Ma during regional cooling (Möller et al., 2007;

1861    Söderlund et al., 2008b). In the Idefjorden lithotectonic unit, the large biotite + muscovite-

1862    bearing Flå and Bohus granite plutons (c. 932–922 Ma) (Eliasson et al., 2003; Eliasson and

1863    Schöberg, 1991; Lamminen et al., 2011) carry a distinctly peraluminous signature (S-type)

1864    and sub-chondritic epsilon Nd values (-8.4 < $\varepsilon_{Ndi}$ < -2.7) (Andersen et al., 2001). These

1865    properties imply a metasedimentary source, most probably in the hosting Stora Le-Marstrand

1866    complex (-8.0 < $\varepsilon_{Nd930}$ < -3.0) (Åhäll and Daly, 1989). In the Telemarkia lithotectonic unit,

1867    large plutons of the HBG granite suite emplaced between c. 985 and 926 Ma (Fig. 22; Fig.

1868    23). There is a significant spread in geochemical and isotopic composition, reflecting a

1869    diversity of sources and petrogenesis (Andersen et al., 2001; Granseth et al., 2020; Vander

1870    Auwera et al., 2011). The HBG suite is characterized by a distinctly ferroan geochemical

1871    signature (Fig. 14). Experimental petrology and geochemical modelling of the representative

1872    Lyngdal pluton in Vest Agder (Bogaerts et al., 2006; Vander Auwera et al., 2008), suggest

1873    that this granodiorite crystallized at shallow conditions corresponding to pressures between

1874    0.2 and 0.4 GPa from a wet (5–6 wt% $H_2O$), oxydized (QFM +1) and hot (c. 975 °C) magma.

1875    This magma can be generated by partial melting of an amphibole-rich mafic source (with c.

1876    1.5 wt% $H_2O$). The near-chondritic to sub-chondritic Nd isotopic signature of the HBG

1877    plutons (-6.4 < $\varepsilon_{Ndi}$ < +1.9, n = 7; -2.0 < $\varepsilon_{Hfi}$ < +1.7, n = 10) overlaps with the evolution trend

1878    of the crust generated at 1520-1480 Ma (Fig. 8; Fig. 13). This implies sources isotopically

1879    similar to those of the Sirdal magmatic belt. However, the geographical overlap between the

1880 HBG suite and the Sirdal magmatic belt suggests that more refractory lower crustal sources

1881 were exploited at higher temperature after 985 Ma for the HBG suite (Granseth et al., 2020;

1882 Vander Auwera et al., 2008).

1883     To the west of the Sirdal magmatic belt, the AMC suite formed between 932 and 915 Ma

1884 in a crust previously metamorphosed to granulite conditions (1030–1005 Ma). The AMC suite

1885 is ferran and alkalic (Fig. 14). Constraints from experimental petrology indicate that the high

1886 alumina basalt parental to the anorthosite plutons is characterized by a too low Mg# (molar

1887 $Mg/(Mg+Fe) = 0.52$) and crystallizes too sodic plagioclase (An55) to be generated by melting

1888 of a mantle peridotite (HLCA and TJ compositions; Duchesne et al., 1999; Longhi, 2005;

1889 Longhi et al., 1999). Instead, its composition is situated on the thermal divide of the

1890 plagioclase + pyroxene liquidus surface at 1.0 to 1.3 GPa, imposing that it was produced by

1891 partial melting of a gabbronoritic source (Longhi, 2005; Longhi et al., 1999). Experiments

1892 show that compositionally adequate melts in equilibrium with plagioclase and orthopyroxene

1893 are found in a temperature range between c. 1180 and 1250 °C at c. 1.1 GPa (Fram and

1894 Longhi, 1992; Longhi et al., 1999; Vander Auwera and Longhi, 1994). The Sm–Nd isochron

1895 of $1041 \pm 17$ Ma defined by the high-aluminium orthopyroxene megacrysts (HAOM) hosted

1896 in the anorthosite plutons (Bybee et al., 2014) suggests that these megacrysts are restitic

1897 crystals from a lower crustal source (Vander Auwera et al., 2014b). The isochron implies that

1898 the gabbronoritic source formed at c. 1040 Ma as an underplate (1.1 GPa) and was remelted at

1899 c. 930 Ma to form the parental magmas of the AMC suite (Vander Auwera et al., 2014b).

1900 Isotopically, this two stage model is realistic, with overlapping positive epsilon Nd values for

1901 the megacrysts ($+3.1 < \varepsilon_{Nd(930\ Ma)} < +5.9$) and mafic rocks in the AMC suite ($\varepsilon_{Nd(930\ Ma)} < +5.8$)

1902 (Fig. 13). However, the wide range of Nd isotopic composition of differentiated rocks in the

1903 AMC suite ($-2.8 < \varepsilon_{Nd(930\ Ma)} < +5.8$), implies a variety of lower crustal sources and crustal

1904 contaminants in the suite, all of them characterized by low water content (Barling et al., 2000;

1905    Duchesne and Wilmart, 1997). This two-stage model requires that hot asthenosphere was

1906    upwelling just under the crust around 930 Ma in order to extensively remelt (high degree of

1907    partial melting) gabbronoritic layers of the 1040 Ma underplate. Heat transfer from the mantle

1908    and the anorthosite plutons to the crust resulted in a second phase of ultra-high temperature

1909    granulite-facies metamorphism (M2; 0.35–0.5 GPa, 900–950 °C, c. 930 Ma) (Laurent et al.,

1910    2018b). Using a conservative geothermal gradient of 20 °C/km, extrapolation of a 900 °C

1911    temperature at 0.4 GPa (15 km depth; M2) to the base of the crust at 1.1 GPa (41.5 km depth)

1912    indeed yield a temperature of 1420 °C, compatible with the presence of asthenosphere at the

1913    base of the crust at c. 930 Ma.

1914    --------------------
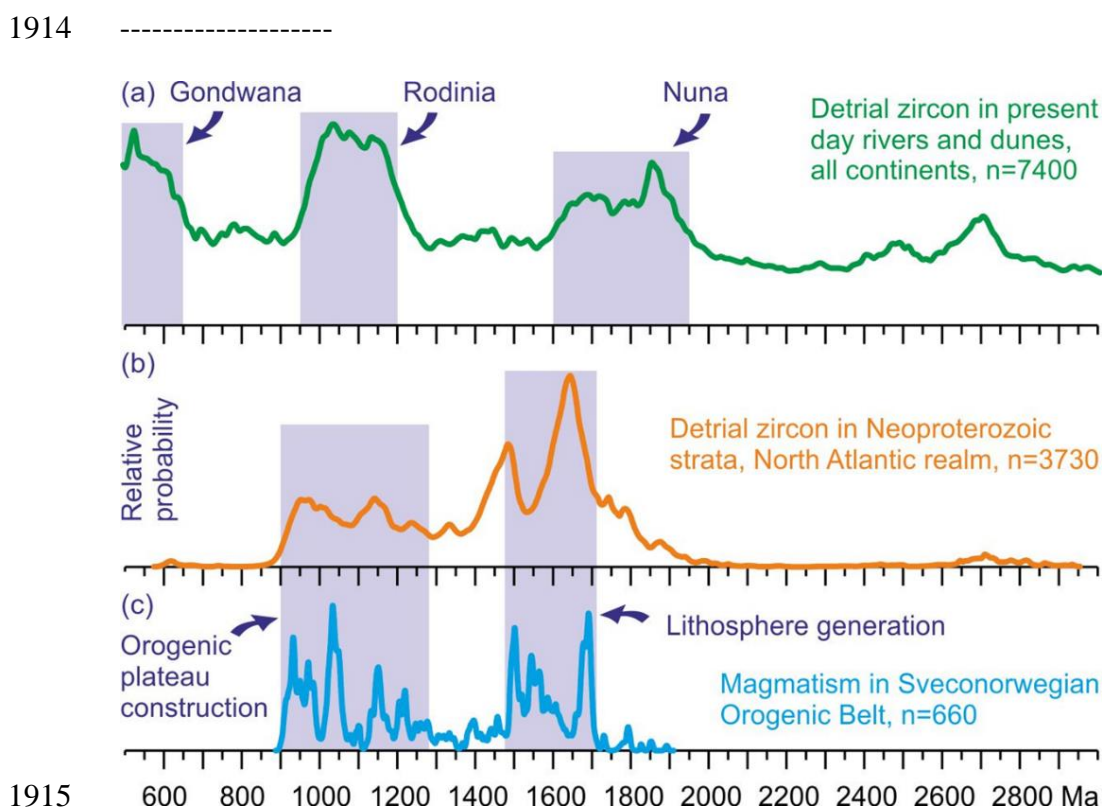


**Figure 24.** Erosion of the Sveconorwegian orogen. (a) Relative probability diagrams of
detrital zircons in present day river sediments and dunes. Peaks in this distribution are
attributed to formation of supercontinents Nuna, Rodinia and Gondwana. Compilation of
Campbell and Allen (2008). (b) Relative probability diagrams of detrital zircons in
Neoproterozoic clastic sediments in the North Atlantic realm, deposited in marine and

1921 continental environment mainly during the Tonian and Cryogenian. The compilation includes

1922 3730 detrital zircons from the Moine Supergroup in Scotland (Kirkland et al., 2008b),

1923 Caledonian Lower and Middle Allochthons in Norway and Sweden (Be'eri-Shlevin et al.,

1924 2011; Bingen et al., 2011; Gee et al., 2015; Kirkland et al., 2007, 2008a; Lamminen et al.,

1925 2015; Zhang et al., 2015, 2016), Timanides in N Norway (Zhang et al., 2015), Northwestern

1926 terrane in Svalbard (Pettersson et al., 2009) and Eleonore Bay Supergroup in E Greenland

1927 (Sláma et al., 2011). Only analyses with discordance < 5% are selected; the $^{206}Pb/^{238}U$ age is

1928 selected for zircon younger than 1500 Ma and the $^{206}Pb/^{207}Pb$ age for older zircons. (c)

1929 Relative probability diagram for magmatic events in the entire Sveconorwegian orogen. The

1930 time intervals for continental lithosphere generation and orogenic plateau development are

1931 highlighted. The similitude in the age distribution between magmatic events in the

1932 Sveconorwegian orogen and the Neoproterozoic strata argues for sourcing in the

1933 Sveconorwegian orogen for these sediments and important transport of detritus northwards

1934 and westwards.

1935 --------------------

1936 ***6.4 Post 920 Ma: late- to post-Sveconorwegian collapse and sedimentation***

1937 The orogenic plateau developed during the Sveconorwegian orogeny (Fig. 17 to Fig. 23)

1938 could not be sustained when convergence came to a halt sometime after c. 930 Ma, and it

1939 collapsed. As noted earlier, syn- to late-Sveconorwegian plutons (1066–920 Ma) exposed

1940 today define a rather uniform depth of intrusion of c. 16 km (0.4–0.5 GPa, Table 1) (Charlier

1941 et al., 2010; Coint et al., 2015; Eliasson et al., 2003; Vander Auwera et al., 2014a; Vander

1942 Auwera and Longhi, 1994). Removal of this c. 16 km thick overburden took place by a

1943 combination of late- to post-Sveconorwegian erosion and extensional tectonics.

1944  Mapping and characterization of extensional shear zones that could explain exhumation of

1945 amphibolite-facies gneiss complexes (infrastructure of the orogenic plateau) relative to low-

1946 grade supracrustal rocks (superstructure) are still in their infancy (Persson-Nilsson and

1947 Lundqvist, 2014; Torgersen et al., 2018; Viola et al., 2011). Extensional reactivation of the

1948 main shear zones in the orogen, including the Sveconorwegian Front, the Mylonite Zone and

1949 the Bamble-Telemarkia boundary zone, are documented between c. 930 and 860 Ma by

1950 muscovite and biotite $^{40}Ar/^{39}Ar$ data (Andréasson and Dallmeyer, 1995; Mulch et al., 2005;

1951 Page et al., 1996b; Viola et al., 2011). Extension was associated with regional cooling, as

1952 documented by regional scale titanite U–Pb and amphibole, muscovite and biotite $^{40}Ar/^{39}Ar$

1953 data (Bingen et al., 1998; Connelly et al., 1996; Johansson et al., 2001; Page et al., 1996a;

1954 Page et al., 1996b; Söderlund et al., 1999; Ulmius et al., 2018; Verschure et al., 1980; Wang

1955 et al., 1998).

1956     Pegmatite bodies represent the youngest magmatism of regional significance in the orogen

1957 between c. 914 and 900 Ma (Hetherington and Harlow, 2008; Müller et al., 2015; Müller et al.,

1958 2017; Pasteels et al., 1979; Scherer et al., 2001; Seydoux-Guillaume et al., 2012). Pegmatites

1959 are locally abundant in the gneiss complexes of the Telemarkia and Idefjorden lithotectonic

1960 units. In the Telemarkia lithotectonic unit, they formed shortly after the regional scale titanite

1961 U–Pb age of c. 918 Ma, interpreted to record regional cooling below c. 600 °C. The

1962 pegmatites are not genetically related to any exposed granite pluton and therefore they

1963 represent small individual batches of fluid-rich melt sourced locally in the gneiss complexes

1964 (Müller et al., 2015; Müller et al., 2017). Their relation to the extensional collapse of the

1965 orogen and the source(s) of fluids necessary to generate the fluid-rich melts remain enigmatic.

1966     Absence of widespread late-Sveconorwegian sedimentation inside the orogen is suggested

1967 by a lack of post-Sveconorwegian sedimentary cover below the sub-Cambrian peneplain in

1968 southern Norway and Sweden (Gabrielsen et al., 2015). The Neoproterozoic Visingsö Group

1969 deposited between c. 885 and 740 Ma along the Sveconorwegian Front is directly and

1970 unconformably overlying Paleoproterozoic basement (Loron and Moczydłowska, 2018;

1971 Moczydłowska et al., 2018; Pulsipher and Dehler, 2019). These observations suggest that the

1972 Sveconorwegian orogen was erodible, i.e. above sea level, at the end of the Sveconorwegian

1973 orogeny.

1974  The rock record supportive for clastic transport towards the Fennoscandia foreland is only

1975 local (Almesåkra Group) (Ripa and Stephens, 2020d). However, thermochronological data

1976 suggest heating of the foreland up to c. 220 °C some 150 km east of the Sveconorwegian

1977 Front between 944 Ma and 851 Ma, which corresponds to burial of the present day surface to

1978 c. 7 km (Guenthner et al., 2017). Clastic transport towards the north and west of the

1979 Sveconorwegian orogen is, instead, quite well established, as Neoproterozoic continental and

1980 marine sediments abound in Caledonian parautochthons and allochthons, Svalbard, and the

1981 Timanides (Nystuen et al., 2008). These sediment sequences contain detrital zircons with age

1982 between 1700 and 1500 Ma and 1280 and 900 Ma (Bingen et al., 2011; Gee et al., 2015;

1983 Kirkland et al., 2007; Kirkland et al., 2008b; Pettersson et al., 2009; Sláma et al., 2011;

1984 Strachan et al., 1995; Strachan et al., 2013; Zhang et al., 2015). These sequences can be, at

1985 least partly, sourced directly from within the Sveconorwegian orogen (Fig. 24).

1986 --------------------

| Time slices [Ma] | 1280 1080 | 1150 1130 | 1065 1020 | 1045 1025 | 1030 1005 | 1040 995 | 990 980 | 985 935 | 980 960 | 935 925 | 935 925 | 925 900 | 980 945 |
|---|---|---|---|---|---|---|---|---|---|---|---|---|---|
| Lithotectonic unit | (yellow) | (green) | (yellow) | (blue) | (yellow) | (blue) | (red) | (yellow) | (red) | (yellow) | (blue) | | (pink) |
| Tectonics | ↔ | ✕ | ✕ | ✕ | ✕ | ✕ | ✕ | ✕ | ✕ | ✕ | ↔ | ↔ | ↔ |
| Pressure [GPa] | | 1.15 | | 1.5 | 0.6 | 1.0 | 1.8 | | 1.1 | 0.4 | | | |
| Temperature [°C] | | 850 | | 740 | 920 | 760 | 870 | | 850 | 920 | | | |
| P-T path | | | | | ↻ | | ↻ | | | ↻ | | | |
| Magmatism: Felsic mafic, anorthosite | (felsic/mafic) | (felsic/mafic) | (felsic/mafic) | | | | (felsic) | | (anorthosite/felsic) | (mafic) | (felsic) | | (mafic) |
| Sedimentation | (basin) | (basin) | | | | | | | | | | | (basin) |

Map views

N ⭡  100 km

Amazonia Andean-Mexican micro-continents

Fennoscandia

Asthenosphere upwelling · Lithospheric mantle retro-delamination · Asthenosphere upwelling

Growing orogenic plateau

**Figure 25.** Summary matrix of Sveconorwegian orogeny. The first line provides the time slices of events. Line 2 represents the lithotectonic units colour coded following the inset map at the bottom. Line 3 (Tectonics) indicates if the tectonic regime is compressional or extensional in the specific time interval and geographic location. Note that for the time interval between 1280 and 1080 Ma, the tectonic regime is extensional in Telemarkia while it is compressional in the Bamble and Kongsberg Lithotectonic Units. Lines 4-5 (Pressure-Temperature) provides the conditions of peak metamorphism and line 6 (P-T path) indicates where this metamorphism follows a clockwise P-T path. Line 7 (magmatism) records plutonic events, with color coding for felsic (purple), mafic (green) or anorthosite (brown). Line 9 records known sedimentation in intermontane basins or foreland basins. The bottom-right figure is a interpretative transect in map view through the orogen between the Amazonia hinterland and Fennoscandia foreland, showing the three step growth of the orogenic plateau from the centre of the orogen. This three steps growth is associated with three steps of retro-delamination of the sub-continental lithospheric mantle (SCLM) towards the foreland, as

2002  recorded by metamorphism with a high-pressure signature. The western part of the orogen is

2003  characterized by upwelling and shallow asthenosphere during the entire orogenic period.

2004  Explanations in the text.

2005  -------------------

2006  **7    Conclusions**

2007  Published models attempting to explain the tectonic evolution of the Sveconorwegian orogeny

2008  vary widely even with respect to their first-order features and boundary conditions. They

2009  range from end-members involving continental collision between Fennoscandia and another

2010  continent to accretion in the absence of collision (Fig. 3). This variation reflects the difficulty

2011  to translate the observed geological record and the analytical data into geodynamic processes

2012  in the Proterozoic.

2013      Based on a review of data and concepts, we favour a model of large, hot and long-duration

2014  continental collision at the margin of Fennoscandia between c. 1065 and 920 Ma, as

2015  synthesized in Fig. 17 to Fig. 23, and by a matrix in Fig. 25. The plate tectonic setting of the

2016  pre-collision events, between 1280 and 1080 Ma, remains uncertain, although it was possibly

2017  a continental back arc setting (Fig. 17; Fig. 18). Although not strictly necessary, the model is

2018  adjusted into a classical Rodinia assembly framework, involving a Baltica–Laurentia–

2019  Amazonia collision (Fig. 1; Fig. 8, Fig. 12; Fig. 13; Fig. 16).

2020      The width of the orogenic zone, the evidence for protracted and widespread crustal melting

2021  and high-temperature metamorphism reaching UHT conditions, the evidence for high pressure

2022  metamorphism recording crustal thickening, the growth of the orogenic zone towards the

2023  foreland, the juxtaposition of low-grade supracrustal rocks and high-grade gneiss complexes,

2024  and the lack of syn-orogenic marine sedimentary sequence, argue for a collisional orogeny.

2025  We suggest that an orogenic plateau started to form around 1280 Ma in the Telemarkia

2026  lithotectonic unit, first as a Cordillera-style (back-arc) orogenic plateau, and that it grew

2027 stepwise both towards the hinterland and foreland, as a Tibetan-style (collisional) orogenic

2028 plateau. Shallow asthenosphere conditions were maintained in the western part of the

2029 orogenic belt at least up to c. 930 Ma, when the formation of anorthosite plutons took place

2030 by remelting of mafic underplates themselves formed at c. 1040 Ma. Formation of the

2031 orogenic plateau was paired with retro-delamination and foundering of the sub-continental

2032 lithospheric mantle. This process is recorded by compression and regional metamorphism

2033 with an increasingly higher pressure signature towards the foreland followed by exhumation.

2034 Three stages of lithosphere foundering are inferred, one at c. 1150–1120 Ma under the

2035 Bamble and Kongsberg Lithotectonic units, one at c. 1050 Ma under the Idefjorden

2036 lithotectonic unit and one at c. 990 Ma under the Eastern Segment. In the Eastern Segment,

2037 peak conditions reached eclogite facies conditions (1.8 GPa-870 °C) and exhumation of

2038 eclogite-bearing units was aided by extrusion of a ductile nappe lubricated by partial melting,

2039 within an overall compressional setting. The increasing peak pressure recorded in time and

2040 space reflects increasing mechanical coupling between the lower crust and colder lithospheric

2041 mantle, as the delamination process progressed toward the Fennoscandia craton.

2042    After c. 930 Ma, convergence came to a halt, the orogenic plateau collapsed, and 16 km of

2043 overburden was removed by extension and erosion.

2044 **8 Declaration of interests**

2045 The authors declare that they have no known competing financial interests or personal

2046 relationships that could have appeared to influence the work reported in this paper.

2047 **9 Acknowledgements**

## 10   References

Åhäll, K.I., Connelly, J.N., 1998. Intermittent 1.53-1.13 Ga magmatism in western Baltica; age constraints and correlations within a postulated supercontinent. Precambrian Research 92, 1-20.

Åhäll, K.I., Connelly, J.N., 2008. Long-term convergence along SW Fennoscandia: 330 m.y. of Proterozoic crustal growth. Precambrian Research 161, 452-474.

Åhäll, K.I., Cornell, D.H., Armstrong, R., 1998. Ion probe zircon dating of metasedimentary units across the Skagerrak: new constraints for early Mesoproterozoic growth of the Baltic Shield. Precambrian Research 87, 117-134.

Åhäll, K.I., Daly, J.S., 1989. Age, tectonic setting and provenance of Östfold-Marstrand Belt supracrustals: westward crustal growth of the Baltic Shield at 1760 Ma. Precambrian Research 45, 45-61.

Åhäll, K.I., Gower, C.F., 1997. The Gothian and Labradorian orogens: variations in accretionary tectonism along a late Paleoproterozoic Laurentia–Baltica margin. GFF 119, 181-191.

Åhäll, K.I., Larson, Å., 2000. Growth-related 1.85-1.55 Ga magmatism in the Baltic Shield; a review addressing the tectonic characteristics of Svecofennian, TIB 1 -related, and Gothian events. GFF 122, 193-206.

Åhäll, K.I., Samuelsson, L., Persson, P.O., 1997. Geochronology and stuctural setting of the 1.38 Ga Torpa granite; implications for charnockite formation in SW Sweden. Geologiska Föreningens i Stockholm Förhandlingar 119, 37-43.

Ahlin, S., Austin Hegardt, E., Cornell, D., 2006. Nature and stratigraphic position of the 1614 Ma Delsjön augen granite-gneiss in the Median Segment of south-west Sweden. GFF 128, 21-32.

2075    Andersen, T., 1997. Radiogenic isotope systematics of the Herefoss granite, South

2076    Norway: an indicator of Sveconorwegian (Grenvillian) crustal evolution in the Baltic shield.

2077    Chemical Geology 135, 139-158.

2078    Andersen, T., Andersson, U.B., Graham, S., Åberg, G., Simonsen, S.L., 2009. Granitic

2079    magmatism by melting of juvenile continental crust: new constraints on the source of

2080    Palaeoproterozoic granitoids in Fennoscandia from Hf isotopes in zircon. Journal of the

2081    Geological Society of London 166, 233-247.

2082    Andersen, T., Andresen, A., Sylvester, A.G., 2001. Nature and distribution of deep crustal

2083    reservoirs in the southwestern part of the Baltic Shield: evidence from Nd, Sr and Pb isotope

2084    data on late Sveconorwegian granites. Journal of the Geological Society of London 158, 253-

2085    267.

2086    Andersen, T., Andresen, A., Sylvester, A.G., 2002a. Timing of late- to post-tectonic

2087    Sveconorwegian granitic magmatism in South Norway. Norges geologiske undersøkelse

2088    Bulletin 440, 5-18.

2089    Andersen, T., Griffin, W.L., Jackson, S.E., Knudsen, T.L., Pearson, N.J., 2004a. Mid-

2090    Proterozoic magmatic arc evolution at the southwest margin of the Baltic shield. Lithos 73,

2091    289-318.

2092    Andersen, T., Griffin, W.L., Pearson, N.J., 2002b. Crustal evolution in the SW part of the

2093    Baltic Shield: the Hf isotope evidence. Journal of Petrology 43, 1725-1747.

2094    Andersen, T., Griffin, W.L., Sylvester, A.G., 2007. Sveconorwegian crustal underplating in

2095    southwestern Fennoscandia: LAM-ICPMS U-Pb and Lu-Hf isotope evidence from granites

2096    and gneisses in Telemark, southern Norway. Lithos 93, 273-287.

2097    Andersen, T., Hagelia, P., Whitehouse, M.J., 1994. Precambrian multi-stage crustal

2098    evolution in the Bamble sector of south Norway: Pb isotopic evidence from a

2099    Sveconorwegian deep-seated intrusion. Chemical Geology (Isotope Geoscience Section) 116,

2100    327-343.

2101        Andersen, T., Laajoki, K., 2003. Provenance characteristics of Mesoproterozoic

2102    metasedimentary rocks from Telemark, South Norway: a Nd-isotope mass-balance model.

2103    Precambrian Research 126, 95-122.

2104        Andersen, T., Laajoki, K., Saeed, A., 2004b. Age, provenance and tectonostratigraphic

2105    status of the Mesoproterozoic Blefjell quartzite, Telemark sector, southern Norway.

2106    Precambrian Research 135, 217-244.

2107        Andersen, T., Munz, I.A., 1995. Radiogenic whole-rock lead in Precambrian

2108    metasedimentary gneisses from South Norway: evidence of Sveconorwegian LILE mobility.

2109    Norsk Geologisk Tidsskrift 75, 156-168.

2110        Andersson, J., Möller, C., Johansson, L., 2002a. Zircon chronology of migmatite gneisses

2111    along the Mylonite Zone (S Sweden): a major Sveconorwegian terrane boundary in the Baltic

2112    Shield. Precambrian Research 114, 121-147.

2113        Andersson, J., Söderlund, U., Cornell, D., Johansson, L., Möller, C., 1999.

2114    Sveconorwegian (-Grenvillian) deformation, metamorphism and leucosome formation in SW

2115    Sweden, SW Baltic Shield: constraints from a Mesoproterozoic granite intrusion. Precambrian

2116    Research 98, 151-171.

2117        Andersson, M., Lie, J.E., Husebye, E.S., 1996. Tectonic setting of post-orogenic granites

2118    within SW Fennoscandia based on deep seismic and gravity data. Terra Nova 8, 558-566.

2119        Andersson, U.B., Neymark, L.A., Billström, K., 2002b. Petrogenesis of Mesoproterozoic

2120    (Subjotnian) rapakivi complexes of central Sweden: implications for U-Pb zircon ages, Nd, Sr

2121    and Pb isotopes. Transactions of the Royal Society of Edinburgh, Earth Sciences 92, 201-228.

2122        Andréasson, P.G., Dallmeyer, R.D., 1995. Tectonothermal evolution of high-alumina rocks

2123    within the Protogine Zone, southern Sweden. Journal of Metamorphic Geology 13, 461-474.

2124    Andréasson, P.G., Rodhe, A., 1994. Ductile and brittle deformation within the Protogine

2125    Zone, southern Sweden: a discussion. Geologiska Föreningens i Stockholm Förhandlingar

2126    116, 115-117.

2127    Appelquist, K., Brander, L., Johansson, Å., Andersson, U.B., Cornell, D., 2011. Character

2128    and origin of variably deformed granitoids in central southern Sweden: implications from

2129    geochemistry and Nd isotopes. Geological Journal 46, 597-618.

2130    Appelquist, K., Cornell, D., Brander, L., 2008. Age, tectonic setting and petrogenesis of

2131    the Habo Volcanic Suite: Evidence for an active continental margin setting for the

2132    Transscandinavian Igneous Belt. GFF 130, 123-138.

2133    Årebäck, H., Andersson, U.B., Petersson, J., 2008. Petrological evidence for crustal

2134    melting, unmixing, and undercooling in an alkali-calcic, high-level intrusion: the late

2135    Sveconorwegian Vinga intrusion, SW Sweden. Mineralogy and Petrology 93, 1-46.

2136    Årebäck, H., Stigh, J., 2000. The nature and origin of an anorthosite associated ilmenite-

2137    rich leuconorite, Hakefjorden Complex, south-west Sweden. Lithos 21, 247-267.

2138    Ashwal, L.D., 1993. Anorthosites. Springer-Verlag, Berlin.

2139    Augland, L.E., Andresen, A., Corfu, F., Agyei-Dwarko, N.Y., Larionov, A.N., 2014. The

2140    Bratten-Landegode gneiss complex: a fragment of Laurentian continental crust in the

2141    Uppermost Allochthon of the Scandinavian Caledonides, in: Corfu, F., Gasser, D., Chew,

2142    D.M. (Eds.), New perspectives on the Caledonides of Scandinavia and related areas.

2143    Geological Society, London, Special Publications, pp. 633-654.

2144    Austin Hegardt, E., 2010. Pressure, temperature and time constraints on tectonic models

2145    for southwestern Sweden, Department of Earth Science. University of Gothenburg, p. 91.

2146    Austin Hegardt, E., Cornell, D.H., Claesson, L., Simakov, S., Stein, H.J., Hannah, J.L.,

2147    2005. Eclogites in the central part of the Sveconorwegian Eastern Segment of the Baltic

2148    Shield: support for an extensive eclogite terrane. GFF 127, 221-232.

2149    Austin Hegardt, E., Cornell, D.H., Hellström, F.A., Lundqvist, I., 2007. Emplacement age

2150    of the mid-Proterozoic Kungsbacka Bimodal Suite, SW Sweden. GFF 129, 227-234.

2151    Bao, X.W., Eaton, D.W., Guest, B., 2014. Plateau uplift in western Canada caused by

2152    lithospheric delamination along a craton edge. Nature Geoscience 7, 830-833.

2153    Barling, J., Weis, D., Demaiffe, D., 2000. A Sr-, Nd- and Pb-isotopic investigation of the

2154    transition between two megacyclic units of the Bjerkreim–Sokndal layered intrusion, south

2155    Norway. Chemical Geology 165, 47-65.

2156    Barnichon, J.D., Havenith, H., Hoffer, B., Charlier, R., Jongmans, D., Duchesne, J.C.,

2157    1999. The deformation of the Egersund-Ogna anorthosite massif, south Norway: finite-

2158    element modelling of diapirism. Tectonophysics 303, 109-130.

2159    Bateman, P.C., Chappell, B.W., 1979. Crystallization, fractionation, and solidification of

2160    the Tuolumne Intrusive Series, Yosemite National Park, California. Geological Society of

2161    America Bulletin 90, 465-482.

2162    Be'eri-Shlevin, Y., Gee, D.G., Claesson, S., Ladenberger, A., Majka, J., Kirkland, C.L.,

2163    Robinson, P., Frei, D., 2011. Provenance of Neoproterozoic sediments in the Särv nappes

2164    (Middle Allochthon) of the Scandinavian Caledonides: LA-ICP-MS and SIMS U-Pb dating of

2165    detrital zircons. Precambrian Research 187, 181-200.

2166    Beaumont, C., Nguyen, M.H., Jamieson, R.A., Ellis, S., 2006. Crustal flow modes in large

2167    hot orogens. Geological Society, London, Special Publications 268, 91-145.

2168    Beckman, V., Möller, C., Söderlund, U., Andersson, J., 2017. Zircon growth during

2169    progressive recrystallization of gabbro to garnet amphibolite, Eastern Segment,

2170    Sveconorwegian orogen. Journal of Petrology 58, 167-187.

2171    Bédard, J., 2010. Parental magmas of Grenville Province massif-type anorthosites, and

2172    conjectures about why massif anorthosites are restricted to the Proterozoic. Earth and

2173 Environmental Science Transactions of the Royal Society of Edinburgh - Earth Sciences 100,

2174 77-103.

2175 Bergerat, F., Angelier, J., Andreasson, P.G., 2007. Evolution of paleostress fields and

2176 brittle deformation of the Tornquist Zone in Scania (Sweden) during Permo-Mesozoic and

2177 Cenozoic times. Tectonophysics 444, 93-110.

2178 Bergman, S., Högdahl, K., Nironen, M., Ogenhall, E., Sjöström, H., Lundqvist, L.,

2179 Lahtinen, R., 2008. Timing of Palaeoproterozoic intra-orogenic sedimentation in the central

2180 Fennoscandian Shield; evidence from detrital zircon in metasandstone. Precambrian Research

2181 161, 231-249.

2182 Bergström, U., Stephens, M.B., Wahlgren, C.H., 2020. Chapter 16 - Polyphase (1.6–1.5

2183 and 1.1–1.0 Ga) deformation and metamorphism of Proterozoic (1.7–1.1 Ga) continental

2184 crust, Idefjorden terrane, Sveconorwegian orogen. Geological Society, London, Memoirs 50,

2185 397-434.

2186 Berthelsen, A., 1980. Towards a palinspastic tectonic analysis of the Baltic Shield, in:

2187 Cogne, J., Slansky, M. (Eds.), Geology of Europe, from Precambrian to the post-Hercyninan

2188 sedimentary basins. Mémoires du B.R.G.M., Paris, pp. 5-21.

2189 Bingen, B., 1989. Geochemistry of Sveconorwegian augen gneisses from SW Norway at

2190 the amphibolite-granulite facies transition. Norsk Geologisk Tidsskrift 69, 177-189.

2191 Bingen, B., Andersson, J., Söderlund, U., Möller, C., 2008a. The Mesoproterozoic in the

2192 Nordic countries. Episodes 31, 29-34.

2193 Bingen, B., Belousova, E.A., Griffin, W.L., 2011. Neoproterozoic recycling of the

2194 Sveconorwegian orogenic belt: detrital-zircon data from the Sparagmite basins in the

2195 Scandinavian Caledonides. Precambrian Research 189, 347-367.

2196 Bingen, B., Birkeland, A., Nordgulen, Ø., Sigmond, E.M.O., 2001. Correlation of

2197 supracrustal sequences and origin of terranes in the Sveconorwegian orogen of SW

2198    Scandinavia: SIMS data on zircon in clastic metasediments. Precambrian Research 108, 293-

2199    318.

2200    Bingen, B., Boven, A., Punzalan, L., Wijbrans, J., Demaiffe, D., 1998. Hornblende

2201    $^{40}Ar/^{39}Ar$ geochronology across terrane boundaries in the Sveconorwegian province of S

2202    Norway. Precambrian Research 90, 159-185.

2203    Bingen, B., Corfu, F., Stein, H.J., Whitehouse, M.J., 2015. U-Pb geochronology of the syn-

2204    orogenic Knaben molybdenum deposits, Sveconorwegian orogen, Norway. Geological

2205    Magazine 152, 537-556.

2206    Bingen, B., Davis, W.J., Hamilton, M.A., Engvik, A., Stein, H.J., Skår, Ø., Nordgulen, Ø.,

2207    2008b. Geochronology of high-grade metamorphism in the Sveconorwegian belt, S Norway:

2208    U-Pb, Th-Pb and Re-Os data. Norwegian Journal of Geology 88, 13-42.

2209    Bingen, B., Demaiffe, D., Hertogen, J., Weis, D., Michot, J., 1993. K-rich calc-alkaline

2210    augen gneisses of Grenvillian age in SW Norway: mingling of mantle-derived and crustal

2211    components. The Journal of Geology 101, 763-778.

2212    Bingen, B., Mansfeld, J., Sigmond, E.M.O., Stein, H.J., 2002. Baltica-Laurentia link

2213    during the Mesoproterozoic: 1.27 Ga development of continental basins in the

2214    Sveconorwegian Orogen, southern Norway. Canadian Journal of Earth Sciences 39, 1425-

2215    1440.

2216    Bingen, B., Nordgulen, Ø., Sigmond, E.M.O., Tucker, R.D., Mansfeld, J., Högdahl, K.,

2217    2003. Relations between 1.19-1.13 Ga continental magmatism, sedimentation and

2218    metamorphism, Sveconorwegian province, S Norway. Precambrian Research 124, 215-241.

2219    Bingen, B., Nordgulen, Ø., Viola, G., 2008c. A four-phase model for the Sveconorwegian

2220    orogeny, SW Scandinavia. Norwegian Journal of Geology 88, 43-72.

2221    Bingen, B., Skår, Ø., Marker, M., Sigmond, E.M.O., Nordgulen, Ø., Ragnhildstveit, J.,

2222    Mansfeld, J., Tucker, R.D., Liégeois, J.P., 2005. Timing of continental building in the

2223    Sveconorwegian orogen, SW Scandinavia. Norwegian Journal of Geology 85, 87-116.

2224    Bingen, B., van Breemen, O., 1998a. Tectonic regimes and terrane boundaries in the high-

2225    grade Sveconorwegian belt of SW Norway, inferred from U-Pb zircon geochronology and

2226    geochemical signature of augen gneiss suites. Journal of the Geological Society of London

2227    155, 143-154.

2228    Bingen, B., van Breemen, O., 1998b. U-Pb monazite ages in amphibolite- to granulite-

2229    facies orthogneisses reflect hydrous mineral breakdown reactions: Sveconorwegian Province

2230    of SW Norway. Contributions to Mineralogy and Petrology 132, 336-353.

2231    Bingen, B., Viola, G., 2018. The early-Sveconorwegian orogeny in southern Norway:

2232    tectonic model involving delamination of the sub-continental lithospheric mantle.

2233    Precambrian Research 313, 170-204.

2234    Bird, P., 1979. Continental delamination and the Colorado Plateau. Journal of Geophysical

2235    Research: Solid Earth 84, 7561-7571.

2236    Blereau, E., Johnson, T.E., Clark, C., Taylor, R.J.M., Kinny, P.D., Hand, M., 2017.

2237    Reappraising the P–T evolution of the Rogaland–Vest Agder Sector, southwestern Norway.

2238    Geoscience Frontiers 8, 1-14.

2239    Bogaerts, M., Scaillet, B., Liégeois, J.P., Vander Auwera, J., 2003. Petrology and

2240    geochemistry of the Lyngdal granodiorite (Southern Norway) and the role of fractional

2241    crystallization in the genesis of Proterozoic ferro-potassic A-type granites. Precambrian

2242    Research 124, 149-184.

2243    Bogaerts, M., Scaillet, B., Vander Auwera, J., 2006. Phase equilibria of the Lyngdal

2244    granodiorite (Norway): implications for the origin of metaluminous ferroan granitoids.

2245    Journal of Petrology 47, 2405-2431.

2246    Bogdanova, S., Bingen, B., Gorbatschev, R., Kheraskova, T., Kozlov, V., Puchkov, V.,

2247    Volozh, Y., 2008. The East European Craton (Baltica) before and during the assembly of

2248    Rodinia. Precambrian Research 160, 23-45.

2249    Boger, S.D., Raetz, M., Giles, D., Etchart, E., Fanning, C.M., 2005. U–Pb age data from

2250    the Sunsas region of Eastern Bolivia, evidence for the allochthonous origin of the Paragua

2251    Block. Precambrian Research 139, 121-146.

2252    Bolle, O., Demaiffe, D., Duchesne, J.C., 2003a. Petrogenesis of jotunitic and acidic

2253    members of an AMC suite (Rogaland anorthosite province, SW Norway): a Sr and Nd

2254    isotopic assessment. Precambrian Research 124, 185-214.

2255    Bolle, O., Diot, H., Duchesne, J.C., 2000. Magnetic fabric and deformation in charnockitic

2256    igneous rocks of the Bjerkreim–Sokndal layered intrusion (Rogaland, Southwest Norway).

2257    Journal of Structural Geology 22, 647-667.

2258    Bolle, O., Diot, H., Liégeois, J.P., Vander Auwera, J., 2010. The Farsund intrusion (SW

2259    Norway): a marker of late-Sveconorwegian (Grenvillian) tectonism emplaced along a newly

2260    defined major shear zone. Journal of Structural Geology 32, 1500-1518.

2261    Bolle, O., Diot, H., Trindade, R.I.F., 2003b. Magnetic fabrics in the Holum granite (Vest-

2262    Agder, southernmost Norway): implications for the late evolution of the Sveconorwegian

2263    (Grenvillian) orogen of SW Scandinavia. Precambrian Research 121, 221-249.

2264    Bolle, O., Diot, H., Vander Auwera, J., Dembele, A., Schittekat, J., Spassov, S.,

2265    Ovtcharova, M., Schaltegger, U., 2018. Pluton construction and deformation in the

2266    Sveconorwegian crust of SW Norway: Magnetic fabric and U-Pb geochronology of the

2267    Kleivan and Sjelset granitic complexes. Precambrian Research 305, 247-267.

2268    Bolle, O., Duchesne, J.C., 2007. The Apophysis of the Bjerkreim-Sokndal layered

2269    intrusion (Rogaland anorthosite province, SW Norway): A composite pluton build up by

2270  tectonically-driven emplacement of magmas along the margin of an AMC igneous complex.

2271  Lithos 98, 292-312.

2272  Bolle, O., Trindade, R.I.F., Bouchez, J.L., Duchesne, J.C., 2002. Imaging downward

2273  granitic magma transport in the Rogaland Igneous Complex, SW Norway. Terra Nova 14, 87-

2274  92.

2275  Bouvier, A., Vervoort, J.D., Patchett, P.J., 2008. The Lu-Hf and Sm-Nd isotopic

2276  composition of CHUR: Constraints from unequilibrated chondrites and implications for the

2277  bulk composition of terrestrial planets. Earth and Planetary Science Letters 273, 48-57.

2278  Brander, L., Appelquist, K., Cornell, D., Andersson, U.B., 2012. Igneous and metamorphic

2279  geochronologic evolution of granitoids in the central Eastern Segment, southern Sweden.

2280  International Geology Review 54, 509-546.

2281  Brander, L., Söderlund, U., 2009. Mesoproterozoic (1.47-1.44 Ga) orogenic magmatism in

2282  Fennoscandia; baddeleyite U-Pb dating of a suite of massif-type anorthosite in S Sweden.

2283  International Journal of Earth Sciences 98, 499-516.

2284  Brander, L., Söderlund, U., Bingen, B., 2011. Tracing the 1271-1246 Ma Central

2285  Scandinavian Dolerite Group mafic magmatism in Fennoscandia: U-Pb baddeleyite and Hf

2286  isotope data on the Moslätt and Børgefjell dolerites. Geological Magazine 148, 632-643.

2287  Brewer, T.S., Åhäll, K.I., Darbyshire, D.P.F., Menuge, J.F., 2002. Geochemistry of late

2288  Mesoproterozoic volcanism in southwestern Scandinavia: implications for Sveconorwegian

2289  /Grenvillian plate tectonic models. Journal of the Geological Society of London 159, 129-144.

2290  Brewer, T.S., Åhäll, K.I., Menuge, J.F., Storey, C.D., Parrish, R.R., 2004. Mesoproterozoic

2291  bimodal volcanism in SW Norway, evidence for recurring pre-Sveconorwegian continental

2292  margin tectonism. Precambrian Research 134, 249-273.

2293  Brewer, T.S., Daly, J.S., Åhäll, K.I., 1998. Contrasting magmatic arcs in the

2294  Palaeoproterozoic of the south-western Baltic Shield. Precambrian Research 92, 297-315.

2295    Brewer, T.S., Menuge, J.F., 1998. Metamorphic overprinting of Sm-Nd isotopic systems in

2296    volcanic rocks: the Telemark Supergroup, southern Norway. Chemical Geology 145, 1-16.

2297    Broekmans, M.A., Nijland, T.G., Jansen, J.B.H., 1994. Are stable isotopic trends in

2298    amphibolite to granulite facies transitions metamorphic of diagenetic? - An answer for the

2299    Arendal area (Bamble sector, S.E. Norway) from mid-Proterozoic carbon bearing rocks.

2300    American Journal of Science 294, 1135-1165.

2301    Brown, M., 2006. Duality of thermal regimes is the distinctive characteristic of plate

2302    tectonics since the Neoarchean. Geology 34, 961-964.

2303    Brown, M., 2013. Granite: From genesis to emplacement. Geological Society of America

2304    Bulletin 125, 1079-1113.

2305    Bruand, E., Storey, C., Fowler, M., 2014. Accessory mineral chemistry of high Ba–Sr

2306    granites from northern Scotland: Constraints on petrogenesis and records of whole-rock

2307    signature. Journal of Petrology 55, 1619-1651.

2308    Brueckner, H.K., 2009. Subduction of continental crust, the origin of post-orogenic

2309    granitoids (and anorthosites?) and the evolution of Fennoscandia. Journal of the Geological

2310    Society of London 166, 753-762.

2311    Buchan, K.L., Mertanen, S., Park, R.G., Pesonen, L.J., Elming, S.-Å., Abrahamsen, N.,

2312    Bylund, G., 2000. Comparing the drift of Laurentia and Baltica in the Proterozoic: the

2313    importance of key palaeomagnetic poles. Tectonophysics 319, 167-198.

2314    Bybee, G.M., Ashwal, L.D., Shirey, S.B., Horan, M., Mock, T., Andersen, T.B., 2014.

2315    Pyroxene megacrysts in Proterozoic anorthosites: Implications for tectonic setting, magma

2316    source and magmatic processes at the Moho. Earth and Planetary Science Letters 389, 74-85.

2317    Cagnard, F., Barbey, P., Gapais, D., 2011. Transition between "Archaean-type" and

2318    "modern-type" tectonics: Insights from the Finnish Lapland Granulite Belt. Precambrian

2319    Research 187, 127-142.

2320    Cameron, K.L., Lopez, R., Ortega-Gutiérrez, F., L, S.A., Keppie, J.D., Schulze, C., 2004.

2321    U-Pb geochronology and Pb isotopic compositions of leached feldspars: constraints on the

2322    origin and evolution of Grenville rocks from eastern and southern Mexico. Geological Society

2323    of America Memoirs 197, 755-769.

2324    Campbell, I.H., Allen, C.M., 2008. Formation of supercontinents linked to increases in

2325    atmospheric oxygen. Nature Geoscience 1, 554-558.

2326    Cardona, A., Chew, D., Valencia, V.A., Bayona, G., Miskovic, A., Ibañez-Mejía, M.,

2327    2010. Grenvillian remnants in the Northern Andes: Rodinian and Phanerozoic

2328    paleogeographic perspectives. Journal of South American Earth Sciences 29, 92-104.

2329    Carr, S.D., Easton, R.M., Jamieson, R.A., Culshaw, N.G., 2000. Geologic transect across

2330    the Grenville orogen of Ontario and New York. Canadian Journal of Earth Sciences 37, 193-

2331    216.

2332    Cawood, P.A., Pisarevsky, S.A., 2017. Laurentia-Baltica-Amazonia relations during

2333    Rodinia assembly. Precambrian Research 292, 386-397.

2334    Cawood, P.A., Strachan, R., Cutts, K., Kinny, P.D., Hand, M., Pisarevsky, S., 2010.

2335    Neoproterozoic orogeny along the margin of Rodinia: Valhalla orogen, North Atlantic.

2336    Geology 38, 99-102.

2337    Cawood, P.A., Strachan, R.A., Merle, R.E., Millar, I.L., Loewy, S.L., Dalziel, I.W.D.,

2338    Kinny, P.D., Jourdan, F., Nemchin, A.A., Connelly, J.N., 2015. Neoproterozoic to early

2339    Paleozoic extensional and compressional history of East Laurentian margin sequences: the

2340    Moine Supergroup, Scottish Caledonides. Geological Society of America Bulletin 127, 349-

2341    371.

2342    Cecys, A., Benn, K., 2007. Emplacement and deformation of the ca. 1.45 Ga Karlshamn

2343    granitoid pluton, southeastern Sweden, during ENE-WSW Danopolonian shortening.

2344    International Journal of Earth Sciences 96, 397-414.

2345    Cecys, A., Bogdanova, S., Janson, C., Bibikova, E., Kornfält, K.A., 2002. The Stenshuvud

2346    and Tåghusa granitoids: new representative of Mesoproterozoic magmatism in southern

2347    Sweden. GFF 124, 149-162.

2348    Chardon, D., Gapais, D., Cagnard, F., 2009. Flow of ultra-hot orogens: A view from the

2349    Precambrian, clues for the Phanerozoic. Tectonophysics 477, 105-118.

2350    Charlier, B., Duchesne, J.C., Vander Auwera, J., 2006. Magma chamber processes in the

2351    Tellnes ilmenite deposit (Rogaland Anorthosite Province, SW Norway) and the formation of

2352    Fe-Ti ores in massif-type anorthosites. Chemical Geology 234, 264-290.

2353    Charlier, B., Duchesne, J.C., Vander Auwera, J., Storme, J.Y., Maquil, R., Longhi, J.,

2354    2010. Polybaric fractional crystallization of high-alumina basalt parental magmas in the

2355    Egersund-Ogna massif-type anorthosite (Rogaland, SW Norway) constrained by plagioclase

2356    and high-alumina orthopyroxene megacrysts. Journal of Petrology 51, 2515-2546.

2357    Chen, M., Niu, F., Tromp, J., Lenardic, A., Lee, C.T.A., Cao, W., Ribeiro, J., 2017.

2358    Lithospheric foundering and underthrusting imaged beneath Tibet. Nature Communications 8,

2359    15659.

2360    Chiarenzelli, J., Lupulescu, M., Cousens, B., Thern, E., Coffin, L., Regan, S., 2010.

2361    Enriched Grenvillian lithospheric mantle as a consequence of long-lived subduction beneath

2362    Laurentia. Geology 38, 151-154.

2363    Christoffel, C.A., Connelly, J.N., Åhäll, K.I., 1999. Timing and characterization of

2364    recurrent pre-Sveconorwegian metamorphism and deformation in the Varberg-Halmstad

2365    region of SW Sweden. Precambrian Research 98, 173-195.

2366    Clemens, J.D., Darbyshire, D.P.F., Flinders, J., 2009. Sources of post-orogenic calcalkaline

2367    magmas: The Arrochar and Garabal Hill–Glen Fyne complexes, Scotland. Lithos 112, 524-

2368    542.

2369     Clough, P.W., Field, D., 1980. Chemical variation in metabasites from a Proterozoic

2370     amphibolite-granulite transition zone, S Norway. Contributions to Mineralogy and Petrology

2371     73, 277-286.

2372     Coint, N., Slagstad, T., Roberts, N.M.W., Marker, M., Røhr, T., Sørensen, B.E., 2015. The

2373     Late Mesoproterozoic Sirdal Magmatic Belt, SW Norway:Relationships between magmatism

2374     and metamorphism and implications for Sveconorwegian orogenesis. Precambrian Research

2375     265, 57-77.

2376     Collins, W.J., 2002. Hot orogens, tectonic switching, and creation of continental crust.

2377     Geology 30, 535-538.

2378     Connelly, J.N., Åhäll, K.I., 1996. The Mesoproterozoic cratonization of Baltica – new age

2379     constraints from SW Sweden, in: Brewer, T.S. (Ed.), Precambrian crustal evolution in the

2380     North Atlantic Region. Geological Society, London, Special Publications, pp. 261-273.

2381     Connelly, J.N., Berglund, J., Larson, S.Å., 1996. Thermotectonic evolution of the Eastern

2382     Segment of southwestern Sweden: tectonic constraints from U-Pb geochronology, in: Brewer,

2383     T.S. (Ed.), Precambrian crustal evolution in the North Atlantic Region. Geological Society,

2384     London, Special Publications, pp. 297-313.

2385     Cooper, D.C., Field, D., 1977. The chemistry and origins of Proterozoic low-potash, high-

2386     iron, charnockitic gneisses from Tromøy, South Norway. Earth and Planetary Science Letters

2387     35, 105-115.

2388     Cordani, U.G., Cardona, A., Jimenez, D.M., Liu, D., Nutman, A.P., 2005. Geochronology

2389     of Proterozoic basement inliers in the Colombian Andes: Tectonic history of remnants of a

2390     fragmented Grenville belt. Geological Society, London, Special Publications 246, 329-346.

2391     Corfu, F., 2019. The Sognefjell volcanic-subvolcanic complex – A late Sveconorwegian

2392     arc imbricated in the central Norwegian Caledonides. Precambrian Research 331, 105353.

2393    Corfu, F., Easton, R.M., 1995. U-Pb geochronology of the Mazinaw terrane, an imbricate

2394    segment of the Central Metasedimentary Belt, Grenville Province, Ontario. Canadian Journal

2395    of Earth Sciences 32, 959-976.

2396    Corfu, F., Laajoki, K., 2008. An uncommon episode of mafic magmatism at 1347 Ma in

2397    the Mesoproterozoic Telemark supracrustals, Sveconorwegian orogen - Implications for

2398    stratigraphy and tectonic evolution. Precambrian Research 160, 299-307.

2399    Cornell, D., Årebäck, H., Scherstén, A., 2000. Ion microprobe discovery of Archaean and

2400    Early Proterozoic zircon xenocrysts in southwest Sweden. GFF 122, 377-383.

2401    Corriveau, L., van Breemen, O., 2000. Docking of the Central Metasedimentary Belt to

2402    Laurentia in geon 12: evidence from the 1.17–1.16 Chevreuil intrusive suite and host

2403    gneisses, Quebec. Canadian Journal of Earth Sciences 37, 253-269.

2404    Cosca, M.A., Mezger, K., Essene, E.J., 1998. The Baltica-Laurentia connection:

2405    Sveconorwegian (Grenvillian) metamorphism, cooling, and unroofing in the Bamble Sector,

2406    Norway. The Journal of Geology 106, 539-552.

2407    Cosca, M.A., O'Nions, R.K., 1994. A re-examination of the influence of composition on

2408    argon retentivity in metamorphic calcic amphiboles. Chemical Geology 112, 39-56.

2409    Couzinié, S., Laurent, O., Moyen, J.F., Zeh, A., Bouilhol, P., Villaros, A., 2016. Post-

2410    collisional magmatism: crustal growth not identified by zircon Hf-O isotopes. Earth and

2411    Planetary Science Letters 456, 182-195.

2412    Cutts, K.A., Hand, M., Kelsey, D.E., Wade, B., Strachan, R.A., Clark, C., Netting, A.,

2413    2009. Evidence for 930 Ma metamorphism in the Shetland Islands, Scottish Caledonides:

2414    implications for Neoproterozoic tectonics in the Laurentia-Baltica sector of Rodinia. Journal

2415    of the Geological Society of London 166, 1033-1047.

2416    Dahlgren, S., Bogoch, R., Magaritz, M., Michard, A., 1993. Hydrothermal dolomite

2417    marbles associated with charnockitic magmatism in the Proterozoic Bamble Shear Belt, south

2418    Norway. Contributions to Mineralogy and Petrology 113, 394-409.

2419    Daly, J.S., McLelland, J.M., 1991. Juvenile Middle Proterozoic crust in the Adirondack

2420    Highlands, Grenville province, northeastern North America. Geology 19, 119-122.

2421    Dalziel, I.W.D., 1997. Neoproterozoic-Paleozoic geography and tectonics: reviews,

2422    hypothesis, environmental speculations. Geological Society of America Bulletin 109, 16-42.

2423    Debon, F., Le Fort, P., 1983. A chemical-mineralogical classification of common plutonic

2424    rocks and associations. Transactions of the Royal Society of Edinburgh, Earth Sciences 73,

2425    135-149.

2426    deHaas, G.J.L.M., Andersen, T., Vestin, J., 1999. Detrital zircon geochronology: new

2427    evidence for an old model for accretion of the SW Baltic Shield. The Journal of Geology 107,

2428    569-586.

2429    deHaas, G.J.L.M., Nijland, T.G., Andersen, T., Corfu, F., 2002a. New constraints on the

2430    timing of deposition and metamorphism in the Bamble sector, south Norway: zircon and

2431    titanite U-Pb data from the Nelaug area. GFF 124, 73-78.

2432    deHaas, G.J.L.M., Nijland, T.G., Valbracht, P.J., Maijer, C., Verschure, R., Andersen, T.,

2433    2002b. Magmatic versus metamorphic origin of olivine-plagioclase coronas. Contributions to

2434    Mineralogy and Petrology 143, 537-550.

2435    Demaiffe, D., Bingen, B., Wertz, P., Hertogen, J., 1990. Geochemistry of the Lyngdal

2436    hyperites (SW Norway): comparison with the monzonorites associated with the Rogaland

2437    anorthosite complex. Lithos 24, 237-250.

2438    Demaiffe, D., Michot, J., 1985. Isotope geochronology of the Proterozoic crustal segment

2439    of southern Norway: a review, in: Tobi, A.C., Touret, J.L. (Eds.), The deep Proterozoic crust

2440    in the north Atlantic provinces. Reidel, Dordrecht, pp. 411-433.

2441    Demaiffe, D., Weis, D., Michot, J., Duchesne, J.C., 1986. Isotopic constraints on the

2442    genesis of the Rogaland anorthositic suite (SW Norway). Chemical Geology 57, 167-179.

2443    Dewey, J.F., 1988. Extensional collapse of orogens. Tectonics 7, 1123-1139.

2444    DeWolf, C.P., Mezger, K., 1994. Lead isotope analyses of leached feldspars: Constraints

2445    on the early crustal history of the Grenville Orogen. Geochimica et Cosmochimica Acta 58,

2446    5537-5550.

2447    Dhuime, B., Hawkesworth, C., Cawood, P., 2011. When continents formed. Science 331,

2448    154-155.

2449    Dickin, A.P., 2000. Crustal formation in the Grenville Province: Nd-isotope evidence.

2450    Canadian Journal of Earth Sciences 37, 165-181.

2451    Dickin, A.P., Higgins, M.D., 1992. Sm/Nd evidence for a major 1.5 Ga crust-forming

2452    event in the Central Grenville Province. Geology 20, 137-140.

2453    Dickin, A.P., McNutt, R.H., 2007. The Central Metasedimentary Belt (Grenville Province)

2454    as a failed backarc rift zone: Nd isotope evidence. Earth and Planetary Science Letters 259,

2455    97-106.

2456    Dickin, A.P., McNutt, R.H., Martin, C., Guo, A., 2010. The extent of juvenile crust in the

2457    Grenville Province: Nd isotope evidence. Geological Society of America Bulletin 122, 870-

2458    883.

2459    Dons, J.A., 1960. The stratigraphy of supracrustal rocks, granitization and tectonics in the

2460    Precambrian Telemark area, southern Norway. Norges geologiske undersøkelse 212h, 1-30.

2461    Dons, J.A., Jorde, K., 1978. Geologisk kart over Norge, berggrunnskart Skien, 1:250000.

2462    Norges geologiske undersøkelse.

2463    Drüppel, K., Elsässer, L., Brandt, S., Gerdes, A., 2013. Sveconorwegian mid-crustal

2464    ultrahigh-temperature metamorphism in Rogaland, Norway: U-Pb LA-ICP-MS

2465 geochronology and pseudosections of sapphirine granulites and associated paragneisses.

2466 Journal of Petrology 54, 305-350.

2467 Duchesne, J.C., 1972. Iron-titanium oxide minerals in the Bjerkrem-Sogndal massif, south-

2468 western Norway. Journal of Petrology 13, 57-81.

2469 Duchesne, J.C., Berza, T., Liégeois, J.P., Vander Auwera, J., 1998. Shoshonitic liquid line

2470 of descent from diorite to granite: the Late Precambrian post-collisional Tismana pluton

2471 (South Carpathians, Romania). Lithos 45, 281-303.

2472 Duchesne, J.C., Charlier, B., 2005. Geochemistry of cumulates from the Bjerkreim-

2473 Sokndal layered intrusion (S. Norway). Part I: Constraints from major elements on the

2474 mechanism of cumulate formation and on the jotunite liquid line of descent. Lithos 83, 229-

2475 254.

2476 Duchesne, J.C., Liégeois, J.P., Vander Auwera, J., Longhi, J., 1999. The crustal tongue

2477 melting model and the origin of massive anorthosites. Terra Nova 11, 100-105.

2478 Duchesne, J.C., Maquil, R., Demaiffe, D., 1985. The Rogaland anorthosites: facts and

2479 speculations, in: Tobi, A.C., Touret, J.L. (Eds.), The deep Proterozoic crust in the north

2480 Atlantic provinces. Reidel, Dordrecht, pp. 449-476.

2481 Duchesne, J.C., Wilmart, E., 1997. Igneous charnockites and related rocks from the

2482 Bjerkreim-Sokndal layered intrusion (SW Norway): a jotunite (hypersthene monzodiorite)-

2483 derived A-type granitoid suite. Journal of Petrology 38, 337-369.

2484 Duchesne, J.C., Wilmart, E., Demaiffe, D., Hertogen, J., 1989. Monzonorites from

2485 Rogaland (southwest Norway): a series of rocks coeval but not comagmatic with massif-type

2486 anorthosites. Precambrian Research 45, 111-128.

2487 Eliasson, T., Ahlin, S., Petersson, J., 2003. Emplacement mechanism and thermobarometry

2488 of the Sveconorwegian Bohus granite, SW Sweden. GFF 125, 113-130.

2489     Eliasson, T., Schöberg, H., 1991. U-Pb dating of the post-kinematic Sveconorwegian

2490     (Grenvillian) Bohus granite, SW Sweden: evidence of restitic zircon. Precambrian Research

2491     51, 337-350.

2492     Elminen, T., Zwingmann, H., Kaakinen, A., 2018. Constraining the timing of brittle

2493     deformation and sedimentation in southern Finland: Implications for Neoproterozoic

2494     evolution of the eastern Fennoscandian shield. Precambrian Research 304, 110-124.

2495     Emslie, R.F., 1985. Proterozoic anorthosite massifs, in: Tobi, A.C., Touret, J.L. (Eds.), The

2496     deep Proterozoic crust in the north Atlantic provinces. Reidel, Dordrecht, pp. 39-60.

2497     Engvik, A.K., Bingen, B., Solli, A., 2016. Localized occurrences of granulite: P-T

2498     modeling, U-Pb geochronology and distribution of early-Sveconorwegian high-grade

2499     metamorphism in Bamble, South Norway. Lithos 240-243, 84-103.

2500     Engvik, A.K., Corfu, F., Solli, A., Austrheim, H., 2017. Sequence and timing of mineral

2501     replacement reactions during albitisation in the high-grade Bamble lithotectonic domain, S-

2502     Norway. Precambrian Research 291, 1-16.

2503     Engvik, A.K., Ihlen, P.M., Austrheim, H., 2014. Characterisation of Na-metasomatism in

2504     the Sveconorwegian Bamble Sector of South Norway. Geoscience Frontiers 5, 659-672.

2505     Engvik, A.K., Mezger, K., Wortelkamp, S., Bast, R., Corfu, F., Korneliussen, A., Ihlen,

2506     P.M., Bingen, B., Austrheim, H., 2011. Metasomatism of gabbro - mineral replacement and

2507     element mobilization during the Sveconorwegian metamorphic event. Journal of

2508     Metamorphic Geology 29, 399-423.

2509     Erlström, M., 2020. Chapter 24 - Carboniferous–Neogene tectonic evolution of the

2510     Fennoscandian transition zone, southern Sweden. Geological Society, London, Memoirs 50,

2511     603-620.

2512    EUGENO-S-working-group, 1988. Crustal structure and tectonic evolution of the

2513    transition between the Baltic Shield and the North German Caledonides (the EUGENO-S

2514    Project). Tectonophysics 150, 253-348.

2515    Evans, D.A.D., Mitchell, R.N., 2011. Assembly and breakup of the core of

2516    Paleoproterozoic-Mesoproterozoic supercontinent Nuna. Geology 39, 443-446.

2517    Falkum, T., 1985. Geotectonic evolution of southern Scandinavia in light of a late-

2518    Proterozoic plate-collision, in: Tobi, A.C., Touret, J.L. (Eds.), The deep Proterozoic crust in

2519    the north Atlantic provinces. Reidel, Dordrecht, pp. 309-322.

2520    Falkum, T., Petersen, J.S., 1980. The Sveconorwegian orogenic belt, a case of late-

2521    Proterozoic plate collision. Geologische Rundschau 69, 622-647.

2522    Field, D., Drury, S.A., Cooper, D.C., 1980. Rare-earth and LIL element fractionation in

2523    high-grade charnockitic gneisses, south Norway. Lithos 13, 281-289.

2524    Field, D., Smalley, P.C., Lamb, R.C., Råheim, A., 1985. Geochemical evolution of the 1.6-

2525    1.5 Ga-old amphibolite- granulite facies terrain, Bamble sector, Norway: dispelling the myth

2526    of grenvillian high-grade reworking, in: Tobi, A.C., Touret, J.L. (Eds.), The deep Proterozoic

2527    crust in the north Atlantic provinces. Reidel, Dordrecht, pp. 567-578.

2528    Fram, M.S., Longhi, J., 1992. Phase equilibria of dikes associated with Proterozoic

2529    anorthosite complexes. American Mineralogist 77, 605-616.

2530    Frost, B.R., Barnes, C.G., Collins, W.J., Arculus, R.J., Ellis, W.J., Frost, D.J., 2001. A

2531    geochemical classification for granitic rocks. Journal of Petrology 42, 2033-2048.

2532    Gabrielsen, R.H., Nystuen, J.P., Jarsve, E.M., Lundmark, A.M., 2015. The Sub-Cambrian

2533    Peneplain in southern Norway: its geological significance and its implications for post-

2534    Caledonian faulting, uplift and denudation. Journal of the Geological Society of London 172,

2535    777-791.

2536    Gammon, J.B., 1966. Fahlbands in the Precambrian of southern Norway. Economic

2537    Geology 61, 174-188.

2538    Gee, D.G., Andréasson, P.G., Lorenz, H., Frei, D., Majka, J., 2015. Detrital zircon

2539    signatures of the Baltoscandian margin along the Arctic Circle Caledonides in Sweden: The

2540    Sveconorwegian connection. Precambrian Research 265, 40-56.

2541    Geraldes, M.C., Van Schmus, W.R., Condie, K.C., Bell, S., Teixeira, W., Babinski, M.,

2542    2001. Proterozoic geologic evolution of the SW part of the Amazonian Craton in Mato

2543    Grosso state, Brazil. Precambrian Research 111, 91-128.

2544    Gerya, T., 2014. Precambrian geodynamics: Concepts and models. Gondwana Research

2545    25, 442-463.

2546    Ghani, A.A., Atherton, M.P., 2006. The chemical character of the Late Caledonian

2547    Donegal granites, Ireland, with comments on their genesis. Transactions of the Royal Society

2548    of Edinburgh-Earth Sciences 97, 437-454.

2549    Godin, L., Grujic, D., Law, R.D., Searle, M.P., 2006. Channel flow, ductile extrusion and

2550    exhumation in continental collision zones: an introduction. Geological Society, London,

2551    Special Publications 268, 1-23.

2552    Gong, Z., Evans, D.A.D., Elming, S.Å., Söderlund, U., Salminen, J.M., 2018.

2553    Paleomagnetism, magnetic anisotropy and U-Pb baddeleyite geochronology of the early

2554    Neoproterozoic Blekinge-Dalarna dolerite dykes, Sweden. Precambrian Research 317, 14-32.

2555    Gorbatschev, R., Bogdanova, S., 2006. Report: Aspects of the Proterozoic boundary

2556    between SE and SW Sweden. Department of Geology, Lund University, Sweden, pp. 1-50.

2557    Gower, C.F., 1985. Correlations between the Grenville Province and Sveconorwegian

2558    orogenic belt - implications for Proterozoic evolution of the southern margins of the Canadian

2559    and Baltic Shields, in: Tobi, A.C., Touret, J.L. (Eds.), The deep Proterozoic crust in the north

2560    Atlantic provinces. Reidel, Dordrecht, pp. 247-258.

2561    Gower, C.F., Kamo, S., Krogh, T.E., 2008. Indentor tectonism in the eastern Grenville

2562    Province. Precambrian Research 167, 201-212.

2563    Granseth, A., Slagstad, T., Coint, N., Roberts, N.M.W., Røhr, T.S., Sørensen, B.E., 2020.

2564    Tectonomagmatic evolution of the Sveconorwegian orogen recorded in the chemical and

2565    isotopic compositions of 1070–920 Ma granitoids. Precambrian Research 340, 105527.

2566    Graversen, O., Pedersen, S., 1999. Timing of Gothian structural evolution in SE Norway: a

2567    Rb-Sr whole-rock age study. Norsk Geologisk Tidsskrift 79, 47-56.

2568    Griffin, W.L., O'Reilly, S.Y., Afonso, J.C., Begg, G.C., 2009. The composition and

2569    evolution of lithospheric mantle: a re-evaluation and its tectonic implications. Journal of

2570    Petrology 50, 1185-1204.

2571    Griffin, W.L., Pearson, N.J., Belousova, E.A., Jackson, S.E., van Achterbergh, E.,

2572    O'Reilly, S.Y., Shee, S.R., 2000. The Hf isotope composition of cratonic mantle: LAM-MC-

2573    ICPMS analysis of zircon megacrysts in kimberlites. Geochimica et Cosmochimica Acta 64,

2574    133-147.

2575    Groulier, P.A., Indares, A., Dunning, G., Moukhsil, A., Jenner, G., 2018a. Syn-orogenic

2576    magmatism over 100 m.y. in high crustal levels of the central Grenville Province:

2577    Characteristics, age and tectonic significance. Lithos 312-313, 128-152.

2578    Groulier, P.A., Indares, A., Dunning, G., Moukhsil, A., Wälle, M., 2018b. Peri-Laurentian,

2579    Pinwarian-age oceanic arc crust preserved in the Grenville Province: Insights from the

2580    Escoumins supracrustal belt. Precambrian Research 311, 37-64.

2581    Grove, T.L., Chatterjee, N., Parman, S.W., Médard, E., 2006. The influence of H2O on

2582    mantle wedge melting. Earth and Planetary Science Letters 249, 74-89.

2583    Guenthner, W.R., Reiners, P.W., Drake, H., Tillberg, M., 2017. Zircon, titanite, and apatite

2584    (U-Th)/He ages and age-eU correlations from the Fennoscandian Shield, southern Sweden.

2585    Tectonics 36, 1254-1274.

2586     Hanmer, S., Corrigan, D., Pehrsson, S., Nadeau, L., 2000. SW Grenville Province, Canada:

2587     the case against post-1.4 Ga accretionary tectonics. Tectonophysics 319, 33-51.

2588     Hansen, E., Johansson, L., Andersson, J., LaBarge, L., Harlov, D., Möller, C., Vincent, S.,

2589     2015. Partial melting in amphibolites in a deep section of the Sveconorwegian Orogen, SW

2590     Sweden. Lithos 236–237, 27-45.

2591     Harley, S., Kelly, N.M., Möller, A., 2007. Zircon behaviour and the thermal histories of

2592     mountain chains. Elements 3, 25-30.

2593     Harley, S.L., 2008. Refining the P–T records of UHT crustal metamorphism. Journal of

2594     Metamorphic Geology 26, 125-154.

2595     Harlov, D.E., 2000. Pressure-temperature estimation in orthopyroxene-garnet bearing

2596     granulite facies rocks, Bamble Sector, Norway. Mineralogy and Petrology 69, 11-33.

2597     Harlov, D.E., Van Den Kerkhof, A., Johansson, L., 2013. The Varberg-Torpa charnockite-

2598     granite association, SW Sweden: Mineralogy, petrology, and fluid inclusion chemistry.

2599     Journal of Petrology 54, 3-40.

2600     Hartz, E.H., Torsvik, T.H., 2002. Baltica upside down: a new plate tectonic model for

2601     Rodinia and the Iapetus Ocean. Geology 30, 255-258.

2602     Haschke, M.R., Scheuber, E., Günther, A., Reutter, K.J., 2002. Evolutionary cycles during

2603     the Andean orogeny: repeated slab breakoff and flat subduction. Terra Nova 14, 49-55.

2604     Hawkesworth, C., Cawood, P., Kemp, T., Storey, C., Dhuime, B., 2009. A Matter of

2605     preservation. Science 232, 49-50.

2606     He, Z.Y., Klemd, R., Yan, L.L., Zhang, Z.M., 2018. The origin and crustal evolution of

2607     microcontinents in the Beishan orogen of the southern Central Asian Orogenic Belt. Earth-

2608     Science Reviews 185, 1-14.

2609     Heaman, L.M., Smalley, P.C., 1994. A U–Pb study of the Morkheia Complex and

2610     associated gneisses, south Norway: implications for disturbed Rb–Sr systems and for the

2611  temporal evolution of Mesoproterozoic magmatism in Laurentia. Geochimica et

2612  Cosmochimica Acta 58, 1899-1911.

2613  Hellström, F.A., Johansson, Å., Larson, S.Å., 2004. Age emplacement of late

2614  Sveconorwegian monzogabbroic dykes, SW Sweden. Precambrian Research 128, 39-55.

2615  Henderson, I.H.C., Ihlen, P.M., 2004. Emplacement of polygeneration pegmatites in

2616  relation to Sveconorwegian contractional tectonics: examples from southern Norway.

2617  Precambrian Research 133, 207-222.

2618  Hervé, F., Pankhurst, R.J., Fanning, C.M., Calderon, M., Yaxley, G.M., 2007. The South

2619  Patagonian batholith: 150 my of granite magmatism on a plate margin. Lithos 97, 373-394.

2620  Herzberg, C., Condie, K., Korenaga, J., 2010. Thermal history of the Earth and its

2621  petrological expression. Earth and Planetary Science Letters 292, 79-88.

2622  Hetherington, C.J., Harlov, D.E., 2008. Metasomatic thorite and uraninite inclusions in

2623  xenotime and monazite from granitic pegmatites, Hidra anorthosite massif, southwestern

2624  Norway: Mechanics and fluid chemistry. American Mineralogist 93, 806-820.

2625  Hoffman, P.F., 1991. Did the breakout of Laurentia turn Gondwanaland inside-out?

2626  Science 252, 1409-1412.

2627  Högdahl, K., Andersson, U.B., Eklund, O., 2004. The Transcandinavian Igneous Belt

2628  (TIB) in Sweden: a review of its character and evolution. Geological Survey of Finland,

2629  Special Paper 37.

2630  Holland, T.J., Babu, E.V., Waters, D.J., 1996. Phase relations of osumilite and dehydration

2631  melting in pelitic rocks: a simple thermodynamic model for the KFMASH system.

2632  Contributions to Mineralogy and Petrology 124, 383-394.

2633  Hynes, A., Rivers, T., 2010. Protracted continental collision - evidence from the Grenville

2634  Orogen. Canadian Journal of Earth Sciences 47, 591-620.

2635    Ibanez-Mejia, M., Pullen, A., Arenstein, J., Gehrels, G.E., Valley, J., Ducea, M.N., Mora,

2636    A.R., Pecha, M., Ruiz, J., 2015. Unraveling crustal growth and reworking processes in

2637    complex zircons from orogenic lower-crust: The Proterozoic Putumayo Orogen of Amazonia.

2638    Precambrian Research 267, 285-310.

2639    Ibanez-Mejia, M., Ruiz, J., Valencia, V.A., Cardona, A., Gehrels, G.E., Mora, A.R., 2011.

2640    The Putumayo Orogen of Amazonia and its implications for Rodinia reconstructions: new U-

2641    Pb geochronological insights into the Proterozoic tectonic evolution of northwestern South

2642    America. Precambrian Research 191, 58-77.

2643    Indares, A., 2020. Deciphering the metamorphic architecture and magmatic patterns of

2644    large hot orogens: Insights from the central Grenville Province. Gondwana Research 80, 385-

2645    409.

2646    INSPIRE_Directive, 2007. INSPIRE Knowledge Base, Infrastructure for spatial

2647    information in Europe, registry. European Commission; http://inspire.ec.europa.eu/registry.

2648    Jagoutz, O., Schmidt, M.W., 2013. The composition of the foundered complement to the

2649    continental crust and a re-evaluation of fluxes in arcs. Earth and Planetary Science Letters

2650    371-372, 177-190.

2651    Jamieson, R.A., Beaumont, C., 2013. On the origin of orogens. Geological Society of

2652    America Bulletin 125, 1671-1702.

2653    Janoušek, V., Konopásek, J., Ulrich, S., Erban, V., Tajčmanová, L., Jeřábek, P., 2010.

2654    Geochemical character and petrogenesis of Pan-African Amspoort suite of the Boundary

2655    Igneous Complex in the Kaoko Belt (NW Namibia). Gondwana Research 18, 688-707.

2656    Jensen, E., Corfu, F., 2016. The U–Pb age of the Finse batholith, a composite bimodal

2657    Sveconorwegian intrusion. Norwegian Journal of Geology 96, 171-178.

2658    Jiménez-Mejía, D.M., Juliani, C., Cordani, U.G., 2006. P–T–t conditions of high-grade

2659    metamorphic rocks of the Garzon Massif, Andean basement, SE Colombia. Journal of South

2660    American Earth Sciences 21, 322-336.

2661    Johansson, Å., 2009. Baltica, Amazonia and the SAMBA connection - 1000 million years

2662    of neighbourhood during the Proterozoic? Precambrian Research 175, 221-234.

2663    Johansson, Å., Waight, T., Andersen, T., Simonsen, S.L., 2016. Geochemistry and

2664    petrogenesis of Mesoproterozoic A-type granitoids from the Danish island of Bornholm,

2665    southern Fennoscandia. Lithos 244, 94-108.

2666    Johansson, L., Lindh, A., Möller, C., 1991. Late Sveconorwegian (Grenville) high-pressure

2667    granulite facies metamorphism in southwest Sweden. Journal of Metamorphic Geology 9,

2668    283-292.

2669    Johansson, L., Möller, C., Söderlund, U., 2001. Geochronology of eclogite facies

2670    metamorphism in the Sveconorwegian Province of SW Sweden. Precambrian Research 106,

2671    261-275.

2672    Johnson, T.E., Brown, M., Kaus, B.J.P., VanTongeren, J.A., 2013. Delamination and

2673    recycling of Archaean crust caused by gravitational instabilities. Nature Geoscience 7, 47.

2674    Kalsbeek, F., Thrane, K., Nutman, A.P., Jepsen, H., 2000. Late Mesoproterozoic to early

2675    Neoproterozoic history of the East Greenland Caledonides: evidence for Grenvillian

2676    orogenesis? Journal of the Geological Society of London 157, 1215-1225.

2677    Kelsey, D.E., Clark, C., Hand, M., 2008. Thermobarometric modelling of zircon and

2678    monazite growth in melt-bearing systems: examples using model metapelitic and

2679    metapsammitic granulites. Journal of Metamorphic Geology 26, 199-212.

2680    Keppie, J.D., Dostal, J., Cameron, K.L., Solari, L.A., Ortega-Gutiérrez, F., Lopez, R.,

2681    2003. Geochronology and geochemistry of Grenvillian igneous suites in the northern Oaxacan

2682    Complex, southern Mexico: tectonic implications. Precambrian Research 120, 365-389.

2683    Keppie, J.D., Ortega-Gutiérrez, F., 2010. 1.3-0.9 Ga Oaxaquia (Mexico): Remnant of an

2684    arc/backarc on the northern margin of Amazonia. Journal of South American Earth Sciences

2685    29, 21-27.

2686    Kirkland, C.L., Daly, J.S., Whitehouse, M.J., 2006. Granitic magmatism of Grenvillian and

2687    late Neoproterozoic age in Finnmark, Arctic Norway – Constraining pre-Scandian

2688    deformation in the Kalak Nappe Complex. Precambrian Research 145, 24-52.

2689    Kirkland, C.L., Daly, J.S., Whitehouse, M.J., 2007. Provenance and terrane evolution of

2690    the Kalak Nappe Complex, Norwegian Caledonides: Implications for Neoproterozoic

2691    paleogeography and tectonics. The Journal of Geology 115, 21-41.

2692    Kirkland, C.L., Daly, J.S., Whitehouse, M.J., 2008a. Basement-cover relationships of the

2693    Kalak Nappe Complex, Arctic Norwegian Caledonides and constraints on Neoproterozoic

2694    terrane assembly in the North Atlantic region. Precambrian Research 160, 245-276.

2695    Kirkland, C.L., Strachan, R.A., Prave, A.R., 2008b. Detrital zircon signature of the Moine

2696    Supergroup, Scotland: contrasts and comparisons with other Neoproterozoic successions

2697    within the circum-North Atlantic region. Precambrian Research 163, 332-350.

2698    Knudsen, T.L., 1996. Petrology and geothermobarometry of granulite facies metapelites

2699    from the Hisøy-Torungen area, south Norway: new data on the Sveconorwegian P-T-t path  of

2700    the Bamble sector. Journal of Metamorphic Geology 14, 267-287.

2701    Knudsen, T.L., Andersen, T., 1999. Petrology and geochemistry of the Tromøy gneiss

2702    complex, South Norway, an alleged example of Proterozoic depleted lower continental crust.

2703    Journal of Petrology 40, 909-933.

2704    Knudsen, T.L., Andersen, T., Whitehouse, M.J., Vestin, J., 1997. Detrital zircon ages from

2705    southern Norway - implications for the Proterozoic evolution of the southwestern Baltic

2706    Shield. Contributions to Mineralogy and Petrology 130, 47-58.

2707    Koistinen, T., Stephens, M.B., Bogatchev, V., Nordgulen, Ø., Wennerström, M.,

2708    Korhonen, J., 2001. Geological map of the Fennoscandian shield, Scale 1:2000000.

2709    Geological Surveys of Finland, Norway and Sweden and the North-West Department of

2710    Natural Resources of Russia.

2711    Korenaga, J., 2008. Urey ratio and the structure and evolution of Earth's mantle. Reviews

2712    of Geophysics 46, RG2007.

2713    Korja, A., Lahtinen, R., Nironen, M., 2006. The Svecofennian orogen: a collage of

2714    microcontinents and island arcs, in: Gee, D.G., Stephenson, R.A. (Eds.), European lithosphere

2715    dynamics. Geological Society, London, Memoirs, pp. 561-578.

2716    Köykkä, J., 2011. The sedimentation and paleohydrology of the Mesoproterozoic stream

2717    deposits in a strike-slip basin (Svinsaga Formation), Telemark, southern Norway.

2718    Sedimentary Geology 236, 239-255.

2719    Köykkä, J., Laajoki, K., 2009. Mesoproterozoic frost action at the base of the Svinsaga

2720    Formation, central Telemark, South Norway. Norwegian Journal of Geology 89, 291-303.

2721    Köykkä, J., Lamminen, J., 2011. Tidally influenced clastic epeiric sea at a

2722    Mesoproterozoic continental margin, Rjukan Rift Basin, southern Norway. Precambrian

2723    Research 185, 164-182.

2724    Krystopowicz, N.J., Currie, C.A., 2013. Crustal eclogitization and lithosphere delamination

2725    in orogens. Earth and Planetary Science Letters 361, 195-207.

2726    Laajoki, K., 2002. The Mesoproterozoic sub-Heddal unconformity, Sauland, central

2727    Telemark, Norway. Norwegian Journal of Geology 82, 139-152.

2728    Laajoki, K., Corfu, F., 2007. Lithostratigraphy of the Mesoproterozoic Vemork formation,

2729    central Telemark, Norway. Bulletin of the Geological Society of Finland 79, 41-67.

2730    Laajoki, K., Corfu, F., Andersen, T., 2002. Lithostratigraphy and U-Pb geochronology of

2731    the Telemark supracrustals in the Bandak-Sauland area, Telemark, South Norway. Norwegian

2732    Journal of Geology 82, 119-138.

2733    Lahtinen, R., Korja, A., Nironen, M., Heikkinen, P., 2009. Palaeoproterozoic accretionary

2734    processes in Fennoscandia. Geological Society, London, Special Publications 318, 237-256.

2735    Lamminen, J., 2011. Provenance and correlation of sediments in Telemark, South Norway:

2736    status of the Lifjell Group and implications for early Sveconorwegian fault tectonics.

2737    Norwegian Journal of Geology 91, 57-75.

2738    Lamminen, J., Andersen, T., Nystuen, J.P., 2011. Zircon U-Pb ages and Lu-Hf isotopes

2739    from basement rocks associated with Neoproterozoic sedimentary successions in the

2740    Sparagmite Region and adjacent areas, South Norway: the crustal architecture of western

2741    Baltica. Norwegian Journal of Geology 91, 35-55.

2742    Lamminen, J., Andersen, T., Nystuen, J.P., 2015. Provenance and rift basin architecture of

2743    the Neoproterozoic Hedmark Basin, South Norway inferred from U-Pb ages and Lu-Hf

2744    isotopes of conglomerate clasts and detrital zircons. Geological Magazine 152, 80-105.

2745    Lamminen, J., Köykkä, J., 2010. The provenance and evolution of the Rjukan Rift Basin,

2746    Telemark, south Norway: The shift from a rift basin to an epicontinental sea along a

2747    Mesoproterozoic supercontinent. Precambrian Research 181, 129-149.

2748    Larsen, B.T., Olaussen, S., Sundvoll, B., Heeremans, M., 2008. The Permo-Carboniferous

2749    Olso Rift through six stages and 65 million years. Episodes 31, 52-58.

2750    Larsson, D., Söderlund, U., 2005. Lu-Hf apatite geochronology of mafic cumulates: an

2751    example from a Fe-Ti mineralization at Smålands Taberg, southern Sweden. Chemical

2752    Geology 224, 201-211.

2753    Lassen, A., Thybo, H., 2012. Neoproterozoic and Palaeozoic evolution of SW Scandinavia

2754    based on integrated seismic interpretation. Precambrian Research 204, 75-104.

2755    Laurent, A., Janoušek, V., Magna, T., Schulmann, K., Míková, J., 2014. Petrogenesis and

2756    geochronology of a post-orogenic calc-alkaline magmatic association: the Žulová Pluton,

2757    Bohemian Massif. Journal of Geosciences 59, 415-440.

2758    Laurent, A.T., Bingen, B., Duchene, S., Whitehouse, M.J., Seydoux-Guillaume, A.M.,

2759    Bosse, V., 2018a. Decoding protracted zircon geochronological record in ultra-high

2760    temperature granulite, and persistence of partial melting in the crust, Rogaland, Norway.

2761    Contributions to Mineralogy and Petrology 173, 29.

2762    Laurent, A.T., Duchene, S., Bingen, B., Bosse, V., Seydoux-Guillaume, A.M., 2018b. Two

2763    successive phases of ultrahigh temperature metamorphism in Rogaland, S. Norway: evidence

2764    from Y-in-monazite thermometry. Journal of Metamorphic Geology 36, 1009-1037.

2765    Laurent, A.T., Seydoux-Guillaume, A.M., Duchene, S., Bingen, B., Bosse, V., Datas, L.,

2766    2016. Sulphate incorporation in monazite lattice and dating the cycle of sulphur in

2767    metamorphic belts. Contributions to Mineralogy and Petrology 171, 1-19.

2768    Laurent, O., Couzinié, S., Zeh, A., Vanderhaeghe, O., Moyen, J.F., Villaros, A., Gardien,

2769    V., Chelle-Michou, C., 2017. Protracted, coeval crust and mantle melting during Variscan

2770    late-orogenic evolution: U–Pb dating in the eastern French Massif Central. International

2771    Journal of Earth Sciences on line, 1-31.

2772    Lawlor, P.J., Ortega-Gutiérrez, F., Cameron, K.L., Ochoa-Camarillo, H., Lopez, R.,

2773    Sampson, D.E., 1999. U-Pb geochronology, geochemistry, and provenance of the Grenvillian

2774    Huiznopala Gneiss of Eastern Mexico. Precambrian Research 94, 73-99.

2775    Levander, A., Schmandt, B., Miller, M.S., Liu, K., Karlstrom, K.E., Crow, R.S., Lee,

2776    C.T.A., Humphreys, E.D., 2011. Continuing Colorado plateau uplift by delamination-style

2777    convective lithospheric downwelling. Nature 472, 461-465.

2778    Li, Z.-H., Liu, M., Gerya, T., 2016. Lithosphere delamination in continental collisional

2779    orogens: A systematic numerical study. Journal of Geophysical Research: Solid Earth 121,

2780    5186-5211.

2781    Li, Z.X., Bogdanova, S.V., Collins, A.S., Davidson, A., De Waele, B., Ernst, R.E.,

2782    Fitzsimons, I.C.W., Fuck, R.A., Gladkochub, D.P., Jacobs, J., Karlstrom, K.E., Lu, S.,

2783    Natapov, L.M., Pease, V., Pisarevsky, S.A., Thrane, K., Vernikovsky, V., 2008. Assembly,

2784    configuration, and break-up history of Rodinia: A synthesis. Precambrian Research 160, 179-

2785    210.

2786    Liégeois, J.P., Navez, J., Hertogen, J., Black, R., 1998. Contrasting origin of post-

2787    collisional high-K calc-alkaline and shoshonitic versus alkaline and peralkaline granitoids.

2788    The use of sliding normalization. Lithos 45, 1-28.

2789    Lindh, A., Gorbatschev, R., Lundegårdh, P.H., 1998. Beskrivning till berggrundskartan

2790    över Värmlands Län; Västra Värmlands Berggrund. Sveriges Geologiska Undersökning Ser.

2791    Ba, 45:2, 1-405.

2792    Longhi, J., 2005. A mantle or mafic crustal source for Proterozoic anorthosites? Lithos 83,

2793    183-198.

2794    Longhi, J., Vander Auwera, J., Fram, M.S., Duchesne, J.C., 1999. Some phase equilibrium

2795    constraints on the origin of Proterozoic (massif) anorthosites and related rocks. Journal of

2796    Petrology 40, 339-362.

2797    Lorenz, H., Gee, D.G., Larionov, A.N., Majka, J., 2012. The Grenville-Sveconorwegian

2798    orogen in the high Arctic. Geological Magazine 149, 875-891.

2799    Loron, C., Moczydłowska, M., 2018. Tonian (Neoproterozoic) eukaryotic and prokaryotic

2800    organic-walled microfossils from the upper Visingsö Group, Sweden. Palynology 42, 220-

2801    254.

2802    Lundmark, A.M., Corfu, F., 2008. Late-orogenic Sveconorwegian massif anorthosite in the

2803    Jotun Nappe Complex, SW Norway, and causes of repeated AMCG magmatism along the

2804    Baltoscandian margin. Contributions to Mineralogy and Petrology 155, 147-163.

2805    Lundmark, A.M., Lamminen, J., 2016. The provenance and setting of the Mesoproterozoic

2806    Dala Sandstone, western Sweden, and paleogeographic implications for southwestern

2807    Fennoscandia. Precambrian Research 275, 197-208.

2808    Lundqvist, I., Skiöld, T., 1993. U-Pb zircon dating of volcanic rocks of the Åmål Group,

2809    western Sweden, in: Lundqvist, T. (Ed.), Radiometric dating results. Sveriges Geologiska

2810    Undersökning, Research Papers, Uppsala, pp. 24-30.

2811    Maijer, C., 1987. Day 7 - The metamorphic envelope of the Rogaland intrusive complex,

2812    in: Maijer, C., Padget, P. (Eds.), The geology of southernmost Norway: an excursion guide.

2813    Norges Geologiske Undersøkelse, Special Publication No 1, pp. 68-73.

2814    Maijer, C., Verschure, R.H., 1998. Petrology and isotope geology of the Hunnedalen

2815    monzonoritic dyke swarm, SW Norway: a possible late expression of Egersund anorthosite

2816    magmatism. Norges Geologiske Undersøkelse Bulletin 434, 83-107.

2817    Marcantonio, F., McNutt, R.H., Dickin, A.P., Heaman, L.M., 1990. Isotopic evidence for

2818    the crustal evolution of the Frontenac Arch in the Grenville Province of Ontario, Canada.

2819    Chemical Geology 83, 297-314.

2820    Mattila, J., Viola, G., 2014. New constraints on 1.7 Gyr of brittle tectonic evolution in

2821    southwestern Finland derived from a structural study at the site of a potential nuclear waste

2822    repository (Olkiluoto Island). Journal of Structural Geology 67, Part A, 50-74.

2823    McLelland, J.M., Daly, J.S., Chiarenzelli, J., 1993. Sm–Nd and U–Pb isotopic evidence of

2824    juvenile crust in the Adirondack Lowlands and implications for the evolution of the

2825    Adirondack Mts. The Journal of Geology 101, 97-105.

2826  Menuge, J.F., 1985. Neodymium, isotope evidence for the age and origin of the

2827  Proterozoic of Telemark, south Norway, in: Tobi, A.C., Touret, J.L. (Eds.), The deep

2828  Proterozoic crust in the north Atlantic provinces. Reidel, Dordrecht, pp. 435-448.

2829  Menuge, J.F., 1988. The petrogenesis of massif anorthosites: a Nd and Sr isotopic

2830  investigation of the Proterozoic of Rogaland-Vest Agder, SW Norway. Contributions to

2831  Mineralogy and Petrology 98, 363-373.

2832  Merdith, A.S., Collins, A.S., Williams, S.E., Pisarevsky, S., Foden, J.D., Archibald, D.B.,

2833  Blades, M.L., Alessio, B.L., Armistead, S., Plavsa, D., Clark, C., Müller, R.D., 2017. A full-

2834  plate global reconstruction of the Neoproterozoic. Gondwana Research 50, 84-134.

2835  Milne, K.P., Starmer, I.C., 1982. Extreme differentiation in the Proterozoic Gjerstad-

2836  Morkeheia complex of South Norway. Contributions to Mineralogy and Petrology 79, 381-

2837  393.

2838  Moczydłowska, M., Pease, V., Willman, S., Wickström, L., Agic, H., 2018. A Tonian age

2839  for the Visingsö Group in Sweden constrained by detrital zircon dating and biochronology:

2840  Implications for evolutionary events. Geological Magazine 155, 1175-1189.

2841  Möller, A., O'Brien, P.J., Kennedy, A., Kröner, A., 2002. Polyphase zircon in ultrahigh-

2842  temperature granulites (Rogaland, SW Norway): constraints for Pb diffusion in zircon.

2843  Journal of Metamorphic Geology 20, 727-740.

2844  Möller, A., O'Brien, P.J., Kennedy, A., Kröner, A., 2003. Linking growth episodes of

2845  zircon and metamorphic textures to zircon chemistry: an example from the ultrahigh-

2846  temperature granulites of Rogaland (SW Norway), in: Vance, D., Müller, W., Villa, I.M.

2847  (Eds.), Geochronology: linking the isotopic record with petrology and textures. Geological

2848  Society, London, Special Publications, pp. 65-81.

2849    Möller, C., 1998. Decompressed eclogites in the Sveconorwegian (-Grenvillian) orogen of

2850    SW Sweden: petrology and tectonic implications. Journal of Metamorphic Geology 16, 641-

2851    656.

2852    Möller, C., 1999. Sapphirine in SW Sweden: a record of Sveconorwegian (-Grenvillian)

2853    late-orogenic tectonic exhumation. Journal of Metamorphic Geology 17, 127-141.

2854    Möller, C., Andersson, J., 2018. Metamorphic zoning and behaviour of an underthrusting

2855    continental plate. Journal of Metamorphic Geology 36, 567-589.

2856    Möller, C., Andersson, J., Dyck, B., Antal Lundin, I., 2015. Exhumation of an eclogite

2857    terrane as a hot migmatitic nappe, Sveconorwegian orogen. Lithos 226, 147-168.

2858    Möller, C., Andersson, J., Lundqvist, I., Hellström, F.A., 2007. Linking deformation,

2859    migmatite formation and zircon U-Pb geochronology in polymetamorphic gneisses,

2860    Sveconorwegian province, Sweden. Journal of Metamorphic Geology 25, 727-750.

2861    Möller, C., Söderlund, U., 1997. Age constraints on the regional deformation within the

2862    Eastern Segment, S Sweden: Late Sveconorwegian granite dyke intrusion and metamorphic

2863    deformational relations. GFF 119, 1-12.

2864    Morton, R.D., 1971. Geological investigations in the Bamble sector of the Fennoscandian

2865    Shield, S. Norway. No II. Metasediments and metapyroclastics (?) within the Precambrian

2866    metamorphic suite of the S Norwegian Skaergaard. Norsk Geologisk Tidsskrift 51, 63-83.

2867    Moyen, J.F., Laurent, O., Chelle-Michou, C., Couzinié, S., Vanderhaeghe, O., Zeh, A.,

2868    Villaros, A., Gardien, V., 2017. Collision vs. subduction-related magmatism: Two contrasting

2869    ways of granite formation and implications for crustal growth. Lithos 277, 154-177.

2870    Mulch, A., Cosca, M.A., Andresen, A., Fiebig, J., 2005. Time scales of deformation and

2871    exhumation in extensional detachment systems determined by high-spatial resolution in situ

2872    UV-laser $^{40}$Ar/$^{39}$Ar dating. Earth and Planetary Science Letters 233, 375-390.

2873    Müller, A., Ihlen, P.M., Snook, B., Larsen, R., Flem, B., Bingen, B., Williamson, B.J.,

2874    2015. The chemistry of quartz in granitic pegmatites of southern Norway: petrogenetic and

2875    economic implications. Economic Geology 110, 1737-1757.

2876    Müller, A., Romer, R.L., Pedersen, R.B., 2017. The Sveconorwegian Pegmatite Province –

2877    Thousands of pegmatites without parental granite. Canadian Mineralogist 55, 283-315.

2878    Munz, I.A., 1990. Whiteschists and orthoamphibole-cordierite rocks and the P-T-t path of

2879    the Modum Complex, South Norway. Lithos 24, 181-200.

2880    Munz, I.A., Morvik, R., 1991. Metagabbros in the Modum Complex, southern Norway: an

2881    important heat source for Sveconorwegian metamorphism. Precambrian Research 52, 97-113.

2882    Munz, I.A., Wayne, D., Austrheim, H., 1994. Retrograde fluid infiltration in the high-grade

2883    Modum Complex, South Norway - Evidence for age, source and REE mobility. Contributions

2884    to Mineralogy and Petrology 116, 32-46.

2885    Neilson, J.C., Kokelaar, B.P., Crowley, Q.G., 2009. Timing, relations and cause of plutonic

2886    and volcanic activity of the Siluro-Devonian post-collision magmatic episode in the Grampian

2887    Terrane, Scotland. Journal of the Geological Society of London 166, 545-561.

2888    Nielsen, F.M., Campbell, I.H., McCulloch, M., Wilson, J.R., 1996. A strontium isotopic

2889    investigation of the Bjerkreim-Sokndal layered intrusion, Southwest Norway. Journal of

2890    Petrology 37, 171-193.

2891    Nijland, T.G., deHaas, G.J.L.M., Andersen, T., 2000. Rifting-related (sub)alkaline

2892    magmatism in the Bamble sector (Norway) during the 'Gothian'–Sveconorwegian interlude.

2893    GFF 122, 297-305.

2894    Nijland, T.G., Harlov, D.E., Andersen, T., 2014. The Bamble Sector, South Norway: a

2895    review. Geoscience Frontiers 5, 635-658.

2896    Nijland, T.G., Maijer, C., 1993. The regional amphibolite to granulite facies transition at

2897    Arendal, Norway: evidence for a thermal dome. Neues Jahrbuch für Mineralogie,

2898    Abhandlungen 165, 191-221.

2899    Nijland, T.G., Maijer, C., Senior, A., Verschure, R.H., 1993. Primary sedimentary

2900    structures and compositions of the high-grade metamorphic Nidelva Quartzite Complex

2901    (Bamble, Norway), and the origin of nodular gneisses. Proceedings Koninklijke Nederlandse

2902    Akademie van Wetenschappen 96, 217-232.

2903    Nijland, T.G., Touret, J.L.R., Visser, D., 1998. Anomalously low temperature

2904    orthopyroxene, spinel, and sapphirine occurrences in metasediments from the Bamble

2905    amphibolite-to-granulite facies transition zone (South Norway): possible evidence for

2906    localized action of saline fluids. The Journal of Geology 106, 575-590.

2907    Nordgulen, Ø., 1999. Geologisk kart over Norge, berggrunnskart Hamar, 1:250000.

2908    Norges geologiske undersøkelse.

2909    Nystuen, J.P., Andresen, A., Kumpulainen, R.A., Siedlecka, A., 2008. Neoproterozoic

2910    basin evolution in Fennoscandia, East Greenland and Svalbard. Episodes 31, 35-43.

2911    Olesen, O., Smethurst, M.A., Torsvik, T.H., Bidstrup, T., 2004. Sveconorwegian igneous

2912    complexes beneath the Norwegian-Danish Basin. Tectonophysics 387, 105-130.

2913    Olivarius, M., Friis, H., Kokfelt, T.F., Wilson, J.R., 2015. Proterozoic basement and

2914    Palaeozoic sediments in the Ringkøbing–Fyn High characterized by zircon U–Pb ages and

2915    heavy minerals from Danish onshore wells. Bulletin of the Geological Society of Denmark

2916    63, 29-43.

2917    Page, L.M., Möller, C., Johansson, L., 1996a. $^{40}$Ar/$^{39}$Ar geochronology across the Mylonite

2918    Zone and the Southwestern Granulite Province in the Sveconorwegian Orogen of S Sweden.

2919    Precambrian Research 79, 239-259.

2920    Page, L.M., Stephens, M.B., Wahlgren, C.H., 1996b. $^{40}Ar/^{39}Ar$ geochronological

2921    constraints on the tectonothermal evolution of the Eastern Segment of the Sveconorwegian

2922    Orogen, south-central Sweden, in: Brewer, T.S. (Ed.), Precambrian crustal evolution in the

2923    North Atlantic Region. Geological Society, London, Special Publications, pp. 315-330.

2924    Paludan, J., Hansen, U.B., Olesen, N.O., 1994. Structural evolution of the Precambrian

2925    Bjerkreim–Sokndal intrusion, South Norway. Norsk Geologisk Tidsskrift 74, 185-198.

2926    Park, R.G., Åhäll, K.I., Boland, M.P., 1991. The Sveconorwegian shear-zone network of

2927    SW Sweden in relation to mid-Proterozoic plate movements. Precambrian Research 49, 245-

2928    260.

2929    Pasteels, P., Demaiffe, D., Michot, J., 1979. U-Pb and Rb-Sr geochronology of the eastern

2930    part of the south Rogaland igneous complex, southern Norway. Lithos 12, 199-208.

2931    Pearce, J.A., Harris, N.B., Tindle, A.G., 1984. Trace element discrimination diagrams for

2932    the tectonic interpretation of granitic rocks. Journal of Petrology 25, 956-983.

2933    Peccerillo, A., Taylor, S.R., 1976. Geochemistry of eocene calc-alkaline volcanic rocks

2934    from the Kastamonu area, Northern Turkey. Contributions to Mineralogy and Petrology 58,

2935    63-81.

2936    Pedersen, S., 1981. Rb-Sr age determinations on late Proterozoic granitoids from the Evje

2937    area, South Norway. Bulletin of the Geological Society of Denmark 29, 129-143.

2938    Pedersen, S., Andersen, T., Konnerup-Madsen, J., Griffin, W.L., 2009. Recurrent

2939    Mesoproterozoic continental magmatism in South-Central Norway. International Journal of

2940    Earth Sciences 98, 1151-1171.

2941    Persson-Nilsson, K., Lundqvist, L., 2014. Abstract. The Gillberga synform - and upper-

2942    crustal orogenic lid?, 31st Nordic Geological Winter Meeting, Lund, Sweden. Geologiska

2943    Föreningen.

2944    Petersson, A., Scherstén, A., Andersson, J., Möller, C., 2015a. Zircon U-Pb and Hf

2945    isotopes from the eastern part of the Sveconorwegian Orogen, SW Sweden: implications for

2946    the growth of Fennoscandia, in: Roberts, N.M.W., van Kranendonk, M., Parman, S., Shirey,

2947    S., Clift, P.D. (Eds.), Continent formation through time. Geological Society, London, Special

2948    Publications, pp. 281-303.

2949    Petersson, A., Scherstén, A., Bingen, B., Gerdes, A., Whitehouse, M.J., 2015b.

2950    Mesoproterozoic continental growth: U-Pb-Hf-O zircon record in the Idefjorden Terrane,

2951    Sveconorwegian Orogen. Precambrian Research 261, 75-95.

2952    Pettersson, C.H., Pease, V., Frei, D., 2009. U-Pb zircon provenance of metasedimentary

2953    basement of the Northwestern Terrane, Svalbard: Implications for the Grenvillian-

2954    Sveconorwegian orogeny and development of Rodinia. Precambrian Research 175, 206-220.

2955    Piñán-Llamas, A., Andersson, J., Möller, C., Johansson, L., Hansen, E., 2015. Polyphasal

2956    foreland-vergent deformation in a deep section of the 1 Ga Sveconorwegian orogen.

2957    Precambrian Research 265, 121-149.

2958    Pisarevsky, S.A., Elming, S.Å., Pesonen, L.J., Li, Z.X., 2014. Mesoproterozoic

2959    paleogeography: Supercontinent and beyond. Precambrian Research 244, 207-225.

2960    Plank, T., Kelley, K.A., Zimmer, M.M., Hauri, E.H., Wallace, P.J., 2013. Why do mafic

2961    arc magmas contain c. 4 wt% water on average? Earth and Planetary Science Letters 364,

2962    168-179.

2963    Poudjom Djomani, Y.H., O'Reilly, S.Y., Griffin, W.L., Morgan, P., 2001. The density

2964    structure of subcontinental lithosphere through time. Earth and Planetary Science Letters 184,

2965    605-621.

2966    Pulsipher, M.A., Dehler, C.M., 2019. U-Pb detrital zircon geochronology, petrography,

2967    and synthesis of the middle Neoproterozoic Visingsö Group, Southern Sweden. Precambrian

2968    Research 320, 323-333.

2969    Rämö, O.T., 1991. Petrogenesis of the Proterozoic rapakivi granites and related basic rocks

2970    of southeastern Fennoscandia: Nd and Pb isotopic and general geochemic constraints.

2971    Geological Survey of Finland Bulletin 355, 1-161.

2972    Rey, P., Vanderhaeghe, O., Teyssier, C., 2001. Gravitational collapse of the continental

2973    crust: definition, regimes and modes. Tectonophysics 342, 435-449.

2974    Rey, P.F., Houseman, G., 2006. Lithospheric scale gravitational flow: the impact of body

2975    forces on orogenic processes from Archaean to Phanerozoic. Geological Society, London,

2976    Special Publications 253, 153-167.

2977    Ripa, M., Stephens, M.B., 2020a. Chapter 9 - Continental magmatic arc and siliciclastic

2978    sedimentation in the far-field part of a 1.7 Ga accretionary orogen. Geological Society,

2979    London, Memoirs 50, 253-268.

2980    Ripa, M., Stephens, M.B., 2020b. Chapter 10 - Magmatism (1.6–1.4 Ga) and

2981    Mesoproterozoic sedimentation related to intracratonic rifting coeval with distal accretionary

2982    orogenesis. Geological Society, London, Memoirs 50, 269-288.

2983    Ripa, M., Stephens, M.B., 2020c. Chapter 12 - Dolerites (1.27–1.25 Ga) and alkaline

2984    ultrabasic dykes (c. 1.14 Ga) related to intracratonic rifting. Geological Society, London,

2985    Memoirs 50, 315-323.

2986    Ripa, M., Stephens, M.B., 2020d. Chapter 13 - Siliciclastic sedimentation in a foreland

2987    basin to the Sveconorwegian orogen and dolerites (0.98–0.95 Ga) related to intracratonic

2988    rifting. Geological Society, London, Memoirs 50, 325-333.

2989    Rivers, T., 2008. Assembly and preservation of lower, mid, and upper orogenic crust in the

2990    Grenville Province-Implications for the evolution of large hot long-duration orogens.

2991    Precambrian Research 167, 237-259.

2992    Rivers, T., 2012. Upper-crustal orogenic lid and mid-crustal core complexes: signature of a

2993    collapsed orogenic plateau in the hinterland of the Grenville Province. Canadian Journal of

2994    Earth Sciences 49, 1-42.

2995    Roberts, N.M.W., 2013. The boring billion? – Lid tectonics, continental growth and

2996    environmental change associated with the Columbia supercontinent. Geoscience Frontiers 4,

2997    681-691.

2998    Roberts, N.M.W., Slagstad, T., 2015. Continental growth and reworking on the edge of the

2999    Columbia and Rodinia supercontinents; 1.86–0.9 Ga accretionary orogeny in southwest

3000    Fennoscandia. International Geology Review 57, 1582-1606.

3001    Roberts, N.M.W., Slagstad, T., Parrish, R.R., Norry, M.J., Marker, M., Horstwood,

3002    M.S.A., 2013. Sedimentary recycling in arc magmas: geochemical and U-Pb-Hf-O constraints

3003    on the Mesoproterozoic Suldal Arc, SW Norway. Contributions to Mineralogy and Petrology

3004    165, 507-523.

3005    Robins, B., Tumyr, O., Tysseland, M., Garmann, L.B., 1997. The Bjerkreim-Sokndal

3006    layered intrusion, Rogaland, SW Norway: Evidence from marginal rocks for a jotunite parent

3007    magma. Lithos 39, 121-133.

3008    Rodhe, A., 1987. Depositional environments and lithostratigraphy of the Middle

3009    Proterozoic Almesåkra group, southern Sweden. Sveriges Geologiska Undersökning Ca 69, 1-

3010    80.

3011    Roffeis, C., Corfu, F., 2014. Caledonian nappes of southern Norway and their correlation

3012    with Sveconorwegian basement domains, in: Corfu, F., Gasser, D., Chew, D.M. (Eds.), New

3013    perspectives on the Caledonides of Scandinavia and related areas. Geological Society,

3014    London, Special Publications, pp. 193-221.

3015    Rogers, J.J.W., Santosh, M., 2002. Configuration of Columbia, a Mesoproterozoic

3016    Supercontinent. Gondwana Research 5, 5-22.

3017    Røhr, T.S., Bingen, B., Robinson, P., Reddy, S.M., 2013. Geochronology of

3018    Paleoproterozoic augen gneisses in the Western Gneiss Region, Norway: evidence for

3019    Sveconorwegian zircon neocrystallization and Caledonian zircon deformation. The Journal of

3020    Geology 121, 105-128.

3021    Romer, R.L., Smeds, S.A., 1996. U-Pb columbite ages of pegmatites from Sveconorwegian

3022    terranes in southwestern Sweden. Precambrian Research 76, 15-30.

3023    Royden, L.H., Burchfiel, B.C., van der Hilst, R.D., 2008. The geological evolution of the

3024    Tibetan Plateau. Science 321, 1054-1058.

3025    Rubatto, D., Hermann, J., Berger, J., Engi, M., 2009. Protracted fluid-induced melting

3026    during Barrovian metamorphism in the Central Alps. Contributions to Mineralogy and

3027    Petrology 158, 703-722.

3028    Ruiz, J., Patchett, P.J., Ortega-Gutierrez, F., 1988. Proterozoic and Phanerozoicbasement

3029    terranes of Mexico from Nd isotopic studies. Geological Society of America Bulletin 100,

3030    274-281.

3031    Saintot, A., Stephens, M.B., Viola, G., Nordgulen, Ø., 2011. Brittle tectonic evolution and

3032    paleostress field reconstruction in the southwestern part of the Fennoscandian Shield,

3033    Forsmark, Sweden. Tectonics 30.

3034    Schärer, U., Wilmart, E., Duchesne, J.C., 1996. The short duration and anorogenic

3035    character of anorthosite magmatism: U-Pb dating of the Rogaland complex, Norway. Earth

3036    and Planetary Science Letters 139, 335-350.

3037    Scheiber, T., Viola, G., Bingen, B., Peters, M., Solli, A., 2015. Multiple reactivation and

3038    strain localization along a Proterozoic orogen-scale deformation zone: the Kongsberg-

3039    Telemark boundary in southern Norway revisited. Precambrian Research 265, 78-103.

3040    Scherer, E., Munker, C., Mezger, K., 2001. Calibration of the lutetium-hafnium clock.

3041    Science 293, 683-687.

3042 Scherstén, A., Årebäck, H., Cornell, D., Hoskin, P., Åberg, A., Armstrong, R., 2000.

3043 Dating mafic-ultramafic intrusions by ion-microprobing contact-melt zircon: examples from

3044 SW Sweden. Contributions to Mineralogy and Petrology 139, 115-125.

3045 Schiellerup, H., Lambert, D.D., Prestvik, T., Robins, B., McBride, J.S., Larsen, R.B., 2000.

3046 Re–Os isotopic evidence for a lower crustal origin of massif-type anorthosites. Nature 405,

3047 781-784.

3048 Seydoux-Guillaume, A.M., Montel, J.M., Bingen, B., Bosse, V., de Parseval, P., Paquette,

3049 J.L., Janots, E., Wirth, R., 2012. Low-temperature alteration of monazite: Fluid mediated

3050 coupled dissolution-precipitation, irradiation damage, and disturbance of the U-Pb and Th-Pb

3051 chronometers. Chemical Geology 330-331, 140-158.

3052 Sigmond, E.M.O., 1975. Geologisk kart over Norge, berggrunnskart Sauda, 1:250000.

3053 Norges geologiske undersøkelse, Trondheim.

3054 Sigmond, E.M.O., 1978. Beskrivelse til det berggrunnsgeologiske kartbladet Sauda

3055 1:250000. Norges geologiske undersøkelse Bulletin 341, 1-94.

3056 Sigmond, E.M.O., 1985. The Mandal–Ustaoset line, a newly discovered major fault zone

3057 in south Norway, in: Tobi, A.C., Touret, J.L. (Eds.), The deep Proterozoic crust in the north

3058 Atlantic provinces. Reidel, Dordrecht, pp. 323-331.

3059 Sigmond, E.M.O., 1998. Geologisk kart over Norge, berggrunnskart Odda, 1:250000.

3060 Norges geologiske undersøkelse, Trondheim.

3061 Sigmond, E.M.O., Ragnhildstveit, J., 2004. Berggrunnskart Kalhovd 1515 II, 1:50000.

3062 Norges geologiske undersøkelse, Trondheim.

3063 Sizova, E., Gerya, T., Brown, M., 2014. Contrasting styles of Phanerozoic and

3064 Precambrian continental collision. Gondwana Research 25, 522-545.

3065 Slagstad, T., Kulakov, E., Kirkland, C.L., Roberts, N.M.W., Ganerød, M., 2019. Breaking

3066 the Grenville–Sveconorwegian link in Rodinia reconstructions. Terra Nova 31, 430-437.

3067    Slagstad, T., Marker, M., Roberts, N.M.W., Saalmann, K., Kirkland, C.L., Kulakov, E.,

3068    Ganerød, M., Røhr, T.S., Møkkelgjerd, S.H.H., Granseth, A., Sørensen, B.E., 2020. The

3069    Sveconorwegian orogeny – Reamalgamation of the fragmented southwestern margin of

3070    Fennoscandia. Precambrian Research 350, 105877.

3071    Slagstad, T., Roberts, N.M.W., Coint, N., Høy, I., Sauer, S., Kirkland, K.L., Marker, M.,

3072    Røhr, T.S., Henderson, I.H.C., Stormoen, M.A., Skår, Ø., Sørensen, B.E., Bybee, G.M., 2018.

3073    Magma-driven, high-grade metamorphism in the Sveconorwegian Province, southwest

3074    Norway, during the terminal stages of Fennoscandian Shield evolution. Geosphere 14, 861-

3075    882.

3076    Slagstad, T., Roberts, N.M.W., Kulakov, E., 2017. Linking orogenesis across a

3077    supercontinent; the Grenvillian and Sveconorwegian margins on Rodinia. Gondwana

3078    Research 44, 109-115.

3079    Slagstad, T., Roberts, N.M.W., Marker, M., Røhr, T.S., Schiellerup, H., 2013. A non-

3080    collisional, accretionary Sveconorwegian orogen. Terra Nova 25, 30-37.

3081    Sláma, J., Walderhaug, O., Fonneland, H., Košler, J., Pedersen, R.B., 2011. Provenance of

3082    Neoproterozoic to Upper Cretaceous sedimentary rocks, eastern Greenland: Implications for

3083    recognizing the sources of sediments in the Norwegian Sea. Sedimentary Geology 238, 254-

3084    267.

3085    Sobolev, A.V., Chaussidon, M., 1996. $H_2O$ concentrations in primary melts from supra-

3086    subduction zones and mid-ocean ridges: Implications for $H_2O$ storage and recycling in the

3087    mantle. Earth and Planetary Science Letters 137, 45-55.

3088    Söderlund, P., Söderlund, U., Möller, C., Gorbatschev, R., Rodhe, A., 2004. Petrology and

3089    ion microprobe U-Pb chronology applied to a metabasic intrusion in southern Sweden: a

3090    study on zircon formation during metamorphism and deformation. Tectonics 23, TC5005,

3091    doi:5010.1029 /2003TC001498.

3092    Söderlund, U., Ask, R., 2006. Evidence for two pulses (1215-1224 and ca. 1205 Ma) of

3093    bimodal magmatism along the Protogine Zone, S Sweden. GFF 128, 303-310.

3094    Söderlund, U., Elming, S.Å., Ernst, R.E., Schissel, D., 2006. The Central Scandinavian

3095    Dolerite Group - Protracted hotspot activity or back-arc magmatism? Constraints from U-Pb

3096    baddeleyite geochronology and Hf isotopic data. Precambrian Research 150, 136-152.

3097    Söderlund, U., Hellström, F.A., Kamo, S.L., 2008a. Geochronology of high-pressure mafic

3098    granulite dykes in SW Sweden; tracking the P-T-t path of metamorphism using Hf isotopes in

3099    zircon and baddeleyite. Journal of Metamorphic Geology 26, 539-560.

3100    Söderlund, U., Isachsen, C.E., Bylund, G., Heaman, L.M., Patchett, P.J., Vervoort, J.D.,

3101    Andersson, U.B., 2005. U-Pb baddeleyite ages, and Hf, Nd isotope chemistry constraining

3102    repeated mafic magmatism in the Fennoscandian Shield from 1.6 to 0.9 Ga. Contributions to

3103    Mineralogy and Petrology 150, 174-194.

3104    Söderlund, U., Jarl, L.G., Persson, P.O., Stephens, M.B., Wahlgren, C.H., 1999. Protolith

3105    ages and timing of deformation in the eastern, marginal part of the Sveconorwegian orogen,

3106    southwestern Sweden. Precambrian Research 94, 29-48.

3107    Söderlund, U., Karlsson, C., Johansson, L., Larsson, K., 2008b. The Kullaberg peninsula -

3108    a glimpse of the Proterozoic evolution of SW Fennoscandia. GFF 130, 1-10.

3109    Söderlund, U., Möller, C., Andersson, J., Johansson, L., Whitehouse, M.J., 2002. Zircon

3110    geochronology in polymetamorphic gneisses in the Sveconorwgian orogen, SW Sweden: ion

3111    microprobe evidence for 1.46-1.42 Ga and 0.98-0.96 Ga reworking. Precambrian Research

3112    113, 193-225.

3113    Solari, L.A., Ortega-Gutiérrez, F., Elías-Herrera, M., Ortega-Obregón, C., Macías-Romo,

3114    C., Reyes-Salas, M., 2014. Detrital provenance of the Grenvillian Oaxacan Complex,

3115    southern Mexico: a zircon perspective. International Journal of Earth Sciences 103, 1301-

3116    1315.

3117    Spear, F.S., 1993. Metamorphic phase equilibria and pressure-temperature-time paths.

3118    Mineralogical Society of America, Monograph, Washington D.C.

3119    Spencer, C.J., Roberts, N.M.W., Cawood, P.A., Hawkesworth, C.J., Prave, A.R., Antonini,

3120    A.S.M., Horstwood, M.S.A., 2014. Intermontane basins and bimodal volcanism at the onset

3121    of the Sveconorwegian Orogeny, southern Norway. Precambrian Research 252, 107-118.

3122    Stacey, J.S., Kramers, J.D., 1975. Approximation of terrestrial lead isotope evolution by a

3123    two-stage model. Earth and Planetary Science Letters 26, 207-221.

3124    Starmer, I.C., 1985. The evolution of the south Norwegian Proterozoic as revealed by the

3125    major and mega-tectonics of the Kongsberg and Bamble sector, in: Tobi, A.C., Touret, J.L.

3126    (Eds.), The deep Proterozoic crust in the north Altantic provinces. Reidel, Dordrecht, pp. 259-

3127    290.

3128    Starmer, I.C., 1991. The Proterozoic evolution of the Bamble sector shear belt, southern

3129    Norway: correlations across southern Scandinavia and the Grenvillian controversy.

3130    Precambrian Research 49, 107-139.

3131    Stein, H.J., Bingen, B., 2002. 1.05-1.01 Ga Sveconorwegian metamorphism and

3132    deformation of the supracrustal sequence at Sæsvatn, South Norway: Re-Os dating of Cu-Mo

3133    mineral occurrences, in: Blundell, D., Neubauer, F., von Quadt, A. (Eds.), The timing and

3134    location of major ore deposits in an evolving orogen. Geological Society, London, Special

3135    Publications, pp. 319-335.

3136    Stephens, M.B., 2020. Chapter 8 - Outboard-migrating accretionary orogeny at 1.9–1.8 Ga

3137    (Svecokarelian) along a margin to the continent Fennoscandia. Geological Society, London,

3138    Memoirs 50, 237-250.

3139    Stephens, M.B., Bergström, U., Wahlgren, C.H., 2020. Chapter 14 - Regional context and

3140    lithotectonic framework of the 1.1–0.9 Ga Sveconorwegian orogen, southwestern Sweden.

3141    Geological Society, London, Memoirs 50, 337-349.

3142     Stephens, M.B., Wahlgren, C.H., 2020a. Chapter 15 - Polyphase (1.9–1.8, 1.5–1.4 and 1.0–

3143     0.9 Ga) deformation and metamorphism of Proterozoic (1.9–1.2 Ga) continental crust, Eastern

3144     Segment, Sveconorwegian orogen. Geological Society, London, Memoirs 50, 351-396.

3145     Stephens, M.B., Wahlgren, C.H., 2020b. Chapter 17 - Accretionary orogens reworked in

3146     an overriding plate setting during protracted continent–continent collision, Sveconorwegian

3147     orogen, southwestern Sweden. Geological Society, London, Memoirs 50, 435-448.

3148     Stephens, M.B., Wahlgren, C.H., Weijermars, R., Cruden, A.R., 1996. Left lateral

3149     transpressive deformation and its tectonic implications, Sveconorwegian Orogen, Baltic

3150     Shield, Southwestern Sweden. Precambrian Research 79, 261-279.

3151     Strachan, R.A., Nutman, A.P., Friderichsen, J.D., 1995. SHRIMP U-Pb geochronology and

3152     metamorphic history of the Smallefjord sequence, NE Greenland Caledonides. Journal of the

3153     Geological Society of London 152, 779-784.

3154     Strachan, R.A., Prave, A.R., Kirkland, C.L., Storey, C.D., 2013. U–Pb detrital zircon

3155     geochronology of the Dalradian Supergroup, Shetland Islands, Scotland: implications for

3156     regional correlations and Neoproterozoic–Palaeozoic basin development. Journal of the

3157     Geological Society of London 170, 905-916.

3158     Thybo, H., 2001. Crustal structure along the EGT profile across the Tornquist Fan

3159     interpreted from seismic, gravity and magnetic data. Tectonophysics 334, 155-190.

3160     Tobi, A.C., Hermans, G.A., Maijer, C., Jansen, J.B.H., 1985. Metamorphic zoning in the

3161     high-grade Proterozoic of Rogaland-Vest Agder, SW Norway, in: Tobi, A.C., Touret, J.L.

3162     (Eds.), The deep Proterozoic crust in the north Atlantic provinces. Reidel, Dordrecht, pp. 477-

3163     497.

3164     Tohver, E., Bettencourt, J.S., Tosdal, R., Mezger, K., Leite, W.B., Payolla, B.L., 2004a.

3165     Terrane transfer during the Grenville orogeny: tracing the Amazonian ancestry of southern

3166    Appalachian basement through Pb and Nd isotopes. Earth and Planetary Science Letters 228,

3167    161-176.

3168    Tohver, E., van der Pluijm, B.A., Mezger, K., Essene, E., Scandolara, J.E., Rizzotto, G.,

3169    2004b. Significance of the Nova Bresilândia metasedimentary belt in western Brazil:

3170    Redefining the Mesoproterozoic boundary of the Amazon craton. Tectonics 23, TC6004, doi:

3171    6010.1029/2003TC001563, 001561-001520.

3172    Tohver, E., van der Pluijm, B.A., Mezger, K., Scandolara, J.E., Essene, E., 2005. Two

3173    stage tectonic history of the SW Amazon craton in the late Mesoproterozoic: identifying a

3174    cryptic suture zone. Precambrian Research 137, 35-59.

3175    Tomkins, H.S., Williams, I.S., Ellis, D.J., 2005. In situ U-Pb dating of zircon formed from

3176    retrograde garnet breakdown during decompression in Rogaland, SW Norway. Journal of

3177    Metamorphic Geology 23, 201-215.

3178    Torgersen, E., Henderson, I.H.C., Bingen, B., Svendby, K., Nasuti, A., 2018. Abstract. The

3179    Nisser Shear Zone – Discovery of a Sveconorwegian crustal-scale detachment zone in

3180    southern Norway 33rd Nordic Geological Winter Meeting. Geological Society of Denmark,

3181    Copenhagen, Denmark p. 59.

3182    Torgersen, E., Viola, G., Zwingmann, H., Henderson, I.H.C., 2015. Inclined K-Ar illite age

3183    spectra in brittle fault gouges: effects of fault reactivation and wall-rock contamination. Terra

3184    Nova 27, 106-113.

3185    Torsvik, T.H., 2003. The Rodinia jigsaw puzzle. Science 300, 1379-1381.

3186    Torsvik, T.H., Smethurst, M.A., Meert, J.G., Van der Voo, R., Mc Kerrow, W.S., Brasier,

3187    M.D., Sturt, B.A., Walderhaug, H.J., 1996. Continental break up and collision in the

3188    Neoproterozoic and Paleozoic - A tale of Baltica and Laurentia. Earth-Science Reviews 40,

3189    229-258.

3190    Touret, J.L., 1971a. Le facies granulite en Norvège méridionale. 1. Les associations

3191    minéralogiques. Lithos 4, 239-249.

3192    Touret, J.L., 1971b. Le facies granulite en Norvège méridionale. 2. Les inclusions fluides.

3193    Lithos 4, 423-436.

3194    Touret, J.L., 1987. Day 2 - The high-grade metamorphic Bamble sector, in: Maijer, C.,

3195    Padget, P. (Eds.), The geology of southernmost Norway: an excursion guide. Norges

3196    Geologiske Undersøkelse, Special Publication No 1, pp. 25-30.

3197    Tual, L., Piñán-Llamas, A., Möller, C., 2015. High-temperature deformation in the basal

3198    shear zone of an eclogite-bearing fold nappe, Sveconorwegian orogen, Sweden. Precambrian

3199    Research 265, 104-120.

3200    Tual, L., Pitra, P., Möller, C., 2017. P–T evolution of Precambrian eclogite in the

3201    Sveconorwegian orogen, SW Sweden. Journal of Metamorphic Geology, n/a-n/a.

3202    Tucker, R.D., Krogh, T.E., Råheim, A., 1990. Proterozoic evolution and age - province

3203    boundaries in the central part of the Western Gneiss Region, Norway: results of U-Pb dating

3204    of accessory minerals from Trondheimsfjord to Geiranger, in: Gower, C.F., Rivers, T., Ryan,

3205    B. (Eds.), Mid-Proterozoic Laurentia-Baltica. Geological Association of Canada, Special

3206    Paper 38, pp. 149-173.

3207    Ulmius, J., Andersson, J., Möller, C., 2015. Hallandian 1.45 Ga high-temperature

3208    metamorphism in Baltica: P-T evolution and SIMS U-Pb zircon ages of aluminous gneisses,

3209    SW Sweden. Precambrian Research 265, 10-39.

3210    Ulmius, J., Möller, C., Page, L., Johansson, L., Ganerød, M., 2018. The eastern boundary

3211    of Sveconorwegian reworking in the Baltic Shield, defined by 40Ar/39Ar geochronology

3212    across the southernmost Sveconorwegian Province. Precambrian Research 307, 201-217.

3213    Vaasjoki, M., 1981. The lead isotopic composition of some Finnish galenas. Geological

3214    Survey of Finland Bulletin 316, 25.

3215    Valentino, D.W., Chiarenzelli, J.R., Regan, S.P., 2019. Spatial and temporal links between

3216    Shawinigan accretionary orogenesis and massif anorthosite intrusion, southern Grenville

3217    province, New York, U.S.A. Journal of Geodynamics 129, 80-97.

3218    Vander Auwera, J., Bogaerts, M., Bolle, O., Longhi, J., 2008. Genesis of intermediate

3219    igneous rocks at the end of the Sveconorwegian (Grenvillian) orogeny (S Norway) and their

3220    contribution to intracrustal differentiation. Contributions to Mineralogy and Petrology 156,

3221    721-743.

3222    Vander Auwera, J., Bogaerts, M., Liégeois, J.P., Demaiffe, D., Wilmart, E., Bolle, O.,

3223    Duchesne, J.C., 2003. Derivation of the 1.0-0.9 Ga ferro-potassic A-type granitoids of

3224    southern Norway by extreme differentiation from basic magmas. Precambrian Research 124,

3225    107-148.

3226    Vander Auwera, J., Bolle, O., Bingen, B., Liégeois, J.P., Bogaerts, M., Duchesne, J.C.,

3227    DeWaele, B., Longhi, J., 2011. Sveconorwegian massif-type anorthosites and related

3228    granitoids result from post-collisional melting of a continental root. Earth-Science Reviews

3229    107, 375-397.

3230    Vander Auwera, J., Bolle, O., Dupont, A., Pin, C., Paquette, J.L., Charlier, B., Duchesne,

3231    J.C., Mattielli, N., Bogaerts, M., 2014a. Source-derived heterogeneities in the composite

3232    (charnockite-granite) ferroan Farsund intrusion (SW Norway). Precambrian Research 251,

3233    141-163.

3234    Vander Auwera, J., Charlier, B., Duchesne, J.C., Bingen, B., Longhi, J., Bolle, O., 2014b.

3235    Comment on Bybee et al. (2014): Pyroxene megacrysts in Proterozoic anorthosites:

3236    Implications for tectonic setting, magma source and magmatic processes at the Moho. Earth

3237    and Planetary Science Letters 401, 378-380.

3238    Vander Auwera, J., Longhi, J., 1994. Experimental study of a jotunite (hypersthene

3239    monzodiorite): constraints on the parent magma composition and crystallization conditions

3240 (P, T, fO₂) of the Bjerkreim-Sokndal layered intrusion (Norway). Contributions to Mineralogy

3241 and Petrology 118, 60-78.

3242 Vander Auwera, J., Longhi, J., Duchesne, J.C., 1998. A liquid line of descent of the

3243 Jotunite (Hypersthene Monzodiorite) suite. Journal of Petrology 39, 439-468.

3244 Vanderhaeghe, O., 2012. The thermal–mechanical evolution of crustal orogenic belts at

3245 convergent plate boundaries: A reappraisal of the orogenic cycle. Journal of Geodynamics 56-

3246 57, 124-145.

3247 Vermeesch, P., 2012. On the visualisation of detrital age distributions. Chemical Geology

3248 312, 190-194.

3249 Verschure, R.H., Andriessen, P.A.M., Boelrijk, N.A.M., Hebeda, E.H., Maijer, C., Priem,

3250 H.N.A., Verdurmen, E.A.T., 1980. On the thermal stability of Rb-Sr and K-Ar biotite

3251 systems: evidence from coexisting Sveconorwegian (ca. 870 Ma) and (ca. 400 Ma) biotites in

3252 SW Norway. Contributions to Mineralogy and Petrology 74, 245-252.

3253 Villaseca, C., Barbero, L., Herreros, V., 1998. A re-examination of the typology of

3254 peraluminous granite types in intracontinental orogenic belts. Transactions of the Royal

3255 Society of Edinburgh: Earth Sciences 89, 113-119.

3256 Viola, G., Bingen, B., Solli, A., 2016. Berggrunnskart Kongsberg lithotectoniske enhet,

3257 Kongsberg-Modum-Hønefoss, M 1:100000 - Bedrock geology map of the Kongsberg

3258 lithotectonic unit, Kongsberg-Modum-Hønefoss, scale 1:100000, 1 sheet. Norges Geologiske

3259 Undersøkelse - Geological Survey of Norway, pp. Scale 1:100000, 100001 sheet.

3260 Viola, G., Henderson, I.H.C., 2010. Inclined transpression at the toe of an arcuate thrust:

3261 an example from the Precambrian "Mylonite Zone" of the Sveconorwegian orogen, in: Law,

3262 R., Butler, R., Holdsworth, R.E., Krabbendam, M., Strachan, R.A. (Eds.), Continental

3263 Tectonics and Mountain Building - The Legacy of Peach and Horne. Geological Society,

3264 London, Special Publications, pp. 715-737.

3265    Viola, G., Henderson, I.H.C., Bingen, B., Hendriks, B.W.H., 2011. The Grenvillian-

3266    Sveconorwegian orogeny in Fennoscandia: Back-thrusting and extensional shearing along the

3267    "Mylonite Zone". Precambrian Research 189, 368-388.

3268    Viola, G., Venvik Ganerød, G., Wahlgren, C.H., 2009. Unraveling 1.5 Ga of brittle

3269    deformation history in the Laxemar-Simpevarp area, southeast Sweden: A contribution to the

3270    Swedish site investigation study for the disposal of highly radioactive nuclear waste.

3271    Tectonics 28, TC5007.

3272    Viola, G., Zwingmann, H., Mattila, J., Käpyaho, A., 2013. K-Ar illite age constraints on

3273    the Proterozoic formation and reactivation history of a brittle fault in Fennoscandia. Terra

3274    Nova 25, 236-244.

3275    Wahlgren, C.H., Cruden, A.R., Stephens, M.B., 1994. Kinematics of a major fan-like

3276    structure in the eastern part of the Sveconorwegian orogen, Baltic Shield, south-central

3277    Sweden. Precambrian Research 70, 67-91.

3278    Wahlgren, C.H., Page, L., Kübler, L., Delin, H., 2015. $^{40}$Ar-$^{39}$Ar biotite age of a

3279    lamprophyre dyke and constraints on the timing of ductile deformation inside the Idefjorden

3280    terrane and along the Mylonite Zone, Sveconorwegian orogen, south-west Sweden. GFF first

3281    view, 1-9.

3282    Wahlgren, C.H., Stephens, M.B., 2020. Chapter 11 - Reworking of older (1.8 Ga)

3283    continental crust by Mesoproterozoic (1.5–1.4 Ga) orogeny, Blekinge–Bornholm orogen,

3284    southeastern Sweden. Geological Society, London, Memoirs 50, 291-312.

3285    Wallace, P.J., 2005. Volatiles in subduction zone magmas: concentrations and fluxes based

3286    on melt inclusion and volcanic gas data. Journal of Volcanology and Geothermal Research

3287    140, 217-240.

3288    Wang, X.D., Söderlund, U., Lindh, A., Johansson, L., 1998. U-Pb and Sm-Nd dating of

3289    high-pressure granulite- and upper amphibolite facies rocks from SW Sweden. Precambrian

3290    Research 92, 319-339.

3291    Weber, B., Köhler, H., 1999. Sm–Nd, Rb–Sr and U–Pb geochronology of a Grenville

3292    Terrane in Southern Mexico: origin and geologic history of the Guichicovi Complex.

3293    Precambrian Research 96, 245-262.

3294    Weber, B., Scherer, E.E., Schulze, C., Valencia, V.A., Montecinos, P., Mezger, K., Ruiz,

3295    J., 2010. U-Pb and Lu-Hf isotope systematics of lower crust from central-southern Mexico -

3296    Geodynamic significance of Oaxaquia in a Rodinia Realm. Precambrian Research 182, 149-

3297    162.

3298    Weis, D., 1986. Genetic implications of Pb isotopic geochemistry in the Rogaland

3299    anorthositic complex (Southwest Norway). Chemical Geology 57, 181-199.

3300    Wickström, L.M., Stephens, M.B., 2020. Chapter 18 - Tonian–Cryogenian rifting and

3301    Cambrian–Early Devonian platformal to foreland basin development outside the Caledonide

3302    orogen. Geological Society, London, Memoirs 50, 451-477.

3303    Wiest, J.D., Jacobs, J., Ksienzyk, A.K., Fossen, H., 2018. Sveconorwegian vs. Caledonian

3304    orogenesis in the eastern Øygarden Complex, SW Norway – Geochronology, structural

3305    constraints and tectonic implications. Precambrian Research 305, 1-18.

3306    Wilmart, E., Demaiffe, D., Duchesne, J.C., 1989. Geochemical constraints on the genesis

3307    of the Tellnes ilmenite deposit, southwest Norway. Economic Geology 84, 1047-1056.

3308    Zhang, S., Li, Z.-X., Evans, D.A.D., Wu, H., Li, H., Dong, J., 2012. Pre-Rodinia

3309    supercontinent Nuna shaping up: A global synthesis with new paleomagnetic results from

3310    North China. Earth and Planetary Science Letters 353-354, 145-155.

Zhang, W., Roberts, D., Pease, V., 2015. Provenance characteristics and regional implications of Neoproterozoic, Timanian-margin successions and a basal Caledonian nappe in northern Norway. Precambrian Research 268, 153-167.

Zhang, W., Roberts, D., Pease, V., 2016. Provenance of sandstones from Caledonian nappes in Finnmark, Norway: Implications for Neoproterozoic–Cambrian palaeogeography. Tectonophysics 691, 198-205.

**11  Figure captions**

Inserted into the document

**12  Table captions and Inline Supplementary Material captions**

**Table 1.** Chart of geological events in the Sveconorwegian orogen. (Austin Hegardt, 2010; Bingen et al., 2003; Bybee et al., 2014; Charlier et al., 2010; Coint et al., 2015; Eliasson et al., 2003; Engvik et al., 2016; Hansen et al., 2015, Lamminen, 2011 #5583; Laurent et al., 2018b; Moczydłowska et al., 2018; Müller et al., 2017; Ripa and Stephens, 2020d; Söderlund et al., 2008a; Söderlund et al., 2005; Spencer et al., 2014; Vander Auwera et al., 2014a; Vander Auwera and Longhi, 1994)

**Table 2.** Summary of sampling and zircon U-Pb data for migmatitic gneisses, Eidsvoll-Auli area, Idefjorden lithotectonic unit.

**Inline Supplementary Material 1.** Text document. New zircon U–Pb geochronological data in the Idefjorden lithotectonic unit.

**Table S2. Inline Supplementary Material 2.** SIMS (SHRIMP) U–Pb analyses of zircon from leucosome samples from the Eidsvoll-Auli area, Idefjorden lithotectonic unit.

**Table S3. Inline Supplementary Material 2.** Compilation of samples of metasediments for which detrital zircon U-Pb data are published and compilation of geochronological data recording magmatic-migmatitic events in the Sveconorwegian orogen.